# Numerical Simulation of Flows at Low Mach Numbers with Heat Sources

Dissertation
zur
Erlangung des akademischen Grades eines
Doktors der Naturwissenschaften (Dr. rer. nat.)

im Fachbereich Mathematik/Informatik
der Universität Kassel

vorgelegt von
**Philipp Birken**
aus
**Leonberg**

Gutachter: Prof. Dr. Andreas Meister
Prof. Dr. Thomas Sonar

Tag der Disputation: 20. Dezember 2005

Nature laughs at the difficulties of integration.
Pierre-Simon Laplace

# Contents


Preface . . . . . 7

**1 Introduction** **9**
1.1 Notation . . . . . 12

**2 The Governing Equations** **13**
2.1 The Navier-Stokes Equations . . . . . 13
2.2 The Mach Number . . . . . 15
2.3 Nondimensionalization for Low Mach Numbers . . . . . 15
2.4 The Tunnel Equations . . . . . 16
2.5 Problems of the Model . . . . . 18
2.6 Nondimensional Euler Equations . . . . . 19
2.7 Asymptotic Analysis of the Euler Equations . . . . . 20
2.8 Boundary and Initial Conditions . . . . . 22
2.9 Hydrostatic Solutions . . . . . 22

**3 The Finite Volume Method** **25**
3.1 Time Integration Schemes . . . . . 26
3.2 Fractional Step Methods for Source Terms . . . . . 27
3.3 The Line Integrals and Numerical Flux Functions . . . . . 28
3.4 Boundary Conditions . . . . . 31
3.4.1 Nonreflecting Boundary Conditions . . . . . 32
3.5 Reconstruction and Limiter . . . . . 32
3.5.1 Modification at the Boundaries . . . . . 33
3.6 Time Integration for the Euler Equations . . . . . 34
3.6.1 Implicit schemes . . . . . 35
3.7 Discrete Asymptotic Analysis . . . . . 40

**4 The Preconditioned Method** **43**
4.1 Uniqueness of the Approach . . . . . 45

4.2 Stability Analysis . . . . . 53
4.2.1 Numerical Experiments . . . . . 59
4.2.2 The Two Dimensional Case . . . . . 61

**5 Gravitation and Heat** **63**
5.1 The Source Terms . . . . . 64
5.2 A First Test Case . . . . . 65
5.2.1 Numerical Experiments . . . . . 66
5.3 Analysis of the Energy Flux . . . . . 66
5.4 Further Results for Buoyant Flows . . . . . 69
5.5 Gravitation and a Heat Source . . . . . 70
5.5.1 Simulation of a Fire Event . . . . . 71
5.5.2 Description of the Results for the Fire Events . . . . . 72
5.5.3 Influence of the CFL Number . . . . . 74

**6 Summary and Outlook** **83**

**A One Dimensional Terms** **85**

**B Rotational Invariance of the Lax-Friedrichs Flux** **87**

**C The Preconditioned Flux** **89**

**Bibliography** **93**

# Preface

This thesis was written while I was at the Group for Analysis and applied Mathematics of the Department for Mathematics and Computer Science of the University of Kassel. Part of the results were obtained while I was at the Institute of Mathematics at the University of Lübeck and a stipendiate in the Graduiertenkolleg 357 "Effiziente Algorithmen und Mehrskalenmethoden", financed by the DFG. I would like to thank the colleagues from both departments for their support and the friendly atmosphere.

Especially, I would like to thank my advisor, Prof. Dr. Andreas Meister. The success of my dissertation was important to him and he supported me whereever he could. Furthermore, I would like to thank Prof. Dr. Thomas Sonar for acting as second referee on this thesis and Dr. Ralf Massjung from the RWTH Aachen for allowing me to use his code and for a lot of fruitful discussions.

My thanks also go to the coders of free software, especially those of Linux, the Open Data Explorer, the GNU Project and LaTeX.

Finally, there is my Margit, who still loves me when the numerical results are bad.

# Chapter 1

# Introduction

This thesis is concerned with the numerical simulation of flows at low Mach numbers which are subject to the gravitational force and strong heat sources. As a specific example for such flows, a fire event in a car tunnel will be considered in detail.

In recent years there were a number of tragic and deadly incidents in car tunnels, for example in the Mont-Blanc tunnel 1999, the Tauern tunnel 1999 or the Kaprun tunnel 2000. This demonstrates the need for more efficient safety measures. However, it is very expensive to shut down a tunnel to perform experiments. Therefore, there is a need to develop numerical methods that can reliably simulate fire events. The crucial problem is to guarantee a hospitable environment for as long it takes to evacuate the people. This demands a layer of cool air with enough oxygen and not too much smoke and furthermore structural stability. The latter part is no real problem in car tunnels and so special attention is paid to the first problem. There exists a variety of codes designed to provide information on smoke and heat development in buildings, see for example the survey [48]. In praxis, often so called zonal models like the Multi Room Fire Code of Max [37] are used, which use extremely coarse grids, a division of each cell in hot and cold zones and conservation of mass and energy. The grid sizes are in the order of 50 meters. These methods are fast and thus allow parameter studies. However, they cannot deal with complicated geometries and provide results that are nonlocal and only roughly in agreement with experiments [30]. Furthermore, they are designed for buildings and, due to the missing momentum equation, cannot simulate buoancy driven flows as those in sloped tunnels.

The alternative to zonal models are so called field models, which correspond to more sophisticated and much more accurate tools provided by computational fluid dynamics (CFD). Those can in principal deal with complicated geometries and buoancy driven flows. The increase in computer power makes the use of these methods applicable to these problems, however there is still need for faster algorithms and faster computers until parameter studies of tunnels can be done in acceptable time.

The arising flows can be characterized by characteristic speeds of one meter per second

and thus a low Mach number ($M \approx 10^{-3}$) and furthermore by high temperature gradients. They are driven by buoancy and the strong heat sources. Caused by these effects, parts of the flow become compressible, although the general situation is nearly compressible. This is similar to a lot of applications, where the Mach number or the compressibility properties vary strongly in time or space. Some examples are nozzle flow, chemically reacting flows or laminar combustion. Thus, the methods developed and analyzed in this thesis, can be applied not only to tunnel fire events, but to a wide range of practical problems.

In the CFD community, the efficient simulation of low Mach number flows is a subject of ongoing discussion. It is well known that purely compressible flow solvers which were developed for transonic flow fields produce wrong results at low Mach numbers on reasonable grids and need an unacceptable fine mesh width to provide correct results. This was demonstrated in detail by Volpe [69]. On the other hand, standard incompressible flow solvers cannot deal with strong temperature or strong density gradients. This sets a demand for codes that can deal with compressible flows at all Mach numbers. As a lot of expertise and development time was put into currently used codes, the desire to expand an existing code as opposed to writing a completely new one is very natural. Consequently, there are two main approaches to the design of numerical methods for the above mentioned flows: use either the compressible or the incompressible Euler or Navier-Stokes equations as the basic model and improve upon the existing methods. Both approaches are pursued and widely used. One important idea in this context was the artificial compressibility method by Chorin [5] that inspired the preconditioner of Turkel [63] for the compressible equations. These methods incorporate a preconditioning of the time derivative of the PDE, thus allowing faster convergence to steady state but sacrificing time accuracy. Along these lines, other preconditioners were proposed [67, 4]. The crucial idea is, that as the Mach number tends to zero, the original system develops a large disparity in wave speeds, as some of the eigenvalues grow to infinity while others remain $\mathcal{O}(1)$. The preconditioner changes all the wave speeds to $\mathcal{O}(1)$, thus greatly improving the condition number of the system.

For incompressible flows, there are two main techniques that are used to expand the validity of the scheme into the compressible regime. One class of schemes is based on the marker and cell method (MAC) by Harlow and Welch [21], which is a finite difference method on a staggered grid. The method is quite fast, but it is very difficult to use the staggered location of the variables in the context of unstructured grids. Recently, Wenneker, Segal and Wesseling proposed a method that faces this difficulty [72]. On the other hand, Patankar and Spalding [49] published their SIMPLE scheme (for Semi-Implicit Method for Pressure Linked Equations) in 1972. Based on an approximation of the pressure, a velocity field is computed using the momentum equations. Then, an elliptic pressure correction equation is solved to improve the approximation of the pressure. These steps are then iterated until convergence is obtained. The approach is not limited to incompressible flows: see [8]. Both SIMPLE and MAC scheme as well as their improved descendants have in common that they work on the velocity field and the pressure distribution. By contrast, codes for compressible flow are usually based on the conserved variables density, momentum and energy. Thus, in the context of methods for all Mach numbers it is useful not to speak of

incompressible and compressible solvers, but of pressure based and density based schemes.

In this thesis, we will concentrate on the case of density based flow solvers. Here, three main techniques to obtain time accuracy can be distinguished. First of all, there is the technique to use the above mentioned preconditioning methods for steady state flows in a pseudo time stepping scheme [58, 64, 71]. Furthermore, there is the flux correction approach, where an approximation to the Euler or Navier-Stokes equations is solved and then corrected via elliptic correction equations [24, 28, 56]. Finally, there is the flux preconditioning approach, where only the dissipation within the numerical flux function of the flow solver is changed by low Mach number preconditioning [18, 43]. This has several advantages. An important one is that the implementation is quite simple. The only part of the flow solver that needs to be changed is the flux function. The other one is that compared to the flux correction approach, the computational effort per time step is smaller.

While the principal feasibility of this method was proven, an analysis of its numerical properties was missing so far, as well as an answer to the question what would happen if additional source terms were added to the governing equations. Furthermore, numerical experiments indicate that the stability region of an explicit preconditioned method deteriorates as the Mach number tends to zero. In order to overcome this severe disadvantage implicit methods are usually employed. This behavior of explicit schemes was often reported and a comprehensive analysis of this phenomenon is presented here.

The outline of the thesis is as follows: In chapter two, we briefly introduce the Navier-Stokes equations and then develop a model for fire incidents, which consists of the Euler equations of gas dynamics with source terms. In order to get a deeper insight into the behavior of the corresponding physical quantities, we summarize the main results of an asymptotic analysis in the low Mach number limit. Thereafter in chapter three, a finite volume approximation of the governing equations using a Lax-Friedrichs type scheme is presented whereby we curtly discuss the asymptotic behavior of this approach as the Mach number tends to zero. Then, in chapter four, a preconditioned variant of the Lax-Friedrichs flux is presented, that satisfies the results of the continuous asymptotic analysis in a discrete sense. Then the question is pursued, how far we can deviate from the preconditioner of Turkel. The core of this chapter is an $L_2$-stability analysis of a class of preconditioned methods, where we will prove the generally unfavorable behavior of the explicit scheme. Besides the method proposed by Guillard and Viozat [18] a more general preconditioning matrix due to Turkel [63] is investigated. Thereby, it is proved that the whole class of these approaches suffers from similar stability problems and thus, an implicit time stepping scheme should be preferred for this kind of method in the regime of low Mach numbers. The theoretical results are after wards confirmed by numerical experiments.

We will proceed in chapter five, to incorporate the source terms via operator splittings. As the correct resolution of the buoancy force is crucial for this problem, we will first integrate the gravitational source term only. After having looked at this in detail by both analysis and numerical experiments we will add heat sources and demonstrate the feasibility of the method by means of several test problems.

The focus of the thesis is on issues of discretization, respectively the properties of the

low Mach preconditioned method. Issues of the solvers and how to solve the appearing equations systems fast and efficiently was not the core topic of the work.

## 1.1 Notation

Troughout the thesis, we will use bold capital letters ($\mathbf{A}$) to indicate matrices and bold small letters ($\mathbf{x}$) to indicated vectors. Small letters represent scalars, and thus the components of vectors are small letters with indeces. Therefore, $\mathbf{u}_1$ is the first vector of a family of vectors, but $u_1$ would be the first component of the vector $\mathbf{u}$. Specifically, the two space directions are $x_1$ and $x_2$ as the components of the vector $\mathbf{x}$. In some proofs we will need single components of matrix vector products. There, the $i$-th component will be denoted by placing the index near the matrix. For example, the first component of the vector $\mathbf{Ax}$ is given by $\mathbf{A}_1\mathbf{x}$.

For reference we will now state the different types of variables employed. They will be explained in the next chapter.

A dimensional quantity will be denoted with a hat: $\hat{\phi}$.

A quantity nondimensionalized using $\hat{p}_{ref} = \hat{\rho}_{ref}\hat{v}^2_{ref}$ will not be denoted in a special way: $\phi$.

Finally, a quantity nondimensionalized using an own pressure reference $\hat{p}_{ref}$ wil be denoted with a tilde: $\widetilde{\phi}$.

# Chapter 2

# The Governing Equations

As mentioned in the introduction, we will base our numerical method on a model of compressible flow, namely the two dimensional Euler equations with additional terms for a heat source and gravitation. The first interesting point is, in how far these equations truly model the flow of a fire incident. Therefore, we will start with the full two dimensional Navier-Stokes equations and analyze which terms are actually relevant for the given problem, before proceeding to present some properties of the Euler equations.

## 2.1 The Navier-Stokes Equations

The Navier-Stokes equations describe the behavior of an ideal gas. They consist of the laws of conservation of mass, momentum and energy. The equations will be presented in differential form, first with dimensional quantities, after which a non-dimensionalized version will be presented. In this form, they are a system of second order partial differential equations of mixed hyperbolic-parabolic type. A more detailed description can be found in the texbooks by Chorin and Marsden [6] and Hirsch [22]. The superscript $\hat{}$ denotes a dimensional quantity. We consider an open domain $\mathcal{U} \in \mathbb{R}^2$, the elements of $\mathcal{U}$ are written as $\mathbf{x} = (x_1, x_2)^T$. The *conservation equation of mass* (also called continuity equation) is given in terms of the density $\hat{\rho}$ by

$$\partial_{\hat{t}} \hat{\rho} + \nabla_{\hat{\mathbf{x}}} \cdot \hat{\mathbf{m}} = 0. \tag{2.1}$$

Here $\hat{\mathbf{m}}$ denotes the momentum vector, divided through the unit volume. With the pressure $\hat{p}$ and the velocity vector $\hat{\mathbf{v}}$, *conservation of momentum* can be described by

$$\partial_{\hat{t}} \hat{m}_i + \sum_{j=1}^{2} \partial_{\hat{x}_j} (\hat{m}_i \hat{v}_j + \hat{p}\delta_{ij}) = \sum_{j=1}^{2} \partial_{\hat{x}_j} \hat{S}_{ij} + \hat{\rho}\hat{g}_i, \qquad i = 1, 2, \tag{2.2}$$

where $\delta_{ij}$ is the Kronecker symbol,

$$\hat{S}_{ij} = \hat{\mu}[(\partial_{\hat{x}_j}\hat{v}_i + \partial_{\hat{x}_i}\hat{v}_j) - \frac{2}{3}\delta_{ij}\sum_{k=1}^{2}\partial_{\hat{x}_k}\hat{v}_k], \qquad i,j = 1,2,$$

represents the viscous shear stress tensor with $\hat{\mu}$ being the dynamic viscosity and $\hat{g}_i$ denotes the $i$'th component of the gravitational acceleration vector. This vector will always be given by $\hat{\mathbf{g}} = (0, -9.81)^T$ and its euclidian length will be denoted by $\hat{g}$, which is equal to 9.81. For simplicity of notation, we will not neglect the first component $\hat{g}_1$ in the equations. We assume that there are no other forces acting on the fluid. Finally, we have the *conservation of total energy*, where $\hat{E}$ is the total energy per unit mass:

$$\partial_{\hat{t}}\hat{\rho}\hat{E} + \nabla_{\hat{\mathbf{x}}}\cdot(\hat{H}\hat{\mathbf{m}}) = \sum_{j=1}^{2}\partial_{\hat{x}_j}\left(\sum_{i=1}^{2}\hat{S}_{ij}\hat{v}_i - \hat{W}_j\right) + \hat{q} - \hat{\rho}\hat{\mathbf{v}}\cdot\hat{\mathbf{g}}. \tag{2.3}$$

$\hat{H} = \hat{E} + \frac{\hat{p}}{\hat{\rho}}$ denotes the enthalpy and $\hat{W}_j$ describes the flow of heat which, using the thermal conductivity coefficient $\hat{\kappa}$, can be written in terms of the gradient of the temperature $\hat{T}$ as

$$\hat{W}_j = -\hat{\kappa}\partial_{\hat{x}_j}\hat{T}.$$

The total energy per unit mass $\hat{E}$ is given by the sum of inner, kinetic and potential energy (measured with respect to a reference height $\hat{x}_{2_r}$) as

$$\hat{E} = \hat{e} + \frac{1}{2}|\hat{\mathbf{v}}^2| + (\hat{x}_2 - \hat{x}_{2_r})|\hat{\mathbf{g}}|.$$

Finally, the source terms $\hat{q}$ and $\hat{\rho}\hat{\mathbf{v}}\cdot\hat{\mathbf{g}}$ on the right hand side of (3) model a heat source and the potential energy. $\hat{q}$ corresponds to the power per unit volume generated by the fire. A heat source was chosen to model the fire instead of a heat flux, because the fire fighters report fires in terms of their power in megawatt, which can be measured effectively, by contrast to the heat flux. We thus have four equations for five variables and the system is closed by the equation of state for the pressure using the adiabatic exponent $\gamma$:

$$\hat{p} = (\gamma - 1)\hat{\rho}(\hat{E} - \frac{1}{2}|\hat{\mathbf{v}}|^2 - (\hat{x}_2 - \hat{x}_{2_r})|\hat{\mathbf{g}}|). \tag{2.4}$$

The thermodynamic quantities density, pressure and temperatur are related through the ideal gas law

$$\hat{T} = \frac{\hat{p}}{\hat{\rho}\hat{R}}.$$

Finally, the adiabatic exponent $\gamma$ and the specific gas constant $\hat{R} = 287 J/Kg/K$ are related through the specific heat coefficients for constant pressure $\hat{c}_p = 1010 J/Kg/K$ respectively constant volume and $\hat{c}_v = 723 J/Kg/K$ through

$$\gamma = \frac{\hat{c}_p}{\hat{c}_v} \approx 1.4$$

and

$$\hat{R} = \hat{c}_p - \hat{c}_v.$$

## 2.2 The Mach Number

An important nondimensional quantity is the Mach number $Ma$, after the german engineer Ernst Mach, which is the quotient of the velocity and the speed of sound $\hat{c}$, which is given by

$$\hat{c} = \sqrt{\gamma \frac{\hat{p}}{\hat{\rho}}}.$$

The flow speed in the tunnel is of the order $1\frac{m}{s}$, which is very small and therefore the flow is nearly incompressible. This is called the low Mach number regime.

## 2.3 Nondimensionalization for Low Mach Numbers

An important topic in the analysis of partial differential equations is the non-dimensionalization of the physical quantities. This is done to achieve two things. First, we want all quantities to be $\mathcal{O}(1)$ due to stability reasons and then we want scalability from real experiments to the mathematical equation and the numerical simulation. For the Navier-Stokes equations, we will obtain several reference numbers which depend on the reference quantities and which allow this scaling.

The process is done by replacing all dimensional quantities with the product of a non-dimensional variable with a dimensional reference number:

$$\hat{\phi} = \phi \cdot \hat{\phi}_{ref}.$$

Given reference values for the variables length, velocity, pressure and density ($\hat{x}_{ref}$, $\hat{v}_{ref}$, $\hat{p}_{ref}$ and $\hat{\rho}_{ref}$), we can compute the reference values for all other variables from these, for example:

$$\hat{t}_{ref} = \frac{\hat{x}_{ref}}{\hat{v}_{ref}}, \qquad \hat{E}_{ref} = \hat{H}_{ref} = \hat{c}^2_{ref} = \frac{\hat{p}_{ref}}{\hat{\rho}_{ref}}.$$

Additionally, we need references for the physical parameters and constants $\hat{\mu}_{ref}$, $\hat{\kappa}_{ref}$, $\hat{R}_{ref} = \hat{c}_{p_{ref}}$, $\hat{q}_{ref}$ and $\hat{g}_{ref}$.

For the nondimensional $\mu$, the Sutherland law gives a relation to the temperature:

$$\mu = T^{\frac{3}{2}} \left( \frac{1+Su}{T+Su} \right),$$

with $Su$ being the Sutherland-constant, which is $Su = \frac{110K}{\hat{T}_{ref}}$ for air. For compressible flows, $\hat{p}_{ref}$ is usually defined as $\hat{\rho}_{ref}\hat{v}^2_{ref}$ which results in dimensionless equations, where the Mach number does not appear as a parameter. However, for low Mach numbers this would result in an unphysical pressure reference and a pressure variable which is not $\mathcal{O}(1)$, due to the small velocity reference. Therefore, we also use an independent pressure reference $\hat{p}_{ref}$. To distinguish between the two kinds of nondimensionalization, the quantities after low Mach nondimensionalization will be denoted with a $\widetilde{}$ (e.g. $\widetilde{p}$), while the nondimensional quantities obtained by the usual nondimensionalization as employed in most flow solvers have no special sign (e.g. $p$). Introducing the low Mach nondimensionalized variables into the equations, we obtain the following set of equations:

$$\begin{aligned}
\partial_t \widetilde{\rho} + \quad & \nabla_{\mathbf{x}} \cdot \widetilde{\mathbf{m}} && = 0, \\
\partial_t \widetilde{m}_i + \quad & \textstyle\sum_{j=1}^{2} \partial_{x_j} (\widetilde{m}_i \widetilde{v}_j + \frac{1}{M^2}\widetilde{p}\delta_{ij}) && = \frac{1}{Re} \sum_{j=1}^{2} \partial_{x_j} \widetilde{S}_{ij} + \widetilde{\rho}\frac{\widetilde{g}_i}{Fr^2} \qquad i = 1,2, \\
\partial_t (\widetilde{\rho}\widetilde{E}) + \quad & \nabla_{\mathbf{x}} \cdot (\widetilde{H}\widetilde{\mathbf{m}}) && = \frac{1}{Re} \sum_{j=1}^{2} \partial_{x_j} \left( \sum_{i=1}^{2} M^2 \widetilde{S}_{ij}\widetilde{v}_i - \frac{\widetilde{W}_j}{Pr} \right) + Q\widetilde{q} + \frac{M^2}{Fr^2}\widetilde{\rho}\widetilde{\mathbf{v}} \cdot \widetilde{\mathbf{g}}.
\end{aligned} \tag{2.5}$$

The Reynolds-, Froude- and Prandtl-number, as well as the parameter $M$ are dimensionless quantities, given by:

$$Re = \frac{\hat{\rho}_{ref}\hat{v}_{ref}\hat{x}_{ref}}{\hat{\mu}_{ref}}, \qquad Fr = \frac{\hat{v}_{ref}}{\sqrt{\hat{x}_{ref}\hat{g}_{ref}}}, \qquad Pr = \frac{\hat{\mu}_{ref}\hat{c}_{p_{ref}}}{\hat{\kappa}_{ref}}, \qquad M = \frac{\hat{v}_{ref}}{\hat{c}_{ref}}.$$

The nondimensional number $M$ is related to the Mach number $Ma$ via $M = \sqrt{\gamma}Ma$ and thus $M = \mathcal{O}_S(Ma)$. It is therefore for the question of asymptotic behavior of no importance which number is used. The dimensionless factor Q in front of the heat source $q$ is $\frac{\hat{q}_{ref}\hat{x}_{ref}}{\hat{p}_{ref}\hat{v}_{ref}}$. Finally, the equation of state transforms into

$$\widetilde{p} = (\gamma - 1)\widetilde{\rho} \left( \widetilde{E} - \frac{1}{2}|\widetilde{\mathbf{v}}^2|M^2 - |\widetilde{\mathbf{g}}|(\widetilde{x}_2 - \widetilde{x}_{2_r})\frac{M^2}{Fr^2} \right). \tag{2.6}$$

## 2.4 The Tunnel Equations

After having presented the full Navier Stokes equations in the last section, we are now going to proceed to look at the application to the tunnel fire problem and identify the

terms in (2.5) which are negligible. For this, we will first present the reference values for the problem and then calculate the dimensionless reference numbers. Most of these correspond to physical properties of air and not on the problem, but the reference length, velocity and heat source have to be chosen.

As in [12] we chose the order of the tunnel height as the length scale and typical velocities in the tunnel are about one meter per second. The heat source $\widetilde{q}$ is a spatial indicator function being one where the fire burns and zero where not. $Q\widetilde{q}$ corresponds to a cross segment of the tunnel, due to the fact that we have a two dimensional and not a three dimensional model and is implemented by a spatial indicator. The total power of a fire due to a burning car or truck is about 1-100 megawatt (MW), but distributed over the domain of the fire. To obtain the correct power, we have to chose $\hat{q}_{ref}$ of the order $10^6$ up to $10^7$.

$$\hat{x}_{ref} = 10m, \qquad \hat{v}_{ref} = 1\frac{m}{s}, \qquad \hat{p}_{ref} \approx 10^5\frac{kg}{ms^2}, \qquad \hat{\rho}_{ref} = 1.2\frac{kg}{m^3}, \qquad \hat{q}_{ref} \in [10^6, 10^7]\frac{W}{m^3},$$

$$\hat{\mu}_{ref} = 18 \cdot 10^{-6}\frac{kg}{m\ s}, \qquad \hat{\kappa}_{ref} = 25 \cdot 10^{-3}\frac{kg\ m}{s^3 K}, \qquad \hat{c}_{p_{ref}} = 1005\frac{m^2}{s^2 K}, \qquad \hat{g}_{ref} = 9.81\frac{m}{s^2}.$$

From these values, we obtain

$$Re = \frac{2}{3} \cdot 10^6, \qquad Pr = 0.72, \qquad M = 3.5 \cdot 10^{-3}, \qquad Fr = 10^{-1}, \qquad Q \in [100, 1000]$$

and

$$M^2 = 1.2 \cdot 10^{-5}, \qquad \frac{M^2}{Fr^2} = 1.2 \cdot 10^{-3} \qquad \frac{M^2}{Re} = 1.8 \cdot 10^{-13}.$$

We will keep all the convection terms and neglect only terms on the right hand side. Immediately we see, that the continuity equation remains unchanged. As for the energy equation, we can omit the loss of energy due to viscosity, which is multiplied with $M^2/Re$. This is not surprising, as due to the small flow velocities, the frictional heat is also low. Regarding the heat conduction, we see that this is multiplied by $1/Re/Pr$, but the gradients $\partial_{x_j}\widetilde{W}_j$ can be very large in the vicinity of the fire, where we have high temperature gradients. We will therefore keep the heat conduction term. By contrast, we will neglect the potential energy. For a properly chosen reference height, the nondimensional height for this problem is between one and zero. Thus the potential energy is globally smaller by orders of magnitude than the heat source term, as we have only small variations of height in the tunnel and furthermore a low Mach number. In the equation of state, we will neglect the kinetic and the potential energy with the same reasoning. The final energy equation is then given by

$$\partial_t(\widetilde{\rho}\widetilde{E}) + \nabla_{\mathbf{x}} \cdot (\widetilde{H}\widetilde{\mathbf{m}}) = -\frac{1}{RePr}\sum_{j=1}^{2} \partial_{x_j}\widetilde{W}_j + Q\widetilde{q} \tag{2.7}$$

and the equation of state is simply

$$\widetilde{p} = (\gamma - 1)\widetilde{\rho}\widetilde{E}. \tag{2.8}$$

We will now look more closely at the viscous terms in the momentum equations. These have an influence only in the boundary layer, which is small due to the high Reynolds number. Nevertheless, it is important to incorporate these terms to obtain the correct flow profile, as these second order terms change the character of the partial differential equations. There are several models to simplify the viscous terms by neglecting some of the stresses, for example the parabolized Navier-Stokes equations or the thin shear layer approximation. Unfortunately, due to the heat source and the low Mach number, none of these are applicable. We will therefore keep all the stresses $\widetilde{S}_{ij}$. The gravitational term in the momentum equations is multiplied with about one hundred, which demonstrates its importance and thus it will of course be kept.

Note that these equations are truly compressible. While the compressible Navier-Stokes equations in the limit of a zero Mach number result in the density dependent incompressible Navier-Stokes equations where the divergence of the velocity is zero, as was shown by Klainermann and Majda [26] in the 1980s, it was shown for example in [12] that in this case the divergence of the velocity is equal to a constant times the heat source. Thus we also see that the stronger the heat source, the more compressible the flow.

## 2.5 Problems of the Model

There are several important effects which are not included in the model. The first one is the radiation of heat, which affects the wall temperature to a great extent. Radiation is however not a fluid mechanical effect and is therefore not included in this thesis.

The other important effect is heat loss at the walls. This is a clearly three dimensional effect, where also in the two dimensional equations, additional source terms are needed to take this into account, as was done in [12] in a onedimensional model. Gasser and Struckmeier use a source term in the energy equation corresponding to a cross section of the tunnel. However, it was beyond the scope of this thesis to incorporate these effects.

Finally, the fire is incorpororated through a heat source only. Thus, there is no flame and no smoke. The flame can be neglected, as the specific shape or composition of the plume has no great effect on the flow field. Smoke however, is an important part of the problem and poses a life threat due to poisoning and asphyxiation independently of the heat. Nevertheless, it is not yet included in the model, as a proper numerical method for the computation of the flow field is the necessary starting point for the simulation of a tunnel fire. Fortunately, the region of hot air is a very good indicator of where the smoke is.

## 2.6 Nondimensional Euler Equations

The Navier-Stokes equations are numerically difficult to solve. If we neglect the viscosity and heat conduction terms, we obtain the Euler equations with source terms for heat and gravity:

$$\begin{aligned} \partial_t \widetilde{\rho} + & \quad \nabla_{\mathbf{x}} \cdot \widetilde{\mathbf{m}} & = 0, & \\ \partial_t \widetilde{m}_i + & \quad \textstyle\sum_{j=1}^{2} \partial_{x_j} (\widetilde{m}_i \widetilde{v}_j + \frac{1}{M^2} \widetilde{p} \delta_{ij}) & = \widetilde{\rho} \dfrac{\widetilde{g}_i}{Fr^2} & \quad i = 1, 2, \\ \partial_t (\widetilde{\rho} \widetilde{E}) + & \quad \nabla_{\mathbf{x}} \cdot (\widetilde{H} \widetilde{\mathbf{m}}) & = Q \widetilde{q}. & \end{aligned} \tag{2.9}$$

They are purely hyperbolic and numerically easier to solve than the Navier-Stokes equations. The solution of these equations is the first step in developing a method for the tunnel equations and we will use them for this thesis. Thus, the asymptotic analysis of the properties of the solutions will be performed on the above equations. However, the standard flow solvers are based on a different nondimensionalization of the flow variables, where $\hat{p}_{ref} = \hat{\rho}_{ref} \hat{v}_{ref}^2$. This leads to the following form of the Euler equations, which is the system the numerical methods in this thesis are designed for:

$$\begin{aligned} \partial_t \rho + \nabla_{\mathbf{x}} \cdot \mathbf{m} &= 0, & \\ \partial_t m_i + \sum_{j=1}^{2} \partial_{x_j} (m_i v_j + p \delta_{ij}) &= \rho \frac{g_i}{Fr^2} & \quad i = 1, 2, \\ \partial_t \rho E + \nabla_{\mathbf{x}} \cdot (H \mathbf{m}) &= \frac{Q}{M^2} q. & \end{aligned} \tag{2.10}$$

The difference lies in the missing factor $M^{-2}$ in front of the pressure gradient and an additional factor $M^{-2}$ for the nondimensional $Q$. This is so, because in the usual nondimensionalization, $\hat{q}$ is nondimensionalized via $\frac{\hat{q}_{ref} \hat{x}_{ref}}{\hat{\rho}_{ref} \hat{v}_{ref}^3} = \frac{Q}{M^2}$. This also fits with the energy variables, which are of the order $\mathcal{O}(M^{-2})$ in this nondimensionalization, which has to be reflected in the source term. In short, using the vector of conservative variables $\mathbf{u} = (\rho, m_1, m_2, \rho E)^T$ and

$$\mathbf{f}_1(\mathbf{u}) = \begin{pmatrix} m_1 \\ m_1 v_1 + p \\ m_1 v_2 \\ \rho H v_1 \end{pmatrix}, \quad \mathbf{f}_2(\mathbf{u}) = \begin{pmatrix} m_2 \\ m_2 v_1 \\ m_2 v_2 + p \\ \rho H v_2 \end{pmatrix} \text{ and } \mathbf{g} = \begin{pmatrix} 0 \\ \rho g_1 / Fr^2 \\ \rho g_2 / Fr^2 \\ Qq / M^2 \end{pmatrix},$$

these equations can be written as

$$\mathbf{u}_t + \partial_{x_1} \mathbf{f}_1(\mathbf{u}) + \partial_{x_2} \mathbf{f}_2(\mathbf{u}) = \mathbf{g}(\mathbf{u}).$$

## 2.7 Asymptotic Analysis of the Euler Equations

We will now focus on the asymptotic behavior of the Euler equations without source terms in the low Mach number limit. Thus we look the equation system:

$$\begin{array}{rcll} \partial_t \widetilde{\rho} + & \nabla_{\mathbf{x}} \cdot \widetilde{\mathbf{m}} & = 0, & \\ \partial_t \widetilde{m}_i + & \sum_{j=1}^{2} \partial_{x_j} (\widetilde{m}_i \widetilde{v}_j + \frac{1}{M^2} \widetilde{p} \delta_{ij}) & = 0 \qquad i = 1, 2, & \\ \partial_t (\widetilde{\rho} \widetilde{E}) + & \nabla_{\mathbf{x}} \cdot (\widetilde{H} \widetilde{\mathbf{m}}) & = 0 & \end{array} \tag{2.11}$$

and

$$\widetilde{p} = (\gamma - 1)\, \widetilde{\rho} \left( \widetilde{E} - \frac{M^2}{2} |\widetilde{\mathbf{v}}|^2 \right). \tag{2.12}$$

Based on the characteristic number $M$ we are now able to investigate the behavior of the physical quantities in the low Mach number limit by means of a formal asymptotic analysis.

Throughout this paragraph we assume that the non-dimensional formulation of the governing equations (2.11) consists exclusively of physical quantities $\widetilde{\varphi}$ satisfying $\widetilde{\varphi} = \mathcal{O}(1)$ if the Mach number tends to zero. This is a prerequisite for a meaningful asymptotic analysis. Asymptotic expansions are defined via asymptotic sequences. These are sequences of functions satisfying $\phi_n(x) = o(\phi_{n-1}(x))$, as $x$ tends to a specific point $x_0$. We are interested in the behavior as the Mach number tends to zero. The specific asymptotic sequence we employ is $\phi_n(M) = M^n$, which obviously satisfies $\phi_n(M) = o(\phi_{n-1}(M)), M \to 0$. Note that some authors use the asymptotic sequence $\phi_n(M) = M^{2n}$, which leads to the same results. However, this will no longer be the case when applying this method to the discrete equations, therefore our choice of the asymptotic sequence. Having selected an asymptotic sequence we can define an asymptotic expansion. Multiple scales expansions could be used to include effects like sound. Klein [27] uses a multiple space scale and single time scale expansion, where Müller [46] employs single space scale and multiple time scale expansions. As sound is not relevant for our problem, we use a single time scale, single space scale asymptotic expansion, following Meister. For a comprehensive survey, consult [40]. There, also the following lemma can be found which justifies the next step:

**Lemma 1** *Let $\{\phi(\epsilon)\}_{n \in \mathbb{N}_0}$ be an asymptotic sequence and $L_n$, $n = 0, ..., N$, arbitrary terms which are independent of $\epsilon$. Then the statement*

$$\sum_{n=0}^{N} \phi_n(\epsilon) L_n = o(\phi_N(\epsilon)),\ \epsilon \to 0,$$

*holds if and only if $L_n = 0$, $n = 0, ..., N$.*

We now expand every physical variable in a single time scale, single space scale asymptotic expansion

$$\widetilde{\varphi}(\mathbf{x},t;M)=\sum_{m=0}^{j}M^m\widetilde{\varphi}^{(m)}(\mathbf{x},t)+o(M^j),\ M\to 0,\ j=0,1,2 \tag{2.13}$$

and introduce it into the system (2.11). In the resulting equations we can, due to the lemma, identify terms multiplied by the same order of the Mach number, as the functions $\widetilde{\varphi}^{(m)}(\mathbf{x},t)$ do not depend on $M$. Thus we immediately see from the momentum equations that $\nabla\widetilde{p}^{(0)}=0$ as well as $\nabla\widetilde{p}^{(1)}=0$ and we obtain the following theorem:

**Theorem 1** *Let $\widetilde{\mathbf{u}}$ be a solution of system* (2.11). *Then the leading order pressure satisfies*

$$\widetilde{p}(\mathbf{x},t;M)=\widetilde{p}^{(0)}(t)+M\widetilde{p}^{(1)}(t)+M^2\widetilde{p}^{(2)}(\mathbf{x},t)+o\left(M^2\right),\quad M\to 0.$$

Therefore, the pressure varies in space with $\mathcal{O}(M^2)$ if the Mach number is sufficiently small. This is an important result that the discrete scheme has to take into account and a point where the failure of conventional schemes can be shown. From the theorem it follows immediately that for low Mach numbers, $\nabla p=\nabla p^{(2)}$. If the Navier-Stokes or Euler equations are adjusted accordingly, they are sometimes called the *low Mach equations.* This is also sometimes exploited in numerical schemes which then use multiple pressure variables, namely the background pressure $\widetilde{p}^{(0)}(t)+M\widetilde{p}^{(1)}(t)$ and the second order pressure $M^2\widetilde{p}^{(2)}(\mathbf{x},t)$. Without proof, we present two further results of the asymptotic analysis.

**Theorem 2** *Let $\widetilde{\mathbf{u}}$ be a solution of system* (2.11). *Thus there holds*

$$\frac{1}{\gamma\widetilde{p}^{(0)}}\frac{d}{dt}\widetilde{p}^{(0)}=-\frac{1}{|\Omega|}\int_{\partial\Omega}\widetilde{\mathbf{v}}^{(0)}\cdot\mathbf{n}\,ds,\quad M\to 0.$$

Theorem 2 implies that the temporal change of the leading order pressure is only due to compression from the boundary or expansion of the gas itself.

**Theorem 3** *Let $\widetilde{\mathbf{v}}$ be a velocity vector corresponding to a solution of* (2.11). *Then it satisfies the divergence constraint*

$$\nabla_{\mathbf{x}}\cdot\widetilde{\mathbf{v}}=\frac{1}{|\Omega|}\int_{\partial\Omega}\widetilde{\mathbf{v}}\cdot\mathbf{n}\,ds+o(1),\quad M\to 0.$$

Note, that for a vanishing right hand side and a vanishing Mach number, we obtain the divergence constraint on the velocity field known from incompressible flow.

## 2.8 Boundary and Initial Conditions

Initially at time $\hat{t}_0$, we have to prescribe values for four variables, where it does not matter if we use the conservative variables or any other set, as long as they are linearly independent. We always use the primitive variables, as these can be measured quite easily, in contrast to e.g. the conservative variables. Further, if we restrict ourselves to a compact set $D \in \mathcal{U}$, we have to prescribe conditions for the solution on the boundary. This is necessary for numerical calculations and therefore, $D$ is also called the computational domain. The number of boundary conditions needed depends on the type of the boundary and can never exceed four, as we have four equations.

**Initial Conditions** At time $\hat{t} = \hat{t}_0$, we define a velocity $\hat{\mathbf{v}}_0$, a density $\hat{\rho}_0$ and a pressure $\hat{p}_0$. All other values like the energy and the momentum will be computed from these.

**Wall Conditions** At the wall we use no-slip conditions, thus the normal velocity should vanish: $\hat{v}_n = 0\frac{m}{s}$. For the Navier-Stokes equations, an additional condition could be to force the normal temperature gradient to be zero: $\partial \hat{T}_n = 0$, which corresponds to no heat conduction through the wall. The wall conditions can also be used to simulate vents or fans.

**Free Boundary** For the left boundary we use subsonic inflow conditions. This means that we have to specify three values, as we have one outgoing wave corresponding to the eigenvalue $u - c < 0$. We will use:

$$\hat{p} = \hat{p}_{in}, \qquad \hat{v}_n = \hat{v}_{in}, \qquad \hat{v}_t = 0\frac{m}{s}$$

with predefined values $\hat{p}_{in}$ and $\hat{v}_{in}$ and the tangential velocity $v_t$. At the right boundary, we have three outgoing waves and one incoming wave, which again corresponds to the eigenvalue $\hat{v}_n - \hat{c}$. Therefore we can prescribe only one value and we choose the pressure $\hat{p}_{out}$, for example to simulate different weather conditions at different ends of the tunnel:

$$\hat{p} = \hat{p}_{out}.$$

## 2.9 Hydrostatic Solutions

For the choice of the inital pressure and density, as well as for the boundary conditions, it is important to look at hydrostatic solutions, where pressure and density are in hydrostatic balance. This means that in horizontal direction, the gravitational force term is balanced out by the pressure gradient. In dimensional variables this can be written as:

$$\partial_{x_2}\hat{p} = \hat{\rho}\hat{g}_2 = \frac{\hat{p}}{\hat{R}\hat{T}}\hat{g}_2, \tag{2.14}$$

where $\hat{R} = \hat{c}_p - \hat{c}_V$ is the specific gas constant and $\hat{g}_2 = -9.81\frac{m}{s^2}$. For flows in hydrostatic equilibrium there is no horizontal movement if there are no other forces acting on the fluid. Thus, all movement is in $\hat{x}_1$-direction and the flows at different heights have no real interaction. In a neutrally stratified atmosphere, the temperature can be written as

$$\hat{T} = \hat{T}_r - \hat{\Gamma}(\hat{x}_2 - \hat{x}_{2_r}),$$

with a reference temperature $\hat{T}_r$ at the reference height $\hat{x}_{2_r}$ and the dry adiabatic lapse rate $\hat{\Gamma} = \hat{g}/\hat{c}_p$, see [55]. Inserting this expression into (2.14) leads to the differential equation

$$\partial_{x_2}\hat{p} = -\frac{\hat{p}\hat{g}}{\hat{R}\hat{T}_r\left(1 - \frac{\hat{\Gamma}(\hat{x}_2 - \hat{x}_{2_r})}{\hat{T}_r}\right)}.$$

This can be solved using separation of variables and integration from $\hat{x}_{2_r}$ to $\hat{x}_2$ to obtain:

$$-\ln\hat{p}(\hat{x}_2) + \ln\hat{p}(\hat{x}_{2_r}) = -\frac{\hat{g}}{\hat{R}\hat{T}_r}\frac{\hat{T}_r}{\hat{\Gamma}}\ln\left(1 - \frac{\hat{\Gamma}(\hat{x}_2 - \hat{x}_{2_r})}{\hat{T}_r}\right).$$

Defining $\hat{p}_r := \hat{p}(\hat{x}_{2_r})$, we can then write the solution as

$$\hat{p}(\hat{x}_2) = \hat{p}_r\left(1 - \frac{\hat{\Gamma}(\hat{x}_2 - \hat{x}_{2_r})}{\hat{T}_r}\right)^{\hat{c}_p/\hat{R}}. \tag{2.15}$$

The pressure thus decays polynomialy of order 3.5 with the height, however at a very small rate compared to the height of a tunnel. From (2.15) we can deduce also the density distribution as a function of height as

$$\hat{\rho}(\hat{x}_2) = \frac{\hat{p}_r}{\hat{R}\hat{T}_r}\left(1 - \frac{\hat{\Gamma}(\hat{x}_2 - \hat{x}_{2_r})}{\hat{T}_r}\right)^{\hat{c}_p/\hat{R}-1}. \tag{2.16}$$

# Chapter 3

# The Finite Volume Method

The equations we are trying to solve are so called conservation respectively balance laws. For these, finite volume methods are the most natural to use. Basis for those is the integral - and physically much more intuitive - form of the equations, which can be transformed to the differential form using Gauss' theorem. An obvious advantage of this formulation is that discontinuous solutions of some regularity are admissible. This is favourable for nonlinear hyperbolic equations, because shocks are a common feature of their solutions. We will present the implemented method only briefly and refer the interested reader for more information to the excellent textbooks [14, 22, 23, 33, 34]. Starting point for the methods derivation is the integral formulation:

$$\frac{d}{dt}\int_{\Omega} \mathbf{u}(\mathbf{x},t)\; d\mathbf{x} + \int_{\partial\Omega} \mathbf{f}(\mathbf{u}(\mathbf{x},t)) \cdot \mathbf{n}\; d\mathbf{s} = \int_{\Omega} \mathbf{g}(\mathbf{x},t,\mathbf{u}(\mathbf{x},t))\; d\mathbf{x}. \tag{3.1}$$

Here, $\Omega$ is the so called control volume or cell. It has the outer normal unit vector $\mathbf{n}$ and is required to have a Lipschitz continuous boundary. Note that there are otherwise no conditions on the cell and thus we can decompose the computational domain $D$ into a finite number of arbitrarily shaped and bounded control volumes, which is another advantage of finite volume schemes. As the geometry of the problems considered in this thesis is quite simple, we will use only quadrilateral cells and no hanging nodes.

We denote the $i$'th cell by $\Omega_i$ and its volume by $|\Omega_i|$. Edges will be called $e$ with the edge between $\Omega_i$ and $\Omega_j$ being $e_{ij}$ with length $|e_{ij}|$. We can therefore rewrite (3.1) for each cell as

$$\frac{d}{dt}\int_{\Omega_i} \mathbf{u}(\mathbf{x},t)\; d\mathbf{x} + \sum_{e_{ij}\subset\partial\Omega_i} \int_{e_{ij}} \mathbf{f}(\mathbf{u}(\mathbf{x},t)) \cdot \mathbf{n}\; d\mathbf{s} = \int_{\Omega_i} \mathbf{g}(\mathbf{x},t,\mathbf{u}(\mathbf{x},t))\; d\mathbf{x}. \tag{3.2}$$

The key step towards a numerical method is now to consider the mean value

$$\mathbf{u}_i(t) := \frac{1}{|\Omega_i|}\int_{\Omega_i} \mathbf{u}(\mathbf{x},t) d\mathbf{x}$$

of $\mathbf{u}(\mathbf{x}, t)$ in every cell $\Omega_i$ and to use this to approximate the solution in the cell. Under the condition that $\Omega_i$ does not change with time we obtain an evolution equation for the mean value in a cell:

$$\frac{d}{dt}\mathbf{u}_i(t) = -\frac{1}{|\Omega_i|}\sum_{e_{ij}\subset\partial\Omega_i}\int_{e_{ij}} \mathbf{f}(\mathbf{u}(\mathbf{x},t))\cdot\mathbf{n}\, ds + \frac{1}{|\Omega_i|}\int_{\Omega_i}\mathbf{g}(\mathbf{x},t,\mathbf{u}(\mathbf{x},t))\, d\mathbf{x}.$$

## 3.1 Time Integration Schemes

Assuming that we have a way to compute the spatial integrals in the above formula, we are faced with the task of solving ordinary differential equations (ODEs) or more precisely, initial value problems

$$\frac{d}{dt}u(t) = f(u(t)), \quad u(0) = u_0.$$

There is a huge variety of numerical methods for this, see for example the book [19]. Using the common abbreviation $u^n = u(t_n)$ and the generating function $\Phi$, they can be written as:

$$u^{n+1} = u^n + \Delta t\Phi, \quad t_{n+1} = t_n + \Delta t.$$

Two important properties by which to distinguish the different schemes are consistency and stability. Consistency is determined by the local error, defined as the difference between the exact solution of an ODE and the numerical solution obtained after one step if exact initial data is used. A method is called consistent of order $p$ if for any initial data function $u \in C^{p+1}$, the norm of the local error is $\mathcal{O}(h^p)$, where $h$ is the time step.

A method is called stable, if it is robust with respect to the initial data, which also means that rounding errors do not accumulate. This is connected to the Dahlquist test equation $\frac{d}{dt}u = \lambda u$ with $u(0) = u_0$. For a $\lambda$ with negative real part, the exact solution decays to zero. Consequently a method with a fixed step size $h$ is called unstable, if the numerical solution to this problem is unbounded. The set of all complex numbers $h\lambda$ for which this is not the case is called the stability region of the method. This stability region differs widely from method to method, see [20]. If the stability region contains the left complex half plane, the method is called A-stable.

A scheme is called implicit if it incorporates the unknown data at $t_{n+1}$, otherwise it is called explicit. Implicit schemes require solving an equation system in every step.

Several time integration schemes are implemented in the code, namely the improved Euler method, which is a second order explicit Runge-Kutta scheme, the implicit midpoint rule, which is a second order implicit Runge-Kutta scheme, and the so called $\Theta$-scheme

$$u^{n+1} = u^n + \Delta t((1-\Theta)f(u^{n+1}) + \Theta f(u^n)),\ \Theta \in [0,1].$$

This includes the explicit and the implicit Euler method, both of first order, as well as the Crank Nicholson scheme by setting $\Theta$ equal to 1, 0 or 1/2, respectively. The Crank-Nicholson scheme is outside the CFD community better known as the trapezoidal rule. The implicit midpoint rule is defined by

$$u^{n+1} = u^n + \Delta t f\left(\frac{u^n + u^{n+1}}{2}\right).$$

Regarding stability, the implicit midpoint rule and the Crank-Nicholson scheme have the same stability region. Together with the implicit Euler method they share the A-stability property.

## 3.2 Fractional Step Methods for Source Terms

The convective parts $\mathbf{f}$ and the source terms $\mathbf{g}$, like gravity and heat, will be treated seperately via *fractional step* or *operator splitting* methods. These allow an easy implementation, as they split the solution process in two parts, for both of which well known methods are available. Therefore, we prefer this approach to others which incorporate the source terms directly in the solver of the Euler equations, for example the well-balanced schemes of Greenberg and Leroux [17]. Given possibly vector valued functions $\mathbf{f}$ and $\mathbf{g}$ and a balance equation for $\mathbf{u}(\mathbf{x}, t)$ on the domain $D \in \mathbb{R}^d$ of the type

$$\partial_t \mathbf{u} + \nabla_{\mathbf{x}} \cdot \mathbf{f}(\mathbf{u}) = \mathbf{g}(\mathbf{u}),\ \mathbf{u}(\mathbf{x}, t_n) = \mathbf{u}^n(\mathbf{x}), \tag{3.3}$$

a first order approximation (for smooth solutions $\mathbf{u}$) to this problem is given by the simple Godunov splitting [15]:

1. Solve $\partial_t \mathbf{u} + \nabla_{\mathbf{x}} \cdot \mathbf{f}(\mathbf{u}) = \mathbf{0}$ with timestep $\Delta t$ and initial data $\mathbf{u}^n$ to obtain intermediate data $\mathbf{u}^*$.

2. Solve $\partial_t \mathbf{u} = \mathbf{g}(\mathbf{u})$ with the same timestep, but inital data $\mathbf{u}^*$ to obtain $\mathbf{u}^{n+1}$.

Here, we require each "solve" to be at least first order accurate. To increase the accuracy and obtain a scheme of second order for smooth solutions, we have to use a slightly more sophisticated method, for example the Strang splitting [59], where again the subproblem solvers have to be at least of first order:

1. Solve $\partial_t \mathbf{u} = \mathbf{g}(\mathbf{u})$ with timestep $\Delta t/2$.

2. Solve $\partial_t \mathbf{u} + \nabla_{\mathbf{x}} \cdot \mathbf{f}(\mathbf{u}) = 0$ with timestep $\Delta t$.

3. Solve $\partial_t \mathbf{u} = \mathbf{g}(\mathbf{u})$ with timestep $\Delta t/2$.

Again, in each step, the intermediate result obtained in the last step is used as inital data. The role of $\mathbf{g}$ and $\mathbf{f}$ can of course be exchanged, however in general they do not commute. This is quite obvious for the heat source, which is locally active. Increasing the heat first and then applying the convective flux leads to a different result compared to doing the convective step first and then increasing the heat locally. For this reason, special care has to be taken in chosing the numerical boundary conditions for the partial differential equation. Otherwise, unphysical effects can be introduced into the solution. As the solution of the equations for the sources is quite cheap and a step of the flow solver is quite expensive, we will apply the Strang splitting as defined above to save one flow solver step and do the same for the Godunov splitting for reasons of simplicity.

Tang and Teng [60] proved for multidimensional scalar balance laws that if the exact solution operator is used for both subproblems, the described schemes converge to the weak entropy solution and furthermore that the $L^1$ convergence rate of both fractional step methods is not worse than $1/2$. This convergence rate is actually optimal, if a monotone scheme is used for the homogenous conservation law in combination with the forward Euler method for the time integration. Langseth, Tveito and Winther [31] proved for scalar one dimensional balance laws that the $L^1$ convergence rate of the Godunov splitting (again using the exact solution operators) is linear and showed corresponding numerical examples, even for systems of equations. A better convergence rate than linear for nonsmooth solutions is not possible, as Crandall and Majda proved already in 1980 [7].

The $L^1$ error does not tell the whole story. Using the Strang or Godunov splitting combined with a higher order method in space and a second order time integration does improve the solution compared with first order schemes and is therefore appropriate for the computation of unsteady flows. This is for example suggested by LeVeque [34].

In our case, the application of a fractional step method thus requires solving the two equations

$$\frac{d}{dt}\mathbf{u}_i(t) + \frac{1}{|\Omega_i|}\sum_{e_{ij}\subset\partial\Omega_i}\int_{e_{ij}} \mathbf{f}(\mathbf{u}(\mathbf{x},t))\cdot\mathbf{n}\; d\mathbf{s} = \mathbf{0}, \tag{3.4}$$

namely the low Mach Euler equations (2.10) without the source terms and

$$\frac{d}{dt}\mathbf{u}_i(t) = \frac{1}{|\Omega_i|}\int_{\Omega_i} \mathbf{g}(\mathbf{x},t,\mathbf{u}(\mathbf{x},t))\; d\mathbf{x}, \tag{3.5}$$

which is an ordinary differential equation for heat and gravity. For the remainder of chapter four, we will explain and analyze the numerical method used to solve equation (3.4) in the context of low Mach number flows. The source terms will again be considered in chapter six.

## 3.3 The Line Integrals and Numerical Flux Functions

In the integral formulation of the Euler equations (3.4) which forms the basis for the finite volume scheme, line integrals of the flux along the edges appear. A numerical method thus

needs a mean to compute them. The line integral along an edge requires knowledge of the value of the flux there. On the edge though, the numerical solution is usually discontinuous, because it consists of the mean values in the cells. Therefore, a numerical flux function is required. This so called Riemann solver takes the states from the left and the righthand side of the edge and approximates the exact solution of a Riemann problem based on these states. In the code, several numerical flux functions are implemented, most importantly Van Leers flux vector splitting [66] and a two dimensional variant of the Lax-Friedrichs flux, which was proposed by Friedrich [11]. We will only explain these two, for information on the other schemes consult [23, 61] and the references therein. The Lax-Friedrichs flux as proposed by Friedrich is given by:

$$\mathbf{f}^{LF}(\mathbf{u}_L, \mathbf{u}_R; \mathbf{n}) = \frac{1}{2}(\mathbf{f}(\mathbf{u}_L) + \mathbf{f}(\mathbf{u}_R))\mathbf{n} - \breve{\mathbf{D}}(\mathbf{u}_L, \mathbf{u}_R; \mathbf{n}) \cdot (\mathbf{u}_R - \mathbf{u}_L)), \tag{3.6}$$

where we have a matrix valued dissipation term

$$\breve{\mathbf{D}}(\mathbf{u}_L, \mathbf{u}_R; \mathbf{n}) = \breve{\mathbf{R}}\left(\frac{\mathbf{u}_L + \mathbf{u}_R}{2}; \mathbf{n}\right) |\breve{\mathbf{\Lambda}}| \left(\mathbf{u}_L, \mathbf{u}_R; \mathbf{n}\right) \breve{\mathbf{R}}^{-1}\left(\frac{\mathbf{u}_L + \mathbf{u}_R}{2}; \mathbf{n}\right). \tag{3.7}$$

The dissipation matrix is denoted with an accent, because throughout most of the thesis, we will consider a modified dissipation matrix, that will be written as $\mathbf{D}$. In the definition of $\breve{\mathbf{D}}$, $\breve{\mathbf{R}}$ is the matrix of the conservative right eigenvectors:

$$\breve{\mathbf{R}}(\mathbf{u}; \mathbf{n}) = \begin{pmatrix} 1 & 0 & \frac{\rho}{2c} & \frac{\rho}{2c} \\ v_1 & \rho n_2 & \frac{\rho}{2c}(v_1 + cn_1) & \frac{\rho}{2c}(v_1 - cn_1) \\ v_2 & -\rho n_1 & \frac{\rho}{2c}(v_2 + cn_2) & \frac{\rho}{2c}(v_2 - cn_2) \\ \frac{|v|^2}{2} & \rho(v_1 n_2 - v_2 n_1) & \frac{\rho}{2c}(E + \frac{p}{\rho} + cv \cdot n) & \frac{\rho}{2c}(E + \frac{p}{\rho} - cv \cdot n) \end{pmatrix},$$

which has the inverse

$$\breve{\mathbf{R}}^{-1}(\mathbf{u}; \mathbf{n}) = \begin{pmatrix} 1 - \frac{\gamma-1}{2}M^2 & (\gamma-1)\frac{v_1}{c^2} & (\gamma-1)\frac{v_2}{c^2} & -\frac{\gamma-1}{c^2} \\ \frac{1}{\rho}(v_2 n_1 - v_1 n_2) & \frac{n_2}{\rho} & -\frac{n_1}{\rho} & 0 \\ \frac{c}{\rho}(\frac{\gamma-1}{2}M^2 - \frac{\mathbf{v}\cdot\mathbf{n}}{c}) & \frac{1}{\rho}(n_1 - (\gamma-1)\frac{v_1}{c}) & \frac{1}{\rho}(n_2 - (\gamma-1)\frac{v_2}{c}) & \frac{\gamma-1}{\rho c} \\ \frac{c}{\rho}(\frac{\gamma-1}{2}M^2 + \frac{\mathbf{v}\cdot\mathbf{n}}{c}) & -\frac{1}{\rho}(n_1 + (\gamma-1)\frac{v_1}{c}) & -\frac{1}{\rho}(n_2 + (\gamma-1)\frac{v_2}{c}) & \frac{\gamma-1}{\rho c} \end{pmatrix}$$

while $|\breve{\mathbf{\Lambda}}|$ is a diagonalmatrix consisting of absolute values of the eigenvalues of the jacobian of the flux. More precisely it is defined as

$$|\breve{\mathbf{\Lambda}}|(\mathbf{u}_L, \mathbf{u}_R; \mathbf{n}) := diag(\max|\mathbf{v}\cdot\mathbf{n}|, \max|\mathbf{v}\cdot\mathbf{n}|, \max|\mathbf{v}\cdot\mathbf{n} + c|, \max|\mathbf{v}\cdot\mathbf{n} - c|),$$

where the maximum is taken over the set $\{\mathbf{u}_L, \mathbf{u}_R, \frac{\mathbf{u}_L + \mathbf{u}_L}{2}\}$. Thus $\breve{\mathbf{D}}$ is obtained from the Jacobian $\mathbf{F}$ of the physical flux through diagonalization, taking the described maximum and then transforming back. We will denote this process via $\breve{\mathbf{D}} = |\mathbf{F}|$. A numerical flux function is called consistent if it reproduces the physical flux if $\mathbf{u}_L = \mathbf{u}_R$. Obviously we have:

$$\mathbf{f}^{LF}(\mathbf{u},\mathbf{u};\mathbf{n}) = \mathbf{f}(\mathbf{u})\cdot\mathbf{n}$$

and thus the Lax Friedrichs flux is consistent. We call a numerical flux function rotationally invariant if with

$$\mathbf{T}(\mathbf{n}) = \begin{pmatrix} 1 & & & \\ & n_1 & n_2 & \\ & -n_2 & n_1 & \\ & & & 1 \end{pmatrix},$$

we obtain

$$\mathbf{T}^{-1}(\mathbf{n})\mathbf{f}^{LF}(\mathbf{T}(\mathbf{n})\mathbf{u}_L, \mathbf{T}(\mathbf{n})\mathbf{u}_R; (1,0)^T) = \mathbf{f}^{LF}(\mathbf{u}_L, \mathbf{u}_R; \mathbf{n}).$$

A proof that the Lax Friedrichs flux indeed has this property can be found in appendix B. The physical Euler flux has this property, therefore it is reasonable to require this also of the numerical flux. We will make use of the rotational invariance in the code, as it allows us to assume that the input of the numerical flux function is aligned in normal direction.

The van Leer flux vector splitting is much simpler than the Lax-Friedrichs flux. It will be used only for the purpose of preconditioning the linear equation systems appearing when an implicit time integration scheme is applied, which will be explained later in this chapter. Justified by its rotational invariance, it is sufficient to define the van Leer flux vector splitting only for $\mathbf{n} = (1,0)^T$. The flux is given in the two dimensional case by the splitting

$$\mathbf{f}^{VL}(\mathbf{u}_L, \mathbf{u}_R; (1,0)^T) = \mathbf{f}^{+}(\mathbf{u}_L) + \mathbf{f}^{-}(\mathbf{u}_R). \tag{3.8}$$

The vectors $\mathbf{f}^{\pm}$ and their Jacobians are continuous functions of the Mach number $Ma = v_1/c$. They are defined, in a way that the Jacobians are positive, respectively negative semidefinit and thus we have a natural upwind scheme. The specific definitions of the split fluxes as given by van Leer are then obtained, using the physical flux $\mathbf{f}_1$, as

$$\mathbf{f}^{-} = \mathbf{f}_1 \text{ and } \mathbf{f}^{+} = \mathbf{0}, \quad \text{if } Ma \le -1,$$

$$\mathbf{f}^{\pm}(\mathbf{q}) = \pm\frac{\rho}{4c}(v_1 \pm c)^2 \begin{pmatrix} 1 \\ \frac{(\gamma-1)v_1 \pm 2c}{\gamma} \\ v_2 \\ \frac{((\gamma-1)v_1 \pm 2c)^2}{2(\gamma^2-1)} \end{pmatrix} \quad \text{if } -1 < Ma < 1,$$

and

$$\mathbf{f}^{-} = \mathbf{0} \text{ and } \mathbf{f}^{+} = \mathbf{f}_1, \quad \text{if } Ma \ge 1.$$

Employing any of the implemented Riemann solvers, we can now compute the line integrals by a quadrature formula. In this thesis we will only use the Lax-Friedrichs flux, respectively a variation if it, for this purpose. A gaussian quadrature rule with one Gauss point in the middle of the edge already achieves second order accuracy, which is sufficient for our purposes. Thus, the discretization in space is complete and we have obtained a semidiscrete form of the Euler equations, namely a finite dimensional nonlinear system of ordinary differential equations. This way of treating a partial differential equation is also called the method of lines approach. For each single cell, this differential equation can be written as:

$$\frac{d}{dt}\mathbf{u}_i(t) + \frac{1}{|\Omega_i|}\sum_{e_{ij}\subset\partial\Omega_i} |e_{ij}|\mathbf{T}^{-1}(\mathbf{n}_{ij})\mathbf{f}^{LF}(\mathbf{T}(\mathbf{n}_{ij})\mathbf{u}_i, \mathbf{T}(\mathbf{n}_{ij})\mathbf{u}_j; (1,0)^T) = \mathbf{0}, \tag{3.9}$$

where the input of the flux function are the states on the left hand, respectively right hand side of the edge. Combined with a suitable time integration method from section 4.1 and appropriate boundary conditions, this equation already represents a numerical scheme.

## 3.4 Boundary Conditions

The code used in this thesis was written by Ralf Massjung for his thesis, therefore the content of the following sections follows mostly [35].

If an edge is part of the boundary of the computational domain, the Riemann problem cannot be defined as before and we have to take a different approach to compute the flux on the edge. First, we have to distinguish between fixed wall boundaries and others. At a fixed wall, we use no-slip conditions as in section 3.8 for the continuous equations, thus we require the solution to have no velocity perpendicular to the boundary. Therefore, at the evalution point on the wall the condition $\mathbf{v}^T \cdot \mathbf{n} = 0$ has to hold.

Other boundaries are artificial ones where the computational domain ends, but not the physical one. The implementation is there always done using one layer of ghost cells. In these, we prescribe values in some way and can then compute a flux on the edge. Several types of boundary conditions are implemented and will be used depending on the problem to solve. For example, there are *constant interpolation boundary conditions* which means that we use von Neumann boundary conditions where we set the derivative on the edge to zero. Thus the same value is used in the ghost cells as in the neighbouring fluid cell. This leads to problems when significant tangential flows are present, thus the conditions employed when the gravitational source term is active are *far field boundary conditions.*

Depending on whether we are at an inlet or outlet boundary, we prescribe three, respectively one value in the ghost cell neighbouring the boundary and use for the remaining variables the values from the computational domain. This approach corresponds to the boundary conditions described in section 3.8. A third variant are *nonreflecting boundary conditions.*

### 3.4.1 Nonreflecting Boundary Conditions

An artificial boundary is an edge, where the computational domain ends, but nevertheless waves are allowed to enter or leave. Essentially, we want outgoing waves to leave the computational domain without any disturbances reflecting backwards. Boundary conditions with this property are called nonreflecting. This is simply achieved by setting all incoming waves to zero. First, we use a formulation of the Euler equations using tangential ($\tau$) and normal ($\mathbf{n}$) derivatives:

$$\partial_t \mathbf{u} + \partial_{\mathbf{n}} \mathbf{f}(\mathbf{u}) + \partial_\tau \mathbf{f}(\mathbf{u}) = \mathbf{0}.$$

We write the normal derivative in quasilinear form to obtain:

$$\partial_t \mathbf{u} + \mathbf{A}_{\mathbf{n}} \partial_{\mathbf{n}} \mathbf{u} + \partial_\tau \mathbf{f}(\mathbf{u}) = \mathbf{0}.$$

Then we replace the Jacobian $\mathbf{A}_{\mathbf{n}}$ by the matrix $\mathbf{A}_{\mathbf{n}}^+ = \mathbf{R}\mathbf{\Lambda}^+\mathbf{R}^{-1}$, which is obtained by diagonalizing $\mathbf{A}_{\mathbf{n}}$, setting all negative eigenvalues to zero and transforming back. The matrix $\mathbf{A}_{\mathbf{n}}^+$ is also known from the theoretical analysis of the van Leer flux vector splitting. Thus the velocity of incoming waves is zero:

$$\partial_t \mathbf{u} + \mathbf{A}_{\mathbf{n}}^+ \partial_{\mathbf{n}} \mathbf{u} + \partial_\tau \mathbf{f}(\mathbf{u}) = \mathbf{0}.$$

At an inlet edge between a ghost cell and an inner cell this equation is then discretized using first order upwinding. Note that the tangential component can be neglected in most applications. For the buoyancy driven flows that we have in mind, a correct implementation of the tangential part is mandatory and therefore we will not use these conditions when the gravitational source term is included in the problem.

## 3.5 Reconstruction and Limiter

Computing the solution using a piecewise constant approximation to $\mathbf{u}(\mathbf{x}, t)$ results in a method that can be at most of first order. To obtain higher order, we will use a reconstruction technique which uses a linear representation $\mathbf{u}_i(t)$ of $\mathbf{u}(\mathbf{x}, t)$ in each cell. As this leads to spurious oscillations near shocks, a limiter is used to reduce the spatial discretization to first order where necessary.

The reconstruction procedure is based on the primitive variables $\mathbf{q} = (\rho, v_1, v_2, p)^T$, as this is numerically more stable than using the conservative variables, see for example [39]. At a given time $t$, the linear representation of a primitive variable $q \in \{\rho, v_1, v_2, p\}$ in a cell $i$ with barycenter $(x_{1_i}, x_{2_i})$ is given by

$$q(x_1, x_2) = q_i + q_{x_1}(x_1 - x_{1_i}) + q_{x_2}(x_2 - x_{2_i}), \tag{3.10}$$

where $q_i$ is the mean value of $q$ in $\Omega_i$. The unknown scalars $q_{x_1}$ and $q_{x_2}$ represent the slopes and are obtained by solving a least square problem that is suitable for unstructured grids.

Let $C$ be the closed polygonal curve that connects the barycenters of the neighbouring cells and the piecewise linear function $q_c$, defined on $C$ by setting

$$q_c(x_{1_j}, x_{2_j}) = q_j$$

for all barycenters of neighbouring cells. The least squares problem, which has to be solved for all primitive variables, is then:

$$\text{Find } q_{x_1}, q_{x_2} \text{ such that } L(q_{x_1}, q_{x_2}) := \int_C (q(x_1, x_2) - q_c(x_1, x_2))^2 ds \text{ is minimized.}$$

Finally, we introduce the slope limiter $\phi$ which is a real number between zero and one and which is responsible for the switching between first and higher order spatial discretization:

$$q(x_1, x_2) = q_i + \phi q_{x_1}(x_1 - x_{1_i}) + \phi q_{x_2}(x_2 - x_{2_i}). \tag{3.11}$$

If the limiter function is zero, the discretization is reduced to first order, while it is of second order for a value of one. We use the limiter proposed by Venkatakrishnan [68], which has a favourable behavior on unstructured grids. It is defined as follows:

$$\overline{\Delta}_{ij} := q_{x_1}(x_{1_{ij}} - x_{1_i}) - q_{x_2}(x_{2_{ij}} - x_{2_i}), \text{with the edge center } (x_{1_{ij}}, x_{2_{ij}}),$$

$$\Delta_{ij} = q_j - q_i, \qquad \text{but if } \overline{\Delta}_{ij}\Delta_{ij} < 0, \text{then } \Delta_{ij} = 0$$

and $\epsilon = 10^{-6}$. The limiter function is then given by

$$\phi = \min_{e_{ij} \in \partial\Omega_i} \frac{(\Delta_{ij}^2 + \epsilon) + 2\Delta_{ij}\overline{\Delta}_{ij}}{\Delta_{ij}^2 + 2\overline{\Delta}_{ij}^2 + \Delta_{ij}\overline{\Delta}_{ij} + \epsilon}. \tag{3.12}$$

### 3.5.1 Modification at the Boundaries

At a fixed wall, the boundary condition requires the flux to satisfy $\mathbf{v}^T \cdot \mathbf{n} = 0$ in the evaluation point, thus the slopes have to satisfy the same condition. Therefore we have to modify the original velocity slopes $(v_1)_{x_1}, (v_1)_{x_2}, (v_2)_{x_1}$ and $(v_2)_{x_2}$. We first define the unit vector $\eta = (\eta_1, \eta_2)^T$ to be the one pointing from the cell barycenter to the evaluation point on the wall and the unit vector $\vartheta = (\vartheta_1, \vartheta_2)^T = (-\eta_2, \eta_1)^T$ to be perpendicular to $\eta$. To ease the following construction, we now restrict the set of possible slope modifications $(\bar{v_1})_{x_1}, (\bar{v_1})_{x_2}, (\bar{v_2})_{x_1}, (\bar{v_2})_{x_2}$ satisfying $\bar{\mathbf{v}}^T \cdot \mathbf{n} = 0$ to those with a constant $\vartheta$ derivative. Thus we only modify the derivatives $(v_1)_\eta$ and $(v_2)_\eta$. This does not define the new slopes uniquely, therefore we require the new slopes to deviate from the old slopes minimally in the euclidian norm. We obtain the least squares problem:

$$\min(((\bar{v_1})_\eta - (v_1)_\eta)^2 + ((\bar{v_2})_\eta - (v_2)_\eta)^2 | (\bar{v_1})_{x_1}, (\bar{v_1})_{x_2}, (\bar{v_2})_{x_1}, (\bar{v_2})_{x_2} : \bar{\mathbf{v}}^T \cdot \mathbf{n} = 0).$$

With $\Delta$ being the euclidian distance from the cell barycenter to the evaluation point on the edge, we can write the modified velocity on the evaluation point as $\bar{\mathbf{v}} = \mathbf{v}_i + \Delta((v_1)_\eta, (v_2)_\eta)^T$, where $\mathbf{v}_i$ is the mean velocity vector of the cell and we obtain:

$$\bar{\mathbf{v}}^T \cdot \mathbf{n} = (\mathbf{v}_i + \Delta((v_1)_\eta, (v_2)_\eta)^T)^T \cdot \mathbf{n} = 0$$

$$\Leftrightarrow (\bar{v}_1)_\eta n_1 + (\bar{v}_2)_\eta n_2 = -\mathbf{v}_i \cdot \mathbf{n}/\Delta.$$

Inserting this condition directly into the least squares functional allows us to solve the minimization problem to obtain the solution $(\bar{v}_1)^\star_\eta, (\bar{v}_2)^\star_\eta$. Then we can compute the modified slopes via

$$(\bar{v}_1)_{x_1} = \eta_1(\bar{v}_1)^\star_\eta - \eta_2(v_1)_\vartheta, \quad (\bar{v}_2)_{x_1} = \eta_1(\bar{v}_2)^\star_\eta - \eta_2(v_2)_\vartheta,$$

$$(\bar{v}_1)_{x_2} = \eta_2(\bar{v}_1)^\star_\eta + \eta_1(v_1)_\vartheta \text{ and } (\bar{v}_2)_{x_2} = \eta_2(\bar{v}_2)^\star_\eta + \eta_1(v_2)_\vartheta.$$

In the ghost cells at the inlet boundaries, the slopes and limiters are computed in the usual way. As the ghost cells are the definite border of the computational domain, no values beyond the ghost edges are interpolated or incorporated in any way.

## 3.6 Time Integration for the Euler Equations

After the discretization in space, we obtain a nonlinear system of ordinary differential equations and any of the methods mentioned in section 3.1 can be used to integrate this. We will now describe these methods, when applied to the Euler equations, in more detail. As the equations are hyperbolic, we know that for stability reasons, the timestep size for explicit schemes is bounded by the Courant-Friedrichs-Levy (CFL) condition

$$\Delta t = CFL \cdot \frac{\Delta x}{\max\limits_{k,|\mathbf{n}|=1} |\lambda_k(\mathbf{u}, \mathbf{n})|}, \tag{3.13}$$

with a CFL number smaller than one, for example 0.9. The $\lambda_k$ are the eigenvalues of the Jacobian of the physical flux. In more than one space dimension, it is not obvious which value to choose in a cell for $\Delta x$. We will use the diameter of the cell and approximate it via the following algorithm:

1. Given a cell $\Omega_i$, determine the minimal edge with respect to length. If there are hanging nodes, do not count the two edges as seperate.

2. Compute the modulus of the cosine of the angle between the minimal edge and the neighbouring edges.

3. Compute the length of the projection of the minimal edge onto the edge corresponding to the smaller angle (greater cosine).

Implicit schemes do not have to satisfy the CFL condition, although we will use the CFL number to describe the timestep size and to compare an implicit scheme with an explicit one.

### 3.6.1 Implicit schemes

The application of an implicit scheme leads to a nonlinear system of equations. For the $\Theta$-scheme we obtain in our case:

$$\Omega\,\underline{\mathbf{u}}^{n+1} = \Omega\,\underline{\mathbf{u}}^{n} + \Delta t((1-\Theta)\underline{\mathbf{f}}(\underline{\mathbf{u}}^{n+1}) + \Theta\underline{\mathbf{f}}(\underline{\mathbf{u}}^{n})),$$

where $\underline{\mathbf{u}}$ is the vector of the conservative variables from all cells. Correspondingly, $\underline{\mathbf{f}}(\underline{\mathbf{u}})$ denotes an evaluation of the numerical flux function on the whole grid. $\mathbf{\Omega}$ is the diagonal matrix of the volumes of the cells, corresponding to the variables in $\underline{\mathbf{u}}$. This equation is solved using an inexact Newton's method in primitive variables with the vector $\underline{\mathbf{q}}$, as then the derivatives are simplified significantly. Due to the inexactness, second order convergence is lost, but it is still superlinear. The starting value is $\underline{\mathbf{q}}^{n}$ and the linear system of equations which has to be solved in every step can be written as (see (3.9))

$$\mathbf{A}\Delta\underline{\mathbf{q}} = \left[\mathbf{\Omega}\frac{\partial\underline{\mathbf{u}}}{\partial\underline{\mathbf{q}}} + \Delta t(1-\Theta)\frac{\partial\underline{\mathbf{f}}(\underline{\mathbf{q}})}{\partial\underline{\mathbf{q}}}\right]_{\underline{\mathbf{q}}^{*}} \Delta\underline{\mathbf{q}} = \underline{\mathbf{rhs}}(\underline{\mathbf{q}}^{*}),$$

where $\underline{\mathbf{q}}^{*}$ is the current Newton iterate, updated in every step via $\underline{\mathbf{q}}^{*} = \underline{\mathbf{q}}^{*} + \Delta\underline{\mathbf{q}}$. For the implicit midpoint rule, we obtain the nonlinear equation system

$$\Omega\,\underline{\mathbf{u}}^{n+1} = \Omega\,\underline{\mathbf{u}}^{n} + \Delta t\underline{\mathbf{f}}\left(\frac{\underline{\mathbf{u}}^{n+1}+\underline{\mathbf{u}}^{n}}{2}\right)$$

and the corresponding Newton linearization

$$\mathbf{A}\Delta\underline{\mathbf{q}} = \left[\mathbf{\Omega}\frac{\partial\underline{\mathbf{u}}}{\partial\underline{\mathbf{q}}} + \frac{\Delta t}{2}\frac{\partial\underline{\mathbf{f}}(\frac{\underline{\mathbf{q}}+\underline{\mathbf{q}}^{n}}{2})}{\partial\underline{\mathbf{q}}}\right]_{\underline{\mathbf{q}}^{*}} \Delta\underline{\mathbf{q}} = \underline{\mathbf{rhs}}(\underline{\mathbf{q}}^{*}).$$

The matrix $\mathbf{A}$ has the property of being sparse, ill conditioned and unsymmetric (though it has a certain block symmetry). We can also deduce that the matrix is close to a block diagonal matrix for small time steps and that thus the linear equation systems become the harder to solve, the bigger the time step is. Appropriate methods to solve this kind of system are those preconditioned Krylov subspace methods [53, 65] that take into account the unsymmetric properties of the matrix, for example the GMRES method by Saad and Schultz or the BiCGSTAB algorithm of van der Vorst. In Krylov subspace methods, the

system matrix appears only in matrix vector products. Thus it is possible for our problem to formulate a matrixfree version, where the matrix vector products are replaced by a difference quotient via

$$\frac{\partial \underline{\mathbf{f}}(\bar{\underline{\mathbf{q}}})}{\partial \underline{\mathbf{q}}} \Delta \underline{\mathbf{q}} \approx \frac{\underline{\mathbf{f}}(\bar{\underline{\mathbf{q}}} + \epsilon \Delta \underline{\mathbf{q}}) - \underline{\mathbf{f}}(\bar{\underline{\mathbf{q}}})}{\epsilon}$$

and thus for the $\Theta$-scheme

$$\mathbf{A}(\underline{\mathbf{q}}^*)\Delta \underline{\mathbf{q}} \approx \mathbf{\Omega} \frac{\partial \underline{\mathbf{u}}^*}{\partial \underline{\mathbf{q}}} \Delta \underline{\mathbf{q}} + \Delta t (1 - \Theta) \left( \frac{\underline{\mathbf{f}}(\underline{\mathbf{q}}^* + \epsilon \Delta \underline{\mathbf{q}}) - \underline{\mathbf{f}}(\underline{\mathbf{q}}^*)}{\epsilon} \right),$$

respectively for the implicit midpoint rule:

$$\mathbf{A}(\underline{\mathbf{q}}^*)\Delta \underline{\mathbf{q}} \approx \mathbf{\Omega} \frac{\partial \underline{\mathbf{u}}^*}{\partial \underline{\mathbf{q}}} \Delta \underline{\mathbf{q}} + \frac{\Delta t}{2} \left( \frac{\underline{\mathbf{f}}(\frac{\underline{\mathbf{q}} + \underline{\mathbf{q}}^n}{2} + \epsilon \Delta \underline{\mathbf{q}}) - \underline{\mathbf{f}}(\frac{\underline{\mathbf{q}} + \underline{\mathbf{q}}^n}{2})}{\epsilon} \right).$$

If the parameter $\epsilon$ is chosen very small, the approximation becomes better, however, cancellation errors become a major problem. A simple choice for the parameter, that avoids cancellation but still is moderately small is given by Quin, Ludlow and Shaw [50] as

$$\epsilon = \frac{\sqrt{eps}}{\|\Delta \underline{\mathbf{u}}\|_2},$$

where *eps* is the machine accuracy. The matrixfree version has several advantages, the most important are low storage and ease of implementation: instead of computing the Jacobian by analytical formulas or difference quotients, we only need flux evaluations. For the flux preconditioning technique we intend to use for low Mach numbers, this simplifies the implementation significantly. See [29] for a survey on matrix-free Newton-Krylov methods with a lot of useful references.

There are several Krylov subspace methods that are suitable for the solution of unsymmetric linear equation systems. In this matrixfree context, the GMRES method was reported by McHugh and Knoll [38] to perform better than others in the context of the incompressible Navier-Stokes equations. We compared GMRES with BiCGSTAB and could confirm this observation, therefore we use the first as solver for the linear equation systems.

### The GMRES Algorithm

Now that we have made the decision for the solver of the linear equation systems $\mathbf{Ax} = \mathbf{b}$, we will explain the generalized minimal residual method (GMRES) [54] in detail. The scheme computes in the $j$-th iteration an orthogonal basis $\mathbf{v}_1, ..., \mathbf{v}_j$ of the $j$-th Krylov subspace

$$\mathcal{K}_j = span\{\mathbf{r}_0, ..., \mathbf{A}^{j-1}\mathbf{r}_0\}$$

by the so called Arnoldi method. GMRES uses this basis to minimize the functional

$$J(\mathbf{x}) = \|\mathbf{A}\mathbf{x} - \mathbf{b}\|_2$$

in the space $\mathbf{x}_0 + \mathcal{K}_j$. The point about Arnoldi's method is that it allows an efficient implementation using a Hessenberg matrix. This has to be updated in every step, which is in our case done with Givens-rotations. Another advantage of this representation is, that the value of the functional $J$ in every step can be obtained by the algorithm without explicit computation of $\mathbf{x}_j$, which can wait until the tolerance is satisfied.

Due to the minimization, GMRES computes the exact solution to an $n \times n$ linear equation system in at most $n$ steps. Furthermore, the residual in the 2-Norm is nonincreasing in every step. From a theorem by Greenbaum, Pták and Strakoš [16] we know that this is also the best global result, as for any convergence history, a matrix can be constructed to which the GMRES algorithm produces this convergence history, in particular is might be possible that the residual is constant until the very last step when it drops to zero. Nevertheless, the method is suitable as an iterative solver. By contrast to for example the CG method, GMRES has no short recurrence and the whole basis has to be stored. Thus the cost and storage per step increases linearly with the iteration number.

However, it is possible to restart the iteration by scrapping the orthogonal basis and starting new with the current approximation. Unfortunately , there are examples where the restart technique does not lead to convergence and examples, where the restart convergence results in a speedup. We compared a restart length of 40 with computations without restart and could not observe a significant difference between the two. In Pseudocode, the algorithm can be formulated as (taken from [41]):

Given $\mathbf{x}_0 \in \mathbb{R}^n$, compute $\mathbf{r}_0 = \mathbf{b}_0 - \mathbf{A}\mathbf{x}_0$.
If $\mathbf{r}_0 = \mathbf{0}$, then END.
$\mathbf{v}_1 = \frac{\mathbf{r}_0}{\|\mathbf{r}_0\|_2}$.
For $j = 1, ..., n$
  For $i = 1, ..., j$ do $h_{ij} = \mathbf{v}_i^T \mathbf{A}\mathbf{v}_j$.
  $\mathbf{w}_j = \mathbf{A}\mathbf{v}_j - \sum_{i=1}^{j} h_{ij}\mathbf{v}_i, \quad h_{j+1,j} = \|\mathbf{w}_j\|_2$.
  For $i = 1, ..., j-1$ do $\begin{pmatrix} h_{ij} \\ h_{i+1,j} \end{pmatrix} = \begin{pmatrix} c_{i+1} & s_{i+1} \\ s_{i+1} & -c_{i+1} \end{pmatrix} \begin{pmatrix} h_{ij} \\ h_{i+1,j} \end{pmatrix}$.
  $\beta = \sqrt{h_{jj}^2 + h_{j+1,j}^2}; \quad s_{j+1} = \frac{h_{j+1,j}}{\beta}$.
  $c_{j+1} = \frac{h_{jj}}{\beta}; \quad h_{jj} = \beta$.
  $\gamma_{j+1} = s_{j+1}\gamma_j; \quad \gamma_j = c_{j+1}\gamma_j$.
  if $\gamma_{j+1} \neq 0$, $\mathbf{v}_{j+1} = \frac{\mathbf{w}_j}{h_{j+1,j}}$.
  else
    for $i = j, ..., 1$ do $\alpha_i = \frac{1}{h_{jj}} \left( \gamma_j - \sum_{k=i+1}^{j} h_{ik}\alpha_k \right)$.
    $\mathbf{x} = \mathbf{x}_0 + \sum_{i=1}^{j} \alpha_i \mathbf{v}_i$.
    END.

### Preconditioning GMRES

More important than the specific Krylov subspace method is the right choice of the preconditioner. As the speed of convergence of Krylov subspace methods depends strongly on the matrix, preconditioners are used to transform the linear equation system to speed up convergence:

$$\mathbf{P}_L\mathbf{A}\mathbf{P}_R\mathbf{x}^P = \mathbf{P}_L\mathbf{b}, \quad \mathbf{x} = \mathbf{P}_R\mathbf{x}^P.$$

Here, $\mathbf{P}_L$ and $\mathbf{P}_R$ are invertible matrices, called a left respectively right preconditioner that approximate the system matrix in a cheap way. From experience, right preconditioning seems to be the better choice in the context of compressible flows. Therefore, we will always employ right preconditioning.

This can be very easily done in Krylov subspace methods. Concerning GMRES, every time a matrix vector product $\mathbf{Av_j}$ appears in the original algorithm, the right preconditioned GMRES method is obtained by applying the preconditioner to the vector in advance and then computing the matrixfree product. Usually, the preconditioner is not given directly, but implicitly via its inverse. Then the application of the preconditioner corresponds to the solution of a linear equation system. Note that right preconditioning does not change the initial residual, because

$$\mathbf{r}_0 = \mathbf{b}_0 - \mathbf{A}\mathbf{x}_0 = \mathbf{b}_0 - \mathbf{A}\mathbf{P}_R\mathbf{x}_0^P,$$

therefore the computation of the initial residual can be done without the right preconditioner. On the other hand, when the tolerance criterion is fulfilled, the right preconditioner has to be applied one last time to change back from the preconditioned approximation to the unpreconditioned. For nonnormal matrices as we have here, the crucial properties that determine the speed of convergence are the pseudospectra that were introduced by Trefethen [62]. Unfortunately, for the matrix dimensions considered here, these cannot be computed in reasonable time. Furthermore, there exist only a few analytical results about the matrices appearing in compressible flow. Therefore, the preconditioner has to be chosen by numerical experiments and heuristics. An overview of preconditioners with special emphasis on application in flow problems can be found in the book by Meister [41] and the study in the context of compressible flow by Meister and Vömel [45].

In our case, the matrix free method somewhat reduces the possible choices, because we want a preconditioner that does not work on the whole matrix but only on blocks at a time. Otherwise, we would have to compute and store the matrix, which is in opposition to the idea of matrix free methods. A suitable choice are for example splitting methods. One such method is the symmetric block Gauss-Seidel-method (SGS), which is a very good preconditioner for compressible flow problems. SGS can be written in short using the block decomposition

$$\mathbf{A} = \mathbf{L} + \mathbf{D} + \mathbf{R},$$

where $\mathbf{L}$ is the strict lower left part of $\mathbf{A}$, $\mathbf{D}$ the diagonal and $\mathbf{R}$ the strict upper right part. Then one application of SGS as a right preconditioner corresponds to solving the equation system

$$(\mathbf{D}+\mathbf{L})\mathbf{D}^{-1}(\mathbf{D}+\mathbf{R})\mathbf{x} = \mathbf{x}^P.$$

For the purpose of preconditioning, one iteration is completely sufficient. The $4 \times 4$-blocks of $\mathbf{L}$ and $\mathbf{R}$ can be computed when required one at a time, so it is not necessary to store the complete matrix. Only the diagonal blocks which appear several times are computed in advance and stored. A common technique to improve the efficiency of a splitting related preconditioner is relaxation, which corresponds for SGS to:

$$\frac{1}{\omega(2-\omega)}(\mathbf{D}+\omega\mathbf{L})\mathbf{D}^{-1}(\mathbf{D}+\omega\mathbf{R})\mathbf{x} = \mathbf{x}^P.$$

In our case, numerical experiments indicate that using $\omega = 1.4$ is a good choice. However, the increase in performance is only marginal. Another simple choice for a splitting method would be Jacobi-preconditioning, corresponding to $\mathbf{P}_R = \mathbf{D}^{-1}$, where we need only the diagonal blocks, thus reducing the cost of applying the preconditioner. However this does not pay, as it turns out that Jacobi is not a good preconditioner for our linear systems.

Another important class of preconditioners for our purposes are block incomplete LU (ILU) decompositions, where the blocks correspond to the $4 \times 4$ units the Jacobian consists of. The computation of a complete LU decomposition is quite expensive and in general needs also for sparse matrices full storage. By prescribing a sparsity pattern, incomplete LU decompositions can be defined. The application of such a decomposition as a preconditioner then corresponds to solving by forward-backward substition the appropriate linear equation system. The sparsity pattern can for example be influenced by the level of fill. This is in short a measure for how much beyond the original sparsity pattern is allowed for the purpose of ILU. Those decompositions with higher levels of fill are very good black box preconditioners for flow problems, see for example the study [1]. However they are also not in line with the philosophy of matrix-free methods. Thus remains ILU(0), which has no additional level of fill beyond the sparsity pattern of the original matrix $\mathbf{A}$. Again, for our cases this was not as good a preconditioner as SGS.

The other question besides which specific preconditioner to use is, on which discretization we base the computation of the blocks. For reasons of stability it is prudent to use a first order discretization, even if the spatial discretization is of higher order. Furthermore, we do not necessarily have to use the same flux, but can chose another one. In [35], the van Leer flux-vector splitting is used for the preconditioner, as then the blocks can be computed quite efficiently. By contrast, the Jacobian of the Lax-Friedrichs flux is extremely complicated and expensive to compute. Using the abbreviations,

$$\lambda^{\pm} = v_n \pm c, \quad f^{\pm} = \pm\rho(\lambda^{\pm})^2/(4c) \text{ and } C^{\pm} = ((\gamma-1)v_n \pm 2c)/\gamma$$

the blocks for the van Leer flux vector (3.8) splitting are obtained via computing the derivative of the identity

$$\mathbf{f}^{\pm}(\mathbf{q};\mathbf{n}) = f^{\pm}\begin{pmatrix} 1 \\ C^{\pm} \\ v_t \\ \frac{\gamma^2}{2(\gamma^2-1)}(C^{\pm})^2 \end{pmatrix},$$

which is valid for $|Ma| < 1$. The derivatives are then given by the relations

$$\frac{\partial f^{\pm}}{\partial \mathbf{q}} = \left(\frac{\lambda^{\pm}}{8}(1 \pm 3Ma), \frac{\rho n_1}{2}(1 \pm Ma), \frac{\rho n_2}{2}(1 \pm Ma), \frac{\rho\lambda^{\pm}}{8p}(1 \mp Ma)\right)$$

and

$$\frac{C^{\pm}}{\partial \mathbf{q}} = \left(\mp\frac{c}{\gamma\rho}, \frac{\gamma-1}{\gamma}n_1, \frac{\gamma-1}{\gamma}n_2, \pm\frac{c}{\gamma p}\right).$$

The finite volume scheme employed in this thesis is now completely outlined and we will proceed to analyse some of its properties in the low Mach number regime. The tool for this is, as in the second chapter for the continuous equations, an asymptotic analysis.

## 3.7 Discrete Asymptotic Analysis

It was proved by Meister in [42, 43] by a discrete asymptotic analysis, that the use of a standard numerical flux function leads to an unphysical pressure distribution which contradicts the statement of theorem 1. There, a single time scale, single space scale asymptotic analysis is applied to the semidiscrete equations (3.9) with a first order discretization in space, by writing every variable in every cell in the following asymptotic expansion:

$$\phi_i = \phi_i^{(0)} + M\phi_i^{(1)} + M^2\phi_i^{(2)} + o\left(M^2\right), \quad M \to 0. \tag{3.14}$$

The expansion depends on the choice of the Riemann solver and thus the analysis has to be done for each numerical flux function separately. The following theorem summarizes the result for the Lax-Friedrichs scheme, the AUSMDV and the Roe scheme.

**Theorem 4** *Let the pressure on the boundary be given by*

$$p(\mathbf{x},t) = konst + M^2 p^{(2)}(\mathbf{x},t) \;\; \forall(\mathbf{x},t) \in \partial D \times \mathbb{R}_0^+.$$

*Then the discrete leading order pressure field satisfies*

$$p_i^{(0)} = p_j^{(0)} \;\; \forall i,j.$$

*Furthermore, on a cartesian grid, given $i, j$, there exists a density and velocity distribution such that for the discrete pressure we have $p_i^{(1)} \neq p_j^{(1)}$. In particular, variations of the first order pressure field are generated on the space scale* $\mathbf{x}$.

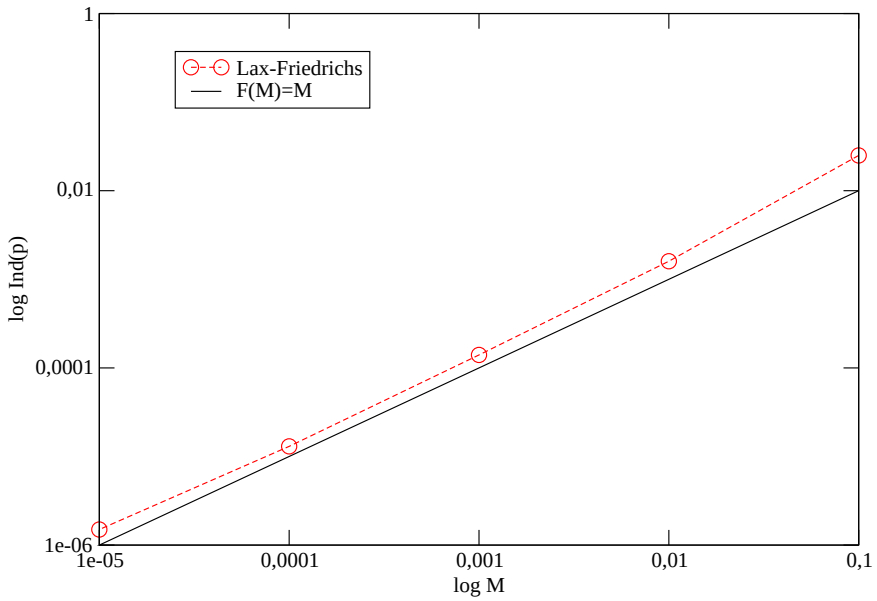


Figure 3.1: Pressure indicator for the unpreconditioned flux

We are not aware of rigorous proofs for other Riemann solvers, but there are numerical results for other flux functions, for example the Osher-Solomon-flux. The theorem is not completely satisfying in the sense that it gives no criteria to tell for a given problem wether the solver produces the correct pressure distribution or generates variations in the first order pressure field. For example, a parallel flow through a channel with a constant pressure field is computed exactly by all Riemann solvers. However, already for slightly more complicated standard test cases, numerical results confirm that the spatial variation in the first order pressure field is not zero.

To show this, we use a NACA0012 profile at zero angle of attack at varying Mach numbers with a fixed grid. In the figure 3.1, the pressure indicator $p_{ind} = \frac{p_{max} - p_{min}}{p_{max}}$ is plotted against the Mach number, for the standard Lax-Friedrichs Flux with nonreflecting boundary conditions. We can clearly see an $\mathcal{O}(M)$ dependence of the indicator on the Mach number, when the results from the continuous analysis would require an $\mathcal{O}(M^2)$ behavior. Figure 3.2 shows the pressure isolines for $Ma = 0.001$. The solution is clearly of a bad quality. Thus, we cannot hope to compute the correct pressure field for nontrivial

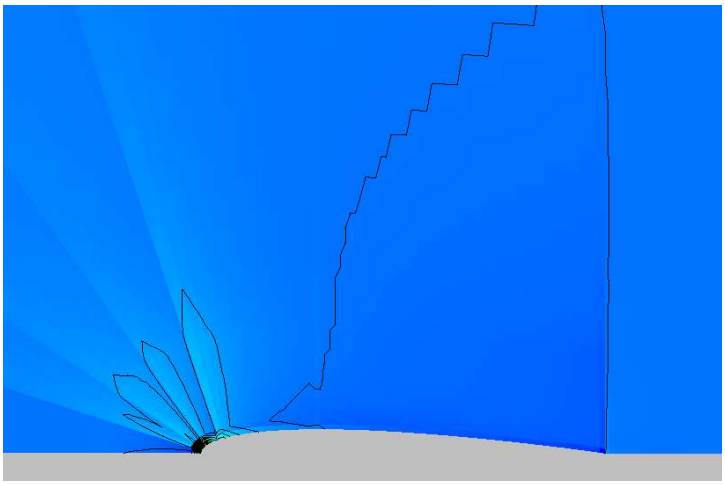

Figure 3.2: Pressure isolines for the NACA0012 profile for the unpreconditioned Flux

flows. Note that, as the method is consistent, we could still compute the correct solution by refining the mesh with decreasing Mach number. However, this is clearly not a desirable strategy, which is why we look for a method that computes the correct pressure distribution on the same grid, as for high Mach numbers.

# Chapter 4

# The Preconditioned Method

To extend the validity of the numerical method into the low Mach number regime, we utilize a preconditioning technique originally proposed by Guillard and Viozat [18] for the Roe scheme and later on derived in the context of the Lax-Friedrichs flux (3.6) by Meister in [43]. It is motivated from an idea by Turkel, where the time derivative of the partial differential equation in entropy variables is multiplied by a preconditioning matrix $\mathbf{P}$, which mainly modifies the pressure equation:

$$\mathbf{P}^{-1}\partial_t \mathbf{q} = \partial_{x_1}\mathbf{g}_1(\mathbf{q}) + \partial_{x_2}\mathbf{g}_2(\mathbf{q}).$$

The time consistency of this equation is of course destroyed, which is why Turkel suggests using the dual time stepping scheme of Jameson. Our method does not use dual time stepping, therefore we have to take a different approach to extend its validity in the low Mach regime. A time consistent scheme is motivated via the following equation:

$$\partial_t \mathbf{q} = \mathbf{P}^{-1}\mathbf{P}\partial_{x_1}\mathbf{g}_1(\mathbf{q}) + \mathbf{P}^{-1}\mathbf{P}\partial_{x_2}\mathbf{g}_2(\mathbf{q}).$$

A discretization of this equation suggests using a flux function where only the dissipation matrix is changed from $\breve{\mathbf{D}} = |\mathbf{F}|$ to $\mathbf{D} = \mathbf{P}^{-1}|\mathbf{P}\mathbf{F}|$. More precise, we use the so called low Mach preconditioned Lax-Friedrichs flux

$$\mathbf{f}^{LFP}(\mathbf{u}_L, \mathbf{u}_R; \mathbf{n}) = \frac{1}{2}(\mathbf{f}(\mathbf{u}_L) + \mathbf{f}(\mathbf{u}_R))\mathbf{n} - \mathbf{D}(\mathbf{u}_L, \mathbf{u}_R; \mathbf{n}) \cdot (\mathbf{u}_R - \mathbf{u}_L)), \tag{4.1}$$

with the new dissipation matrix

$$\mathbf{D}(\mathbf{u}_i, \mathbf{u}_j, \mathbf{n}) \;=\; \mathbf{P}^{-1}\left(\frac{\mathbf{u}_j + \mathbf{u}_i}{2}\right)\mathbf{R}\left(\frac{\mathbf{u}_j + \mathbf{u}_i}{2}, \mathbf{n}\right)|\mathbf{\Lambda}|(\mathbf{u}_i, \mathbf{u}_j, \mathbf{n})\mathbf{R}^{-1}\left(\frac{\mathbf{u}_j + \mathbf{u}_i}{2}, \mathbf{n}\right). \tag{4.2}$$

Herein, $\mathbf{R}(\mathbf{u}, \mathbf{n})$ represents the matrix of the right eigenvectors of the corresponding preconditioned Jacobian

$$\mathbf{F}^P(\mathbf{u}, \mathbf{n}) = \mathbf{P}(\mathbf{u})\mathbf{F}(\mathbf{u}, \mathbf{n})$$

and $|\mathbf{\Lambda}|(\mathbf{u}_i, \mathbf{u}_j, \mathbf{n})$ denotes the diagonal matrix defined by

$$|\mathbf{\Lambda}|(\mathbf{u}_i, \mathbf{u}_j, \mathbf{n}) = \operatorname{diag}\left\{ \max_{\mathbf{u}\in\left\{\mathbf{u}_i, \mathbf{u}_j, \frac{\mathbf{u}_i+\mathbf{u}_j}{2}\right\}} |\lambda_1(\mathbf{u}, \mathbf{n})|, \ldots, \max_{\mathbf{u}\in\left\{\mathbf{u}_i, \mathbf{u}_j, \frac{\mathbf{u}_i+\mathbf{u}_j}{2}\right\}} |\lambda_4(\mathbf{u}, \mathbf{n})| \right\},$$

where $\lambda_i(\mathbf{u}, \mathbf{n})$, $i = 1, \ldots, 4$ are chosen to be the eigenvalues of the matrix $\mathbf{F}^P(\mathbf{u}, \mathbf{n})$. This approach of modifying the flux function only has obvious advantages in the context of the matrix-free solution algorithm chosen, as we do not have to recompute and reimplement the flux Jacobian.

The properties of the derived method strongly depend on the preconditioning matrix used. Obviously, arranging $\mathbf{P}(\mathbf{u}, \mathbf{n})$ to be the identity yields the Lax-Friedrichs-type scheme including a matrix-valued local dissipation term proposed by Friedrich [10]. In order to overcome the failure of the standard Lax-Friedrichs scheme with respect to the pressure distribution in the low Mach number regime it is quite natural to multiply the pressure by a factor associated with the Mach number. Therefore, we extract the pressure by consideration of the so-called entropy variables $\mathbf{w} = (p, v_1, v_2, s)^T$, whereby $s$ denotes the entropy determined as $s = \ln \frac{p}{\rho^\gamma}$. Following Turkel [63] we introduce

$$\mathbf{P}(\mathbf{u}) = (\mathbf{UQW})(\mathbf{u}), \tag{4.3}$$

where $\mathbf{U} = \frac{\partial \mathbf{u}}{\partial \mathbf{w}}$, $\mathbf{W} = \frac{\partial \mathbf{w}}{\partial \mathbf{u}}$ and

$$\mathbf{Q} = \begin{pmatrix} \beta^\nu & 0 & 0 & 0 \\ -\frac{\alpha v_1}{\rho c^2} & 1 & 0 & 0 \\ -\frac{\alpha v_2}{\rho c^2} & 0 & 1 & 0 \\ 0 & 0 & 0 & 1 \end{pmatrix}, \text{ with } \beta = \mathcal{O}_S(M),\ M \to 0, \tag{4.4}$$

$\alpha \in \mathbb{C}$ and $\nu \in [0, 2]$. The expression $u = \mathcal{O}_S(v)$ is used to indicate that $u = \mathcal{O}_S(v)$ and $v = \mathcal{O}_S(u)$, see [25]. It is necessary to point this out, as a $\beta$ tending to zero of a higher order than $M^2$ would not achieve the desired result. To ensure that the matrix is always nonsingular we additionally require that $\beta \neq 0$ for all $M > 0$. Simple but time-consuming calculations give

$$\begin{aligned} \mathbf{P}(\mathbf{u}) \;=\; & \mathbf{I} + \frac{\gamma - 1}{c^2} \left\{ (\beta^\nu - 1) \begin{pmatrix} \frac{|v|^2}{2} & -v_1 & -v_2 & 1 \\ \frac{|v|^2 v_1}{2} & -v_1^2 & -v_1 v_2 & v_1 \\ \frac{|v|^2 v_2}{2} & -v_1 v_2 & -v_2^2 & v_2 \\ \frac{|v|^2 H}{2} & -H v_1 & -H v_2 & H \end{pmatrix} \right. \\ & \left. -\alpha \begin{pmatrix} 0 & 0 & 0 & 0 \\ \frac{|v|^2 v_1}{2} & -v_1^2 & -v_1 v_2 & v_1 \\ \frac{|v|^2 v_2}{2} & -v_1 v_2 & -v_2^2 & v_2 \\ \frac{|v|^4}{2} & -v_1 |v|^2 & -v_2 |v|^2 & |v|^2 \end{pmatrix} \right\} \end{aligned}$$

and

$$\lambda_{1,2}(\mathbf{u},\mathbf{n}) = v_{\mathbf{n}} := \mathbf{v}\cdot\mathbf{n}, \tag{4.5}$$

$$\lambda_{3,4}(\mathbf{u},\mathbf{n}) = \frac{1}{2}\left[(1-\alpha+\beta^{\nu})v_{\mathbf{n}} \pm \sqrt{(1-\alpha+\beta^{\nu})^2 v_{\mathbf{n}}^2 - 4v_{\mathbf{n}}^2\beta^{\nu} + 4\beta^{\nu}c^2}\right]. \tag{4.6}$$

Note that the choice $\alpha = 0$ and $\nu = 2$ yields the preconditioning matrix proposed by Guillard and Viozat [18]. The unpreconditioned method is recovered by chosing $\alpha = 0$ and $\nu = 0$. The specific entries of the vector $\mathbf{D}\Delta\mathbf{u}$ will be needed in the following proofs. They can be found, together with a description of the implementation of this product in the appendix C.

It was recently proven by Meister in [42] that utilizing the preconditioned Lax-Friedrichs flux (3.6) for the choice $\beta = \mathcal{O}(M)$, $M \to 0$, and $\alpha = 0$ within the finite volume method associated with (4.22) yields a pressure distribution satisfying the statement of theorem 1 in a discrete sense. Furthermore, a discrete divergence constraint corresponding to theorem 3 is shown for this scheme by Meister in [44] in the absence of compression and expansion over the boundary of the computational domain.

This theorem can be confirmed by numerical resuls. We use again a NACA0012 profile at zero angle of attack at varying Mach numbers with a fixed grid. The pressure indicator $p_{ind} = \frac{p_{max}-p_{min}}{p_{max}}$ is plotted in figure 4.1 against the Mach number, for the preconditioned Lax-Friedrichs Flux with nonreflecting boundary conditions. We can clearly see a $\mathcal{O}(M^2)$ dependence of the indicator on the Mach number, as predicted by the analysis. Figure 4.2 shows the pressure isolines for $Ma = 0.001$, which are as expected and much better than in figure 3.2. Thus, the preconditioned method is able to compute flows at all Mach numbers without the need to refine the mesh width as the Mach number tends to zero.

At this point we would like to mention that some authors suggest using two pressure variables, namely one for the background pressure, which only depends on time and another for the rest. This is mainly done to diminish cancellation errors which can occur as shown by Sesterhenn [57]. However, if using double precision variables, these errors appear only for extremely small Mach number which is not the case for our problems and thus we do not employ a pressure splitting.

Further results about the preconditioned scheme were so far missing. For the remainder of the chapter we will analyze properties of the preconditioned flux function to obtain more insight in the proper choice of parameters or what is to be regarded when applying this method.

## 4.1 Uniqueness of the Approach

One question is, whether another preconditioning Matrix $\mathbf{P}$ results in a physically correct asymptotic behavior. The parameter $\alpha$ does not influence the asymptotic behavior of the pressure, therefore we set it to zero for this paragraph. The following theorems then show that $\nu = 2$ is indeed the only possible choice, because when smaller values are used, there will be pressure variations of the order $\mathcal{O}(M^{1+\frac{\nu}{2}})$.

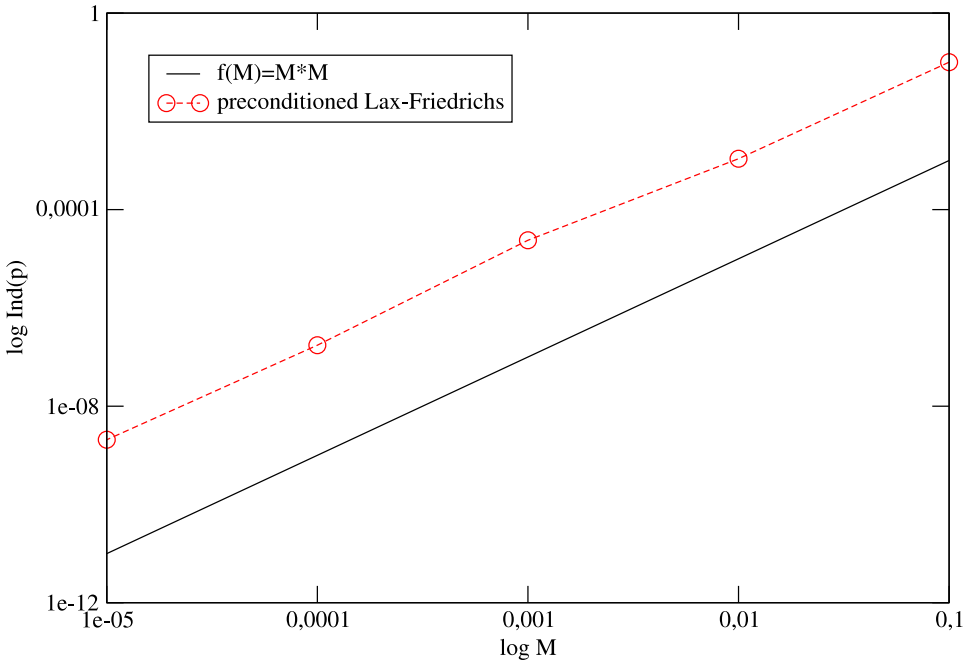


Figure 4.1: Pressure indicator for the preconditioned flux

**Theorem 5** *Let the preconditioner be given by*

$$\mathbf{P}^{-1} = \begin{pmatrix} \beta^{\nu} & & & \\ & 1 & & \\ & & 1 & \\ & & & 1 \end{pmatrix}, \ \nu \in (0,2], \ \beta = \mathcal{O}_S(M).$$

*Then the discrete leading and first order pressure of the preconditioned Lax-Friedrichs-flux satisfy*

$$p_i^{(0)} = p_j^{(0)} \text{ and } p_i^{(1)} = p_j^{(1)} \ \forall i, j.$$

*Proof:* The core idea of the proof is to perform a discrete asymptotic analysis of the mass flux and plug this into the finite volume scheme. Throughout this proof, all Landau symbols are defined for $M \to 0$. We consider the preconditioned Lax-Friedrichs flux (4.1):

$$\mathbf{f}^{LFP}(\mathbf{u}_L, \mathbf{u}_R, \mathbf{n}) = \frac{1}{2}\left(\mathbf{f}(\mathbf{u}_L; \mathbf{n}) + \mathbf{f}(\mathbf{u}_R; \mathbf{n}) - \mathbf{D}\left(\mathbf{u}_L, \mathbf{u}_R; \mathbf{n}\right)\left(\mathbf{u}_R - \mathbf{u}_L\right)\right).$$

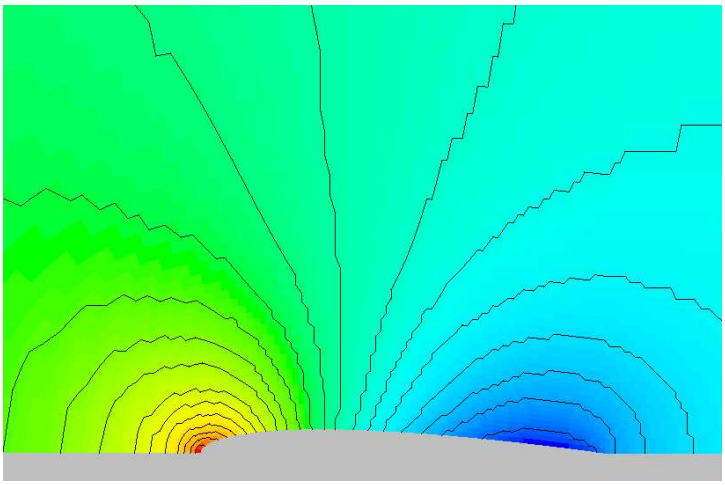

Figure 4.2: Pressure isolines for the NACA0012 profile for the preconditioned flux

The eigenvalues of the preconditioned Jacobian for $\alpha = 0$ are obtained from (5.5) and (5.6) as $|\lambda_{1/2}| = |v_n|$ and

$$\lambda_{3,4}(\mathbf{u}, \mathbf{n}) = \frac{1}{2}\left[(1+\beta^\nu)v_\mathbf{n} \pm \sqrt{(1+\beta^\nu)^2 v_\mathbf{n}^2 - 4v_\mathbf{n}^2\beta^\nu + 4\beta^\nu c^2}\right].$$

We have $|\lambda_{1/2}| = |v_n| = \mathcal{O}(1)$. Furthermore, because $\beta = \mathcal{O}(M)$ and $c = \mathcal{O}(M^{-1})$, we see that $|\lambda_{3/4}| = \mathcal{O}(M^{\frac{\nu}{2}-1})$. Thus, we obtain

$$\xi_1 = \lambda_3 - \beta^\nu v_n = \mathcal{O}(M^{\frac{\nu}{2}-1}), \quad \xi_2 = \lambda_4 - \beta^\nu v_n = \mathcal{O}(M^{\frac{\nu}{2}-1})$$

and

$$\xi_3 = \frac{\lambda_4 - \lambda_3}{2} = \mathcal{O}(M^{\frac{\nu}{2}-1}).$$

We should now keep in mind that the analysis is aimed at a standard compressible solver, which uses not the low Mach nondimenzionalization of the Euler equations, but the usual pressure reference $p_{ref} = \rho_{ref} v_{ref}^2$. Then, the nondimensionalized energy $E$ scales with $M^{-2}$. To illuminate this, we define auxiliary variables via

$$E = \frac{\tilde{E}}{M^2} \quad p = \frac{\tilde{p}}{M^2}. \tag{4.7}$$

These new variables $\tilde{E}$ and $\tilde{p}$ are then $\mathcal{O}(1)$ as the Mach number tends to zero and are thus suitable for an asymptotic analysis. We employ the ˜ notation, beacuse the axiliary variables are the same as those obtained when using the low Mach nondimensionalization. The mass component of the dissipation term then reads (see appendix C)

$$\mathbf{D}_1(\mathbf{u}_R - \mathbf{u}_L) = |\lambda_1|\eta_1 + \eta_4\left[|\lambda_3|\eta_2 + |\lambda_4|\eta_3 + \frac{\gamma-1}{M^2}(|\lambda_3|\xi_2 - |\lambda_4|\xi_1)\Delta_{ji}(\rho\tilde{E})\right], \tag{4.8}$$

with

$$\eta_1 = \Delta_{ji}\rho + \frac{\gamma-1}{c^2}\left(-\frac{|v|^2}{2}\Delta_{ji}\rho + v_1\Delta_{ji}m_1 + v_2\Delta_{ji}m_2 - \frac{\Delta_{ji}(\rho\tilde{E})}{M^2}\right) = \mathcal{O}(1),$$

$$\begin{aligned}\eta_2 &= \left(\xi_2\frac{(\gamma-1)|v|^2}{2} + \beta^\nu c^2 v_n\right)\Delta_{ji}\rho - (\xi_2(\gamma-1)v_1 + \beta^\nu c^2 n_1)\Delta_{ji}m_1 - (\xi_2(\gamma-1)v_2 \\ &\quad +\beta^\nu c^2 n_2)\Delta_{ji}m_2 = \mathcal{O}(M^{\nu-2}),\end{aligned}$$

$$\begin{aligned}\eta_3 &= -\left(\xi_1\frac{(\gamma-1)|v|^2}{2} + \beta^\nu c^2 v_n\right)\Delta_{ji}\rho + (\xi_1(\gamma-1)v_1 + \beta^\nu c^2 n_1)\Delta_{ji}m_1 + (\xi_1(\gamma-1)v_2 \\ &\quad +\beta^\nu c^2 n_2)\Delta_{ji}m_2 = \mathcal{O}(M^{\nu-2})\end{aligned}$$

and

$$\eta_4 = \frac{1}{2\beta^\nu c^2\xi_3} = \mathcal{O}(M^{3-\frac{3}{2}\nu}).$$

We can thus rewrite (4.8) as

$$\begin{aligned}\mathbf{D}_1(\mathbf{u}_R - \mathbf{u}_L) &= \mathcal{O}(1) + \eta_4\left[\mathcal{O}(M^{\frac{3}{2}\nu-3}) + \mathcal{O}(M^{\frac{3}{2}\nu-3}) + \frac{\gamma-1}{M^2}(|\lambda_3^P|\xi_2 - |\lambda_4^P|\xi_1)\Delta_{ji}(\rho\tilde{E})\right] \\ &= \mathcal{O}(1) + \mathcal{O}(1) + \frac{(\gamma-1)}{M^2 2\beta^\nu c^2\xi_3}(|\lambda_3|\xi_2 - |\lambda_4|\xi_1)\Delta_{ji}(\rho\tilde{E}). \qquad (4.9)\end{aligned}$$

If the Mach number is small enough, $|\lambda_3| = \lambda_3$ and $|\lambda_4| = -\lambda_4$, so we obtain with $2\lambda_3\lambda_4 = \frac{1}{2}\left(((1+\beta^\nu)v_n)^2 - ((1+\beta^\nu)v_n)^2 - 4\beta^\nu c^2\right)$:

$$\begin{aligned}|\lambda_3|\xi_2 - |\lambda_4|\xi_1 &= \lambda_3\xi_2 + \lambda_4\xi_1 = 2\lambda_3\lambda_4 - \beta^\nu\frac{v_n^2}{2}(1+\beta^\nu) \\ &= -2\beta^\nu c^2 + \frac{1}{2}\beta^\nu v_n^2 - \frac{1}{2}\beta^{2\nu}v_n^2 = -2\beta^\nu c^2 + \mathcal{O}(M^\nu),\end{aligned}$$

We insert this into (4.9) which results in

$$\mathbf{D}_1(\mathbf{u}_R - \mathbf{u}_L) = -\frac{\gamma-1}{\xi_3 M^2}\Delta_{ji}(\rho\tilde{E}) + \mathcal{O}(1) + \mathcal{O}\left(\frac{1}{\xi_3}\right).$$

From the equation of state we know that $\rho\tilde{E} = \frac{\tilde{p}}{\gamma-1} + \mathcal{O}(M^2)$ and therefore:

$$\mathbf{D}_1(\mathbf{u}_R - \mathbf{u}_L) = -\frac{1}{\xi_3 M^2}\Delta_{ji}\tilde{p} + \mathcal{O}(1) + \mathcal{O}(M^{1-\frac{\nu}{2}}), \qquad (4.10)$$

where we can neglect the last Landau symbol, as the functions are either $\mathcal{O}(1)$ for $\nu = 2$ or of higher order. Now that we have a simple expression for the dissipative part of the flux, we go back to the complete Lax Friedrichs mass flux. As the contributions from the convective mass flux is $\mathcal{O}(1)$, we obtain:

$$f_1^{LFP} = -\frac{1}{2\xi_3 M^2}\Delta_{ji}\tilde{p} + \mathcal{O}(1).$$

Applying this flux in a finite volume scheme, using the discrete asymptotic expansion $\phi_i = \phi_i^{(0)} + \mathbf{M}\phi_i^{(1)} + \mathbf{M}^2\phi_i^{(2)} + o\left(\mathbf{M}^2\right)$ and identifying the terms of lowest order, we see for an interior cell $i$:

$$0 = \sum_{j\in N(i)} \underbrace{|e_{ij}|\frac{-1}{2\xi_3^{(0)} M^2}}_{>0} \Delta_{ji}\tilde{p}^{(0)}. \tag{4.11}$$

From this we deduce that the maximum and the minimum leading pressure have to be at the boundary, otherwise (4.11) could not be zero for all interior cells. Now we assume that we have constant interpolation boundary conditions. The contribution from the dissipation term to the boundary flux is thus zero and the boundary flux itself is $\mathcal{O}(1)$. Therefore, it has no influence on the equation above, as the order is too high. Let $\tilde{p}_i^{(0)}$ be the maximum of the leading order pressure. Thus $\Delta_{ji}\tilde{p}^{(0)} \geq 0$ and we obtain from (4.11):

$$\Delta_{ji}\tilde{p}^{(0)} = 0 \; \forall j \in N(i).$$

Repeating the argument in the cells neighbouring $\Omega_i$, we conclude that $\tilde{p}^{(0)}$ is spatially constant. For the first order pressure, we obtain the following perturbation equation:

$$\begin{aligned} 0 &= \sum_{j\in N(i)} |e_{ij}|\frac{-1}{2\xi_3^{(0)} M^2}\Delta_{ji}\tilde{p}^{(1)} + \sum_{j\in N(i)} |e_{ij}|\frac{-1}{2\xi_3^{(1)} M^2}\Delta_{ji}\tilde{p}^{(0)} && (4.12)\\ &= \sum_{j\in N(i)} \underbrace{|e_{ij}|\frac{-1}{2\xi_3^{(0)} M^2}}_{>0} \Delta_{ji}\tilde{p}^{(1)}, && (4.13) \end{aligned}$$

as the leading order pressure is spatially constant. We conclude, using the same argument as before, that also the first order pressure does not vary in space. As the auxiliary variable $\tilde{p}$ differs from the real pressure $p$ only by a constant, this proves the theorem. □

Although we have no spatial variation of the first order pressure, which is in line with theorem 1, the last theorem makes no assertion about higher orders. The next theorem shows that there are spatial pressure variations on an order between one and two. Note that for the case $\nu = 2$, it was already proven that the pressure distribution is as desired, therefore it is excluded in the theorem.

**Theorem 6** *Let the preconditioner be given by*

$$\mathbf{P}^{-1} = \begin{pmatrix} \beta^\nu & & & \\ & 1 & & \\ & & 1 & \\ & & & 1 \end{pmatrix}, \ \nu \in (0,2), \ \beta = \mathcal{O}_S(M).$$

*Furthermore, assume that $\rho$ is constant in space.*

*Then there exists a velocity distribution, such that the discrete pressure of the preconditioned Lax-Friedrichs flux varies in space with a lower order than $M^2$.*

*Proof:* The idea of the proof is to use a fitting asymptotic expansion of the pressure and insert this into the momentum flux, the dissipation term of which can be found in appendix C. Then an appropriately chosen velocity field will yield the result. As in the last proof, all Landau symbols are for $M \to 0$. Furthermore, the asymptotic behavior of $\xi_1, \xi_2$ and $\xi_3$ is also the same as in the last proof. Again using the auxiliary variables (4.7), namely $\tilde{E} = \frac{E}{M^2}$ and $\tilde{p} = \frac{p}{M^2}$, as in the last proof, the first component of the momentum flux is given by:

$$\begin{aligned}
f_2^{LFP} &= \frac{1}{2}(f_2(\mathbf{u}_i;\mathbf{n}) + f_2(\mathbf{u}_j;\mathbf{n}) - \mathbf{D}_2(\mathbf{u}_i,\mathbf{u}_j;\mathbf{n})(\mathbf{u}_j - \mathbf{u}_i)) \\
&= \frac{1}{2}\Bigg(m_{i,1}v_{i,n} + n_1\frac{\tilde{p}_i}{M^2} + m_{j,1}v_{j,n} + n_1\frac{\tilde{p}_j}{M^2}) \\
&\quad -|v_n|[\frac{v_1(\gamma-1)}{c^2}(\frac{c^2}{\gamma-1}\Delta_{ji}\rho - \frac{|v|^2}{2}\Delta_{ji}\rho + v_1\Delta_{ji}m_1 + v_2\Delta_{ji}m_2 - \frac{\Delta_{ji}\rho\tilde{E}}{M^2}) \\
&\quad +n_2(v_t\Delta_{ji}\rho + n_2\Delta_{ji}m_1 - n_1\Delta_{ji}m_2)] \\
&\quad -\frac{1}{2\beta^\nu c^2\xi_3}\,[|\lambda_3|(v_1+\xi_1 n_1) \\
&\quad \Bigg((\xi_2(\gamma-1)\frac{|v|^2}{2} + \beta^\nu c^2 v_n)\Delta_{ji}\rho - (\xi_2(\gamma-1)v_1 + \beta^\nu c^2 n_1)\Delta_{ji}m_1 \\
&\quad -(\xi_2(\gamma-1)v_2 + \beta^\nu c^2 n_2)\Delta_{ji}m_2 + (\gamma-1)\xi_2\frac{\Delta_{ji}(\rho\tilde{E})}{M^2}\Bigg) \\
&\quad +|\lambda_4|(v_1+\xi_2 n_1)\Bigg(-(\xi_1(\gamma-1)\frac{|v^2|}{2} + \beta^\nu c^2 v_n)\Delta_{ji}\rho + (\xi_1(\gamma-1)v_1 + \beta^\nu c^2 n_1)\Delta_{ji}m_1 \\
&\quad +(\xi_1(\gamma-1)v_2 + \beta^\nu c^2 n_2)\Delta_{ji}m_2 - (\gamma-1)\xi_1\frac{\Delta_{ji}(\rho\tilde{E})}{M^2}\Bigg)\Bigg]\Bigg).
\end{aligned}$$

Now we group all terms together that are obviously $\mathcal{O}(1)$ or of higher order and obtain:

$$\begin{aligned} f_2^{LFP} &= \frac{n_1(\tilde{p}_i+\tilde{p}_j)}{2M^2} - \frac{1}{4\beta^\nu c^2 \xi_3}\Big[|\lambda_3|\xi_1 n_1 \beta^\nu c^2 (v_n \Delta_{ji}\rho - n_1\Delta_{ji}m_1 - n_2\Delta_{ji}m_2) \\ &\quad -|\lambda_4|\xi_2 n_1 \beta^\nu c^2 (v_n \Delta_{ji}\rho - n_1\Delta_{ji}m_1 - n_2\Delta_{ji}m_2) \\ &\quad +\frac{(\gamma-1)}{M^2}(|\lambda_3|\xi_1 n_1 \xi_2 \Delta_{ji}(\rho\tilde{E}) - |\lambda_4|\xi_2 n_1 \xi_1 \Delta_{ji}(\rho\tilde{E}))\Big] + \text{higher order terms} \\ &= \frac{n_1(\tilde{p}_i+\tilde{p}_j)}{2M^2} - \frac{(|\lambda_3|\xi_1 - |\lambda_4|\xi_2)n_1}{4\xi_3}(v_n\Delta_{ji}\rho - n_1\Delta_{ji}(\rho v_1) - n_2\Delta_{ji}(\rho v_2)) \\ &\quad -\frac{(\gamma-1)(|\lambda_3|-|\lambda_4|)n_1\xi_1\xi_2}{M^2c^2 4\beta^\nu\xi_3}\Delta_{ji}(\rho\tilde{E}) + \text{higher order terms} \end{aligned}$$

Using that $\rho$ is spatially constant, $\rho\tilde{E} = \frac{\tilde{p}}{\gamma-1} + \mathcal{O}(M^2)$, as well as $|\lambda_3| = \lambda_3$ and $|\lambda_4| = -\lambda_4$ if the Mach number is small enough, we can simplify this further. The nominator of the second fraction reads $|\lambda_3|\xi_1 - |\lambda_4|\xi_2 = 2\beta^\nu c^2 + \mathcal{O}(1)$ and thus we obtain

$$\begin{aligned} f_2^{LFP} &= \frac{n_1(\tilde{p}_i+\tilde{p}_j)}{2M^2} - \frac{\beta^\nu c^2 n_1}{2\xi_3}(n_1\Delta_{ji}(\rho v_1) + n_2\Delta_{ji}(\rho v_2)) - \frac{n_1\xi_1\xi_2}{M^2c^2 4\beta^\nu\xi_3}(1+\beta^\nu)v_n\Delta_{ji}\tilde{p} \\ &\quad +\text{higher order terms} \\ &= \frac{n_1(\tilde{p}_i+\tilde{p}_j)}{2M^2} - \underbrace{\frac{\beta^\nu c^2 n_1 \rho}{2\xi_3}}_{\mathcal{O}(M^{\frac{\nu}{2}-1})}(n_1\Delta_{ji}v_1 + n_2\Delta_{ji}v_2) - \underbrace{\frac{n_1\xi_1\xi_2 v_n}{M^2c^2 4\beta^\nu\xi_3}}_{\mathcal{O}(M^{-1-\frac{\nu}{2}})}\Delta_{ji}\tilde{p} \\ &\quad +\text{higher order terms} \end{aligned}$$

We now employ the asymptotic expansion

$$\tilde{p} = \tilde{p}^{(0)} + M\tilde{p}^{(1)} + M^{1+\frac{\nu}{2}}\tilde{p}^{(2)} + o(M^{1+\frac{\nu}{2}})$$

for the pressure where we know from theorem 5, that $\tilde{p}^{(0)}$ and $\tilde{p}^{(1)}$ depend only on $t$ and not on $\mathbf{x}$. Then the first momentum equation of a semidiscrete finite volume scheme can be written as:

$$\begin{aligned} \frac{d}{dt}m_1 &= \sum_{j\in N(i)} n_{ij}|e_{ij}| \\ &\quad \left( n_1\frac{M^{1+\frac{\nu}{2}}(\tilde{p}_i^{(2)}+\tilde{p}_j^{(2)})}{2M^2} - \frac{\beta^\nu c^2\rho n_1}{2\xi_3}(n_1\Delta_{ji}v_1 + n_2\Delta_{ji}v_2) - \underbrace{\frac{v_n\xi_1\xi_2 M^{1+\frac{\nu}{2}}}{M^2c^2 4\beta^\nu\xi_3}n_1\Delta_{ji}\tilde{p}^{(2)}}_{\mathcal{O}(1)} \right) \end{aligned}$$

Using the asymptotic expansion $\phi = \phi^{(0)} + M\phi^{(1)} + M^2\phi^{(2)} + o(M^2)$ for all other quantities except the pressure, the perturbation equation of order $M^{\frac{\nu}{2}-1}$ reads:

$$0 = \sum_{j \in N(i)} n_{ij}|e_{ij}| \left( n_1 \frac{\tilde{p}_i^{(2)} + \tilde{p}_j^{(2)}}{2M^{1-\frac{\nu}{2}}} - \left( \frac{\beta^\nu c^2 \rho n_1}{2\xi_3} \right)^{(0)} (n_1 \Delta_{ji} v_1^{(0)} + n_2 \Delta_{ji} v_2^{(0)}) \right).$$

We now assume that we have a cartesian grid consisting of squares, from which follows that $|e_{ij}|$ is constant. Furthermore, we choose a velocity field that varies only in $x$ and is zero in $y$-direction. Given three neighbouring cells $k$, $i$ and $l$, which form a strip in $x$-direction, we obtain:

$$\tilde{p}_k^{(2)} - \tilde{p}_l^{(2)} = \left( \frac{\beta^\nu c^2 \rho}{2\xi_3} \right)^{(0)} M^{1-\frac{\nu}{2}} n_1^2 \Delta_{ki} v_1^{(0)} + \left( \frac{\beta^\nu c^2 \rho}{2\xi_3} \right)^{(0)} M^{1-\frac{\nu}{2}} n_1^2 \Delta_{il} v_1^{(0)}. \tag{4.14}$$

By assumption, $\rho$ is constant in space and so is $\rho^{(0)}$, which is furthermore nonzero. Consequently, $c^{(0)} = \sqrt{\gamma \frac{p}{\rho}}^{(0)}$ is constant in space and nonzero. $\beta$ can be written as $k\frac{v}{c}$, thus $\beta^{(0)} = k\frac{v^{(0)}}{c^{(0)}}$, where $v^{(0)}$ does vary in space. We have

$$\frac{\beta^\nu}{2\xi_3} = -\frac{k v^\nu}{c^\nu \sqrt{(1-\beta^\nu)^2 v_n^2 + 4\beta^\nu c^2}}$$

and therefore

$$\left( \frac{\beta^\nu}{2\xi_3} \right)^{(0)} = -\frac{k {v^{(0)}}^\nu}{{c^{(0)}}^\nu 2{\beta^{(0)}}^{\frac{\nu}{2}} c^{(0)}} = -\frac{k {v^{(0)}}^\nu {c^{(0)}}^{\frac{\nu}{2}}}{{c^{(0)}}^{\nu+1} k^{\frac{\nu}{2}} {v^{(0)}}^{\frac{\nu}{2}}} = -k^{\frac{\nu}{2}} {v^{(0)}}^{\frac{\nu}{2}} {c^{(0)}}^{-\frac{\nu}{2}-1}.$$

Inserting this into (4.14), we obtain

$$\tilde{p}_k^{(2)} - \tilde{p}_l^{(2)} = \underbrace{-k^{\frac{\nu}{2}} {c^{(0)}}^{-\frac{\nu}{2}+1} \rho^{(0)} M^{1-\frac{\nu}{2}} n_1^2}_{\neq 0} ({v^{(0)}}^{\frac{\nu}{2}} \Delta_{ki} v_1^{(0)} + {v^{(0)}}^{\frac{\nu}{2}} \Delta_{il} v_1^{(0)}),$$

from which it follows that we have spatial variations in $\tilde{p}^{(2)}$, if the expression ${v^{(0)}}^{\frac{\nu}{2}} \Delta_{ki} v_1^{(0)} + {v^{(0)}}^{\frac{\nu}{2}} \Delta_{il} v_1^{(0)}$ is nonzero. We have:

$${v^{(0)}}^{\frac{\nu}{2}} \Delta_{ki} v_1^{(0)} + {v^{(0)}}^{\frac{\nu}{2}} \Delta_{il} v_1^{(0)} = \left( \frac{v_k^{(0)} + v_i^{(0)}}{2} \right)^{\frac{\nu}{2}} (v_{1,i}^{(0)} - v_{1,k}^{(0)}) + \left( \frac{v_i^{(0)} + v_l^{(0)}}{2} \right)^{\frac{\nu}{2}} (v_{1,l}^{(0)} - v_{1,i}^{(0)}).$$

This is obviously nonzero, if we have a strictly monotone velocity distribution in $x$-direction. Thus, there exists a velocity distribution, such that we have spatial variations in the $\tilde{p}^{(2)}$ field of a lower order than $M^2$. Again, as the auxiliary variable $\tilde{p}$ differs from the real pressure $p$ only by a constant, this proves the theorem. □

The theorem also shows that the transition between the preconditioner of Guillard and Viozat and the unpreconditioned method is linear in $\nu$ for the leading order of the pressure field as it varies in space.

## 4.2 Stability Analysis

Now that we have established that the spatial discretization computes an asymptotically correct pressure distribution for low Mach numbers only for $\nu = 2$, we will restrict ourselves from now on to this case and proceed to examine other properties of the preconditioned scheme with preconditioner (4.4). A very important topic is stability, which governs the maximal time steps which can be used in a time stepping procedure for the solution of (3.4). This analysis can also be found in more compact form in [2].

Due to the characteristic propagation speeds associated with the governing equations, i.e.

$$v_{\mathbf{n}} = \mathcal{O}(1) \text{ and } v_{\mathbf{n}} \pm c = \mathcal{O}\left(\frac{1}{M}\right), \quad M \to 0,$$

we can directly conclude that the step size of an explicit time integration scheme decreases at least linearly as the Mach number tends to zero, i.e. we expect

$$\Delta t = \mathcal{O}\left(M\right), \quad M \to 0,$$

in order to fulfill the CFL condition that the numerical domain of dependence always covers the physical one. However, for the specific scheme used a different condition on the time step could be valid. To obtain a deeper insight into the behavior of the method we perform a von Neumann stability analysis.

Parallel flows show that without stability in the one-dimensional case, we cannot expect stability in higher dimensions. Therefore, the one-dimensional Euler equations are of interest also in our applications, but tremendously easier to analyze. Thus, for the sake of simplicity we restrict ourselves to the consideration of the spatially one-dimensional case. The relevance for multi-dimensional flow fields is obvious and after wards confirmed by numerical experiments.

It is well known that the standard Lax-Friedrichs scheme combined with the explicit Euler time integration is stable in the sense of von Neumann if the CFL-condition is satisfied. In order to perform a von Neumann stability analysis we have to linearize the governing equations as well as the preconditioning matrix. Thus, we consider the linearized one-dimensional Euler equations in the form

$$\partial_t \mathbf{u} + \mathbf{A}\partial_x(\mathbf{u}) = \mathbf{0} \tag{4.15}$$

where $\mathbf{A} = \mathbf{A}(\bar{\mathbf{u}}) = \frac{\partial f}{\partial u}(\bar{\mathbf{u}})$ with $\bar{\mathbf{u}} = \mathbf{u}_i$ for an arbitrary but fixed vector of conserved variables corresponding to an inner control volume $\Omega_i$. Quantities derived from $\bar{\mathbf{u}}$ will also be denoted with a bar. Note that in one spatial dimension, the conserved variables are $\rho$, $m$ and $\rho E$, while the entropy variables are $p$, $v$ and $s$. Due to the linearization it is appropriate to define the preconditioner also in a global manner by using $\bar{\mathbf{u}}$ instead of the average value of $\mathbf{u}_i$ and $\mathbf{u}_j$ as suggested in (4.2). Consequently, the preconditioned Lax-Friedrichs scheme for the linearized Euler equations (4.15) reads

$$\mathbf{f}^{LFP}(\mathbf{u}_i, \mathbf{u}_j, n) = \frac{1}{2}\left(\mathbf{A}(\bar{\mathbf{u}})(\mathbf{u}_j + \mathbf{u}_i)n - \mathbf{D}(\bar{\mathbf{u}}, \bar{\mathbf{u}}, n)(\mathbf{u}_j - \mathbf{u}_i)\right). \tag{4.16}$$

with

$$\mathbf{D}(\bar{\mathbf{u}}, \bar{\mathbf{u}}, n) = \mathbf{P}^{-1}(\bar{\mathbf{u}})\,\mathbf{R}(\bar{\mathbf{u}}, n)\,|\mathbf{\Lambda}|(\bar{\mathbf{u}}, \bar{\mathbf{u}}, n)\mathbf{R}^{-1}(\bar{\mathbf{u}}, n)\,. \tag{4.17}$$

The one-dimensional preconditioning matrix is obtained from (4.4) by omitting the third row and column. For the investigation of appropriate stability requirements for the preconditioned approach it is necessary to analyze the spectrum of the dissipation matrix $\mathbf{D}(\bar{\mathbf{u}}, \bar{\mathbf{u}}, n)$. At first, we focus on the case of a vanishing parameter $\alpha$. Thereafter, we will extend the statement to the general case.

**Lemma 2** *Let $\mu_i$, $i = 1, 2, 3$ represent the eigenvalues of the linearized dissipation matrix $\mathbf{D}$ corresponding to (4.17) of the preconditioned Lax-Friedrichs scheme (3.6) for equation (4.15) in one spatial dimension with $\beta = \mathcal{O}_S(M)$, $M \to 0$, $\beta \neq 0$, and $\alpha = 0$. Then the appropriately renumbered eigenvalues of $\mathbf{D}$ have the properties*

$$\mu_1, \mu_2 = \mathcal{O}(1)\,, \quad M \to 0$$

*and*

$$\mu_3 = \mathcal{O}_S\left(\frac{1}{M^2}\right), \quad M \to 0.$$

*Proof:* Analogously to the two-dimensional case the eigenvalues of the one-dimensional preconditioned Jacobian $\mathbf{F}^P(\bar{\mathbf{u}}, n)$ read

$$\lambda_1 = \bar{v}_n \;\text{ and }\; \lambda_{2,3} = \frac{1}{2}\left[(1+\beta^2)\bar{v}_n \pm \sqrt{(1-\beta^2)^2\bar{v}^2 + (2\beta\bar{c})^2}\right].$$

In the case that $M$ is sufficiently small one gets $\bar{c}^2 > \bar{v}^2$ by which it follows that

$$(1-\beta^2)^2\bar{v}^2 + 4\beta^2\bar{c}^2 > (1+\beta^2)^2\bar{v}^2. \tag{4.18}$$

This inequality yields $\lambda_2 > 0$ and $\lambda_3 < 0$, and consequently

$$|\lambda_2| - |\lambda_3| = \lambda_2 + \lambda_3 = (1+\beta^2)\bar{v}_n. \tag{4.19}$$

For the investigation of the spectrum of $\mathbf{D}$ it is advantageous to consider the matrix with respect to the entropy variables. Hence, we write the dissipation matrix in the form

$$\mathbf{D} = \mathbf{U}\mathbf{Q}^{-1}\mathbf{S}|\mathbf{\Lambda}|\mathbf{S}^{-1}\mathbf{W}$$

with $\mathbf{S} = \mathbf{W}\mathbf{R}$. Since $\mathbf{W} = \mathbf{U}^{-1}$ the matrices $\mathbf{D}$ and

$$\bar{\mathbf{D}} = \mathbf{Q}^{-1}\mathbf{S}|\mathbf{\Lambda}|\mathbf{S}^{-1} \tag{4.20}$$

are related by means of a similarity transformation which maintains the eigenvalues. Utilizing the abbreviations

$$\xi_1 = \lambda_2 - \lambda_1\beta^2, \quad \xi_2 = \lambda_3 - \lambda_1\beta^2, \quad \text{and} \quad \xi_3 = \frac{\lambda_3 - \lambda_2}{2}$$

in combination with equation (4.19) one can write (see Appendix A)

$$\bar{\mathbf{D}} = \begin{pmatrix} \frac{|\lambda_2|\xi_2 - |\lambda_3|\xi_1}{2\xi_3\beta^2} & -\frac{\bar{c}^2\rho}{2\xi_3}(1+\beta^2)\bar{v}_n & 0 \\ \frac{\xi_1\xi_2}{2\xi_3\beta^2\bar{c}^2\rho}(1+\beta^2)\bar{v}_n & \frac{1}{2\xi_3}(\xi_2|\lambda_3| - \xi_1|\lambda_2|) & 0 \\ 0 & 0 & |\lambda_1| \end{pmatrix}$$

for sufficiently small $M$. By means of straightforward but lengthy calculations we obtain the eigenvalues

$$\mu_1 = |\lambda_1| = |\bar{v}_n| = \mathcal{O}(1)$$

and

$$\mu_{2,3} = -\frac{1}{2\xi_3}\left((1+\beta^2)\bar{c}^2 \mp \sqrt{(1-\beta^2)^2(\bar{c}^4 - \bar{v}^2\bar{c}^2 + \bar{v}^4) + (2\beta\bar{v}\bar{c})^2}\right).$$

Due to the fact that the speed of sound $\widetilde{c}$ is always positive independent of the Mach number we get $\bar{c} = \mathcal{O}_S(M^{-1})$, $M \to 0$ and as a result

$$\begin{aligned} \xi_3 &= -\frac{1}{2}\sqrt{(1-\beta^2)^2\bar{v}^2 + (2\beta\bar{c})^2} = \underbrace{-\frac{1}{2}\sqrt{\bar{v}^2 + (2\beta\bar{c})^2}}_{=\mathcal{O}(1)} + \mathcal{O}(M^2) \\ &= \mathcal{O}(1), \quad M \to 0 \end{aligned} \tag{4.21}$$

and $\xi_3 < 0$ for all $M$. Similar to (4.18) we obtain

$$(1-\beta^2)^2(\bar{c}^4 - \bar{v}^2\bar{c}^2 + \bar{v}^4) + (2\beta\bar{v}\bar{c})^2 > (1-\beta^2)^2\bar{v}^4 + (2\beta\bar{v}\bar{c})^2 \geq 0$$

for a sufficient small Mach number and hence the eigenvalues $\mu_{2,3}$ are real in the low Mach number regime. Using (4.21) in combination with

$$(1+\beta^2)^2\bar{c}^2 = \mathcal{O}_S(M^{-2}), \quad M \to 0$$

and

$$\sqrt{(1-\beta^2)^2(\bar{c}^4 - \bar{v}^2\bar{c}^2 + \bar{v}^4) + (2\beta\bar{v}\bar{c})^2} = \mathcal{O}_S(M^{-2}), \quad M \to 0$$

directly yields

$$\begin{aligned} \mu_3 &= -\underbrace{\frac{1}{2\xi_3}}_{=\mathcal{O}_S(1)}\left(\underbrace{(1+\beta^2)\bar{c}^2}_{=\mathcal{O}_S(M^{-2})} + \underbrace{\sqrt{(1-\beta^2)^2(\bar{c}^4 - \bar{v}^2\bar{c}^2 + \bar{v}^4) + (2\beta\bar{v}\bar{c})^2}}_{=\mathcal{O}_S(M^{-2})}\right) \\ &= \mathcal{O}_S(M^{-2}), \quad M \to 0. \end{aligned}$$

Now we can deduce the asymptotic behavior of the remaining eigenvalue $\mu_2$ via

$$\mu_2 = \frac{\mu_2\mu_3}{\mu_3} = \frac{4\bar{c}^4\beta^2 + \bar{v}^2\bar{c}^2 + \mathcal{O}(1)}{(2\xi_3)^2\mu_3} = \mathcal{O}_S(1), \quad M \to 0$$

and have thus proved the last part of the lemma. □

Interpreting the cell average $\mathbf{u}_i(t)$ as a piecewise constant function on $\Omega_i$ and using a simple explicit time marching procedure leads to the first order scheme

$$\mathbf{u}_i^{n+1} = \mathbf{u}_i^n - \frac{\Delta t}{|\Omega_i|} \sum_{e_{ij} \subset \partial\Omega_i} |e_{ij}| \mathbf{f}^{LFP}(\mathbf{u}_i^n, \mathbf{u}_j^n, \mathbf{n}_{ij}) \tag{4.22}$$

with $\mathbf{u}_i^n = \mathbf{u}_i(t^n)$, $t^{n+1} = t^n + \Delta t$ and $\mathbf{n}_{ij}$ represents the unit outer normal vector on $e_{ij} \subset \partial\Omega_i$.

Let us now consider the preconditioned Lax-Friedrichs scheme (4.16) on an equidistant grid with fixed mesh size $\Delta x > 0$. Using the explicit Euler time integration and taking into account that the normal vector in one dimension is $n = \pm 1$ gives

$$\begin{aligned}
\mathbf{u}_i^{m+1} &= \mathbf{u}_i^m - \frac{\Delta t}{\Delta x} \sum_{j \in \{i-1, i+1\}} \mathbf{f}^{LFP}(\mathbf{u}_i^m, \mathbf{u}_j^m, n) \\
&= \mathbf{u}_i^m - \frac{\Delta t}{\Delta x} \left( \mathbf{f}^{LFP}(\mathbf{u}_i^m, \mathbf{u}_{i-1}^m, -1) + \mathbf{f}^{LFP}(\mathbf{u}_i^m, \mathbf{u}_{i+1}^m, 1) \right) \\
&= \mathbf{u}_i^m - \frac{\Delta t}{2\Delta x} \Big( \mathbf{A}(\bar{\mathbf{u}}) \left( \mathbf{u}_{i-1}^m - \mathbf{u}_{i+1}^m \right) \\
&\qquad + \mathbf{D}(\bar{\mathbf{u}}, \bar{\mathbf{u}}, 1) \left( \mathbf{u}_{i+1}^m - 2\mathbf{u}_i^m + \mathbf{u}_{i-1}^m \right) \Big).
\end{aligned} \tag{4.23}$$

Starting from this formulation we are now able to prove the following stability condition in the case of a vanishing parameter $\alpha$.

**Theorem 7** *A necessary condition to ensure stability of the linearized preconditioned Lax-Friedrichs scheme with $\beta = \mathcal{O}_S(M)$, $M \to 0$, $\beta \neq 0$ and $\alpha = 0$ is*

$$\Delta t = \mathcal{O}(M^2), \quad M \to 0.$$

*Proof:* The investigation of the $L_2$-stability, known as the von Neumann stability, is based on a Fourier analysis. Therefore, we replace $\mathbf{u}_i^m$ by the corresponding Fourier expansion

$$\mathbf{u}_i^m = \sum_{j=-\infty}^{\infty} \mathbf{h}_j^m e^{ij\Delta x I},$$

where $I$ represents the imaginary unit. Introducing $\phi = j\Delta x$ we obtain the evolution of the $j^{th}$ mode in the form

$$\begin{aligned}\mathbf{h}_j^{m+1} e^{i\phi I} &= \mathbf{h}_j^m e^{i\phi I} + \frac{\Delta t}{2\Delta x}\Big(\mathbf{A}(\bar{\mathbf{u}})\mathbf{h}_j^m \left(e^{(i-1)\phi I} - e^{(i+1)\phi I}\right) \\ &\qquad + \mathbf{D}(\bar{\mathbf{u}}, \bar{\mathbf{u}}, 1)\mathbf{h}_j^m \left(e^{(i+1)\phi I} - 2e^{i\phi I} + e^{(i-1)\phi I}\right)\Big).\end{aligned}$$

Division by $e^{i\phi I}$ yields

$$\mathbf{h}_j^{m+1} = \mathbf{H}(j, \Delta x, \Delta t)\mathbf{h}_j^m$$

with the amplification matrix

$$\begin{aligned}\mathbf{H}(j, \Delta x, \Delta t) &= \mathbf{I} + \frac{\Delta t}{2\Delta x}\left(\mathbf{A}(\bar{\mathbf{u}})\left(e^{-\phi I} - e^{\phi I}\right) + \mathbf{D}(\bar{\mathbf{u}}, \bar{\mathbf{u}}, 1)\left(e^{\phi I} - 2 + e^{-\phi I}\right)\right) \\ &= \mathbf{I} - \frac{\Delta t}{\Delta x}\mathbf{D}(\bar{\mathbf{u}}, \bar{\mathbf{u}}, 1) + \frac{\Delta t}{\Delta x}\mathbf{D}(\bar{\mathbf{u}}, \bar{\mathbf{u}}, 1)\cos\phi - I\frac{\Delta t}{\Delta x}\mathbf{A}(\bar{\mathbf{u}})\sin\phi.\end{aligned}$$

The scheme is stable in the sense of von Neumann if the spectral radius of the amplification matrix is less than one for all $\phi$. The eigenvalues of the matrix $\mathbf{A}(\bar{\mathbf{u}})$ are known to be

$$\nu_1 = v = \mathcal{O}(1), \quad M \to 0$$

and

$$\nu_{2,3} = v \pm c = \mathcal{O}(M^{-1}), \quad M \to 0.$$

Consequently, for fixed $\Delta x > 0$ Lemma 2 yields with $\mathbf{A} = \mathbf{I} - \frac{\Delta t}{\Delta x}\mathbf{D}(\bar{\mathbf{u}}, \bar{\mathbf{u}}, 1) + \frac{\Delta t}{\Delta x}\mathbf{D}(\bar{\mathbf{u}}, \bar{\mathbf{u}}, 1)\cos\phi$ and $\mathbf{B} = -\frac{\Delta t}{\Delta x}\mathbf{A}(\bar{\mathbf{u}})\sin\phi$ for some matrix norm:

$$\rho(\mathbf{H}) = \rho(\mathbf{A} + I\mathbf{B}) \quad \geq \quad \|\mathbf{A} + I\mathbf{B}\| - \epsilon \geq \|\mathbf{A}\| - \epsilon = \mathcal{O}(\frac{\Delta t}{M^2}), \quad M \to 0,$$

where the second inequality is due to $\mathbf{A}$ and $\mathbf{B}$ being real matrices. This property proves the requirement $\Delta t = \mathcal{O}(M^2)$, $M \to 0$, which completes the proof. □

Let us now generalize the statement of Lemma 2 to the case of an arbitrary parameter $\alpha$. It is worth mentioning that the parameter $\alpha$ can of course depend on the physical quantities.

**Lemma 3** *If $\beta = \mathcal{O}_S(M)$, $M \to 0$, $\beta \neq 0$, then there exists an eigenvalue $\mu$ of the linearized dissipation matrix $\mathbf{D}$ corresponding to* (4.17) *of the linearized preconditioned Lax-Friedrichs scheme* (3.6) *such that*

$$\mu = \mathcal{O}_S\left(\frac{1}{M^2}\right), \quad M \to 0$$

*independent of $\alpha$.*

*Proof:* As we can learn from the elaborated description of the eigenvalues $\mu_i$, $i = 1, 2, 3$ of the dissipation matrix $\mathbf{D}$ in Appendix A the crucial eigenvalues can be written as

$$\mu_{2,3} = \frac{a \pm \frac{1}{2}\sqrt{b}}{2\xi_3} \tag{4.24}$$

with

$$a = \underbrace{-\beta^2 c^2}_{\mathcal{O}(1)} - \underbrace{c^2}_{\mathcal{O}_S\left(\frac{1}{M^2}\right)} + \frac{\alpha}{2}\underbrace{\left(3v^2 - \beta^4 v + \beta^2 v^2 - \beta^2 v\right)}_{\mathcal{O}(1)} + \frac{\alpha^2}{2}\underbrace{\left(\beta^2 v - v^2\right)}_{\mathcal{O}(1)}. \tag{4.25}$$

In order to ensure that neither $\mu_2$ nor $\mu_3$ is any longer $\mathcal{O}\left(\frac{1}{M^2}\right)$, the parameter $\alpha$ has to be chosen such that the leading order terms cancel out. Due to the fact that the parameter $\alpha$ always appears in form of a product $\alpha v$ within the preconditioner (4.4) it is obvious that one cannot improve the stability properties in the case of a vanishing velocity field. This is also documented by equation (4.25) which shows that $a = \mathcal{O}_S\left(\frac{1}{M^2}\right)$, $M \to 0$ independent of $\alpha$, if $v = 0$.

If $v \neq 0$ we deduce from (4.25) that we have to define

$$\alpha = \sqrt{-\frac{2c^2}{v^2}} \in \mathbb{C} \tag{4.26}$$

in order to remove the leading order term. However, introducing (4.26) into the second addend of (4.24) yields

$$b = 4c^4 + v^4\alpha^4 + o\left(\frac{1}{M^4}\right) = 8c^4 + o\left(\frac{1}{M^4}\right) = \mathcal{O}_S\left(\frac{1}{M^4}\right), \quad M \to 0.$$

This implies $\sqrt{b} = \mathcal{O}_S\left(\frac{1}{M^2}\right)$, $M \to 0$ and consequently there exists always an eigenvalue

$$\mu = \mathcal{O}_S\left(\frac{1}{M^2}\right), \quad M \to 0,$$

which is the assertion of the lemma. □

We are now able to employ the statement of the above mentioned lemma to prove the following proposition exactly in the way we perform the evidence of theorem 7.

**Theorem 8** *A necessary condition to ensure stability of the linearized preconditioned Lax-Friedrichs scheme with $\beta = \mathcal{O}_S(M)$, $M \to 0$, $\beta \neq 0$ and arbitrary $\alpha$ is*

$$\Delta t = \mathcal{O}(M^2), \quad M \to 0.$$

This theoretical result is only valid for the linearized scheme and therefore only a necessary stability condition. Later on we will confirm the significance of the results of the one-dimensional linear theory by numerical tests in the context of the two-dimensional Euler equations. Furthermore, we would like to point out that the proof works analogously for other schemes, for example the Roe-scheme [52] or the AUSMDV scheme [70] and thus these schemes have the same stability properties.

Due to the fact that a numerical method without dissipation is inherently unstable it is not surprising that a preconditioning of the dissipation term influences the stability of the whole numerical method. In the specific situation under consideration, the eigenvalues of the matrix $|\mathbf{PF}|$ are $\mathcal{O}(1)$. Thus, from a heuristical point of view, the multiplication by means of $\mathbf{P}^{-1}$ may introduce a difference on a scale of $\beta^{-2} = \mathcal{O}(M^{-2})$ in the spectrum of the dissipation matrix.

As for the choice of $\alpha$, we will from now on neglect it, as the increase in computational cost due to the more complicated preconditioner is not justified by numerical or theoretical results in this context.

### 4.2.1 Numerical Experiments

Our first test problem is a NACA0012 profile at zero angle of attack with varying inflow Mach numbers. A C-Type grid with 7487 cells was used, the smallest cell directly at the nose having a boundary of 0.0015. Due to the angle, the solution is symmetric and thus it is sufficient to discretize only the upper half of the domain, if fixed wall boundary conditions are used at the dividing interface. For the rest of the free boundary, nonreflecting boundary conditions are employed. We used the finite volume scheme described in this chapter with a first order spatial discretization, the explicit Euler scheme in time and nonreflecting boundary conditions. The time step then tends to zero quadratically with $M$ in the case of a preconditioned Lax-Friedrichs flux. If we do not employ preconditioning, the time step still goes to zero, but only linearly in $M$. These experiments thus confirm the theorem for the nonlinear scheme. The results can be seen in the first tabular. The CFL numbers are accurate up to the leading digit: 0.1 thus means that a CFL number of 0.2 leads to instabilities.

| NACA0012 | Preconditioned | | Unpreconditioned | |
|---|---|---|---|---|
| M | CFL number | $\Delta t$ | CFL number | $\Delta t$ |
| 0.1 | 0.1 | $7 \cdot 10E-7$ | 0.9 | $6 \cdot 10E-5$ |
| 0.01 | 0.01 | 10E-8 | 0.9 | $7 \cdot 10E-6$ |
| 0.001 | 0.001 | 10E-10 | 0.9 | $7 \cdot 10E-7$ |
| 0.0001 | 0.0001 | 10E-12 | 0.9 | $7 \cdot 10E-8$ |
| 0.00001 | 0.00001 | 10E-14 | 0.9 | $7 \cdot 10E-9$ |

The second test problem is a circular bump in a channel, again with varying inflow Mach numbers. We employed the same numerical scheme as above on a cartesian grid of

4000 cells with minimal boundary length 0.012. The asymptotic behavior predicted by the theorem can be clearly seen. For the case $M = 0.1$, the preconditioned scheme is as stable as the unpreconditioned one. This is not a contradiction to the theoretical results, where the Mach number is assumed to be small enough, thus the numerical results show that the asymptotic behavior of the scheme does not yet start at $M = 0.1$. The difference in $\Delta t$ compared to the first problem is due to a different grid with different cell sizes.

| Bump | Preconditioned | | Unpreconditioned | |
|---|---|---|---|---|
| M | CFL number | $\Delta t$ | CFL number | $\Delta t$ |
| 0.1 | 0.9 | $5 \cdot 10E-4$ | 0.9 | $5 \cdot 10E-4$ |
| 0.01 | 0.01 | $6 \cdot 10E-7$ | 0.9 | $5 \cdot 10E-5$ |
| 0.001 | 0.001 | $6 \cdot 10E-9$ | 0.9 | $5 \cdot 10E-6$ |
| 0.0001 | 0.0001 | $6 \cdot 10E-11$ | 0.9 | $5 \cdot 10E-7$ |
| 0.00001 | 0.00001 | $6 \cdot 10E-13$ | 0.9 | $5 \cdot 10E-8$ |

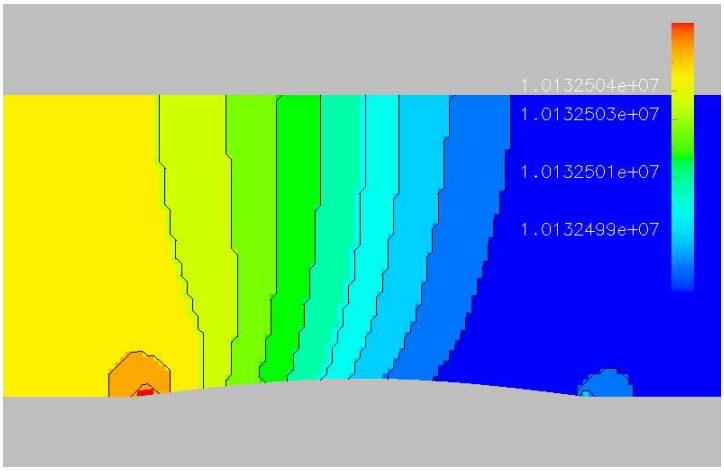


Figure 4.3: Pressure isolines at Ma=0.001 for the circular bump using the preconditioned flux.

If we use the implicit Euler scheme instead of the explicit Euler for the time integration, we observe no bound on the CFL number. Not surprisingly, the von Neumann stability analysis reveals no bound on the time step. Only for $M = 10^{-5}$, a restriction of the CFL number was observed. However, it should be pointed out that the linear equation systems are much more difficult to solve, the smaller the Mach number gets. This is probably due to the strong Mach number dependence of the eigenvalues of the preconditioned flux, which results in a worsening condition number of the matrix. For the NACA profile at $Ma = 0.0001$, in the steady state using the nonpreconditioned flux, one Newton iteration is needed for the nonlinear relative tolerance of 100 and seven GMRES iterations when a linear realtive tolerance of $10^5$ is required. By contrast, if the preconditioned flux is used,

three Newton iterations are not sufficient to reduce the nonlinear relative residual by a factor of 100 and more than 100 GMRES iterations per Newton step.

However, we believe that choosing a different linear preconditioner than the one implemented here will lessen this effect significantly: the discretization the preconditioner is based on, namely the van Leer flux vector splitting (3.8), differs from the preconditioned Lax-Friedrichs flux. This lessens the speed of convergence already in the transsonic regime [36], but there the efficient computation of the blocks of the jacobian makes up for that. Furthermore, it is demonstrated by Reusken in [51] that for the linearized one dimensional Euler equations, the speed of convergence of the symmetric Gauss-Seidel method with the van Leer flux vector splitting as a discretization has an unfavorable Mach number dependence for low Mach numbers.

### 4.2.2 The Two Dimensional Case

As argued before, we cannot hope for two dimensional stability without onedimensional. With the results obtained we can now substantiate this argument straightforwardly.

**Lemma 4** *In the two dimensional case three eigenvalues of the dissipation matrix are* $\mathcal{O}(1)$ *for* $M \to 0$ *and one eigenvalues is* $\mathcal{O}_S(1/M^2)$ *as the Mach number tends to zero.*

*Proof:* We will first consider the case that we have an edge with normal vector $\mathbf{n}_{ij} = (1,0)^T$. Then we have for sufficiently small $M$:

$$\mathbf{D}(\mathbf{u}_i, \mathbf{u}_j; (1,0)^T) = \mathbf{U} \begin{pmatrix} \frac{|\lambda_3|\xi_2 - |\lambda_4|\xi_1}{2\xi_3\beta^2} & -\frac{\bar{c}^2\rho}{2\xi_3}(1+\beta^2)\bar{v}_n & 0 & 0 \\ \frac{\xi_1\xi_2}{2\xi_3\beta^2\bar{c}^2\rho}(1+\beta^2)\bar{v}_n & -\frac{1}{2\xi_3}(\xi_1|\lambda_3| + \xi_2|\lambda_4|) & 0 & 0 \\ 0 & 0 & |\lambda_2| & 0 \\ 0 & 0 & 0 & |\lambda_1| \end{pmatrix} \mathbf{W},$$

where we have used the abbreviations

$$\xi_1 = \lambda_3 - \lambda_1\beta^2, \quad \xi_2 = \lambda_4 - \lambda_1\beta^2, \quad \text{and} \quad \xi_3 = \frac{\lambda_4 - \lambda_3}{2}.$$

The eigenvalues of this matrix are known from Lemma 2. They have the properties that three are $\mathcal{O}(1)$ and one eigenvalue is $\mathcal{O}_S(1/M^2)$ as the Mach number tends to zero. Now as the Lax-Friedrichs flux is rotationally invariant, so is the dissipation term and we have $\mathbf{D}(\mathbf{u}_i, \mathbf{u}_j; \mathbf{n}_{ij}) = \mathbf{T}^{-1}\mathbf{D}(\mathbf{T}\mathbf{u}_i, \mathbf{T}\mathbf{u}_j; \mathbf{T}\mathbf{n}_{ij})$. Choosing the rotation matrix such that the normal vector $\mathbf{n}$ gets rotated onto $(1,0)^T$, we obtain

$$\mathbf{D}(\mathbf{u}_i, \mathbf{u}_j; \mathbf{n}_{ij}) = \mathbf{T}^{-1}\mathbf{D}(\mathbf{T}\mathbf{u}_i, \mathbf{T}\mathbf{u}_j; (1,0)^T).$$

The matrix $\mathbf{T}^{-1}$ is nonsingular and independent of $M$. Therefore, while an application of $\mathbf{T}^{-1}$ changes the eigenvalues of $\mathbf{D}(\mathbf{T}\mathbf{u}_i, \mathbf{T}\mathbf{u}_j; (1,0)^T)$, it does not change their asymptotic

behavior as the Mach number tends to zero. □

Now we can prove the stability result in two dimensions:

**Theorem 9** *Theorem 7 is also valid in the two dimensional case.*

*Proof:* The proof is done by a von Neumann stability analysis on the linearized Euler equations

$$\partial_t \mathbf{u} + \mathbf{A}\partial_{x_1}(\mathbf{u}) + \mathbf{B}\partial_{x_2}(\mathbf{u}) = \mathbf{0}$$

discretized using the explicit Euler method and the preconditioned Lax Friedrichs flux. □

Of course, the same technique can be used to prove the stability result for three dimensional flows.

# Chapter 5

# Gravitation and Heat

For the tunnelfire problem, the gravitational force is responsible for the transport of hot air to the ceiling of the tunnel. A correct computation of the effect of gravitation is thus mandatory for a successful simulation of a tunnel fire event.

The simulation of buoancy is a subject of ongoing discussion, especially in the meteorological community. There the flows are near the hydrostatic balance and several numerical methods exist, see for example the textbook of Durran [9]. Botta, Klein, Langenberg and Lützenkirchen point out in [3] that some of these methods have problems. To illustrate this, we consider a vertical equidistant onedimensional grid. Furthermore we assume that the solution is near hydrostatic balance, that means that $\partial_{x_2} p - \rho g = \mathcal{O}(\epsilon)$. This assumption is valid when there are other disturbances in the flow resulting for example from a heat source. Discretizing this with mesh width $\Delta x = h$ using a method that is $r$-th order consistent, we obtain a discretization error of

$$(\partial_{x_2} p - \rho g)_h - \partial_{x_2} p + \rho g = \mathcal{O}(h^r).$$

If $\epsilon$ tends to zero while $h$ remains fixed, the discretization error $\mathcal{O}(h^r)$ completely dominates the solution. Thus as we come nearer the hydrostatic equilibrium the quality of the solution does not increase: it is unbalanced. If we know beforehand the correct hydrostatic equilibrium $p^H$ and $\rho^H$, we have a decomposition $p = \delta p + p^H$ and $\rho = \delta\rho + \rho^H$ satisfying $\partial_{x_2} p^H - \rho^H g = 0$. If furthermore $\partial_{x_2}\delta p$ and $\delta\rho g$ are $\mathcal{O}(\epsilon)$ we obtain, using the discretization

$$\partial_{x_2}\delta p(x_i) \approx \frac{\delta p(x_{i+1}) - \delta p(x_{i-1})}{2h}$$

and exact data for pressure and density, by a Taylor expansion for the discretization error of $\partial_{x_2} p - \rho g = \partial_{x_2}\delta p - \delta\rho g$:

$$\frac{\delta p(x_{i+1}) - \delta p(x_{i-1})}{2h} - \delta\rho(x_i) g \;=\; \partial_{x_2}\delta p(x_i) - \delta\rho(x_i) g + \frac{h^2}{12}\partial^3_{x_2}\delta p(x_i) + \frac{h^3}{48}\partial^4_{x_2}\delta p(\xi)$$

$$= \mathcal{O}(\epsilon) + \frac{h^2}{12}\epsilon\partial_{x_2}^2\phi(x_i) + \frac{h^3}{48}\epsilon\partial_{x_2}^3\phi(\xi),$$

with $\phi(x_i) = \mathcal{O}(1)$, as $\partial_{x_2}p(x_i) = \mathcal{O}(\epsilon)$ and $\xi \in [x_{i-1}, x_{i+1}]$. Thus, the discretization error for fixed $h$ when using this decomposition tends to zero if $\epsilon$ tends to zero. However, when using the original discretization without a splitting, it is not immediately clear from the analysis, how small $\epsilon$ can become for a given mesh width and a particular problem, before the discretization error dominates the solution. As a remedy, a reconstruction procedure is suggested in [3], that uses a "discrete Archimedes buoancy principle" to obtain a well-balanced scheme.

Nguyen-Bui, Dubroca and Maire [47] applied a low Mach preconditioned method to a free convection problem, where air was cooled and heated between plates and, being subject to buoancy, started to circulate. There they observed errors in their numerical calculations. As a remedy they tried a similar decomposition of the pressure and could improve their results, though no explanation was given.

Therefore, we will first try a simple Godunov splitting to include the gravitational force, as this is the simplest thing to do. Only after having examined this in detail will we proceed to include the heat source in addition to gravity. The heat source in our problems is constant in time and space and affects the solution only locally and not globally, as the gravitational term does. Therefore it is much easier to simulate.

## 5.1 The Source Terms

The equation we have to solve for the incorporation of the source terms via operator splitting is (3.5). This simplifies, because the source terms are spatially and temporally constant, to

$$\frac{d}{dt}\mathbf{u}_i(t) = \mathbf{g}(\mathbf{u}(\mathbf{x}, t)).$$

If we consider only the gravitational source term, we see from (2.10) that the equation to solve in step two of the Godunov splitting is

$$\frac{d}{dt}\mathbf{u} = -\begin{pmatrix} 0 \\ 0 \\ \rho/Fr^2 \\ 0 \end{pmatrix}.$$

Note that while only one of the conservative variables is changed, in primitive variables both the vertical velocity component and the pressure are affected, which has to be considered in the implementation. On the other hand, the heat source is modeled by

$$\frac{d}{dt}\mathbf{u} = \begin{pmatrix} 0 \\ 0 \\ 0 \\ Qq/M^2 \end{pmatrix}.$$

Thus, there is only an increase in the total energy component. As $p = (\gamma-1)(\rho E - \rho\frac{|\mathbf{v}|^2}{2})$, this increase has to be multiplied by $\gamma - 1$ before being added to the pressure, which is the only primitive variable to be changed. As $Qq$ is a constant, this equation can be integrated exactly by any first or higher order numerical scheme and the explicit Euler scheme will be used. We will also use the explicit Euler method for the gravitational source term.

## 5.2 A First Test Case

To analyze the behavior of our methods for flows subject to a buoyant force, we use a simple test problem. We consider a two dimensional longitudal section of a tunnel of five meter height with the bottom of the tunnel being at zero altitude, thus $\hat{x}_{2_r} = 0m$. For the velocity we use the initial data

$$\hat{v}_1 = const = 1\frac{m}{s} \text{ and } \hat{v}_2 = const = 0\frac{m}{s}.$$

We choose a pressure and density distribution which varies only in horizontal direction, such that the gravitational force term is balanced out by the pressure gradient. Thus we choose $\hat{p}(\hat{x}_2)$ and $\hat{\rho}(\hat{x}_2)$ according to (2.15):

$$\hat{p}(\hat{x}_2) = \hat{p}_r \left(1 - \frac{\hat{\Gamma}\hat{x}_2}{\hat{T}_r}\right)^{\hat{c}_p/\hat{R}}.$$

The pressure thus decays polynomially of order 3.5 with the height, thus in this case at a very small rate due to the height of a tunnel. From (2.16) we see that also the density distribution is a function of height:

$$\hat{\rho}(\hat{x}_2) = \frac{\hat{p}_r}{\hat{R}\hat{T}_r}\left(1 - \frac{\hat{\Gamma}\hat{x}_2}{\hat{T}_r}\right)^{\hat{c}_p/\hat{R}-1}.$$

For the discrete initial pressure, we simply use the above formula to determine pressure and density in the cell centers, which results in no variations in $x_1$-direction. For a reference pressure of 101325 $Pa$, we obtain an exact pressure difference from top to bottom of 63,4 $Pa$. Thus, the initial data corresponds approximately to a steady state. Approximately only, because the discrete equations have a slightly different steady state than the continuous equations. Nevertheless, the physical flux of the flow should balance with the gravitational force and there should be almost no energy flux in $x_2$-direction. The $\epsilon$ from the introduction is in this example zero, because we are exactly in hydrostatic balance. Thus the discretization error can be seen very well. We will use a cartesian grid with quadratic cells, where we employ twenty cells in $x_2$-direction.

### 5.2.1 Numerical Experiments

Given the above initial conditions, we use our method to compute a steady state numerically. The Mach number corresponding to the initial data is $Ma = 0.0036$. A first order operator splitting to take the gravitation into account is used, combined with the explicit Euler method in time and a first order discretization in space. The explicit Euler method is used despite the bad stability properties to eliminate possible influences from errors of the inner iterations. At the tunnel ends, Neumann boundary conditions are used.

For the first run, we use the unpreconditioned Lax-Friedrichs flux and a CFL number of 0.9. The solution after 5000 time steps is already a steady state and only slightly different from the initial conditions. A correct nearly linear distribution of the density is obtained and the pressure distribution changes slightly, while preserving the pressure difference of 63,4 $Pa$. This is probably due to the coarse grid and the fact that the discretization is only of first order.

The second run is done using the low Mach preconditioned Lax-Friedrichs flux. Here, also a nearly linear distribution of the density is obtained, but the pressure difference from top to bottom reduces to three Pascal after 5000 time steps with a CFL number of 0.0036. Then it increases again, but only slowly and after 100.000 time steps, a pressure difference of 54 $Pa$ is obtained.

The unpreconditioned method thus produces a physically reasonable result, while the preconditioned method does not. In particular, the scheme does not converge to the steady solution in a monotone way, which is not promising for unsteady computations. To illustrate the problem, we make a new experiment with the same initial data, but this time, only one time step of the flow solver without source terms is performed in both cases. For a cell in the middle of the tunnel, we obtain the following conservative fluxes:

| Preconditioned | Unpreconditioned |
|---|---|
| $1.58499 \cdot 10E-10$ | $1.88016 \cdot 10E-8$ |
| $1.58499 \cdot 10E-10$ | $1.88016 \cdot 10E-8$ |
| -0.324404 | -0.324404 |
| -1.83711 | -0.0034101 |

The physical flux update in the first step is $\mathbf{f} = (0, 0, \Delta p, 0)^T$. The energy flux in both cases is thus too big, but much worse so in the preconditioned case. This explains the different behavior in the pressure field which is connected to the inner energy.

## 5.3 Analysis of the Energy Flux

To understand this phenomenon, we compute the flux updates in an interior cell in the first step. The fluxes in $x_1$-direction cancel out, but along horizontal borders they differ and therefore the reason for the above demonstrated behavior must lie in the horizontal flux. We have for the preconditioned flux function with $\mathbf{n} = (0, 1)^T$:

$$\mathbf{f}^{LFP}(\mathbf{u}_L,\mathbf{u}_R;\mathbf{n}) = \frac{1}{2}(\mathbf{f}_L+\mathbf{f}_R-\mathbf{D}\Delta\mathbf{u}) = \frac{1}{2}(\begin{pmatrix}0\\0\\2p\\0\end{pmatrix} - \mathbf{D}\begin{pmatrix}\Delta\rho\\\Delta\rho\cdot v_1\\0\\\Delta E\end{pmatrix}).$$

The preconditioned flux is the same, though with the different dissipation matrix $\breve{\mathbf{D}}$. The energy component we are interested in depends only on the dissipation term and we obtain for the preconditioned case (see appendix C):

$$\begin{aligned}
\mathbf{D}_4\Delta\mathbf{u} &= |\lambda_1|\frac{|\mathbf{v}|^2}{2}\Big\{(1-\frac{(\gamma-1)|\mathbf{v}|^2}{2c^2})\Delta\rho+\frac{\gamma-1}{c^2}v_1(\Delta\rho v_2)+\frac{\gamma-1}{c^2}v_2\Delta(\rho v_2)\\
&\quad -\frac{\gamma-1}{c^2}\Delta(\rho E)\Big\}\\
&\quad -|\lambda_2|v_t[v_t\Delta\rho+n_2\Delta(\rho v_1)-n_1\Delta(\rho v_2)]\\
&\quad +\frac{1}{2\beta^2c^2\xi_3}\Big\{|\lambda_3|(H+\xi_1v_n)\Big[(\xi_2(\gamma-1)\frac{|\mathbf{v}|^2}{2}+\beta^2c^2v_n)\Delta\rho\\
&\quad -(\xi_2(\gamma-1)v_1+\beta^2c^2n_1)\Delta(\rho v_1)-(\xi_2(\gamma-1)v_2+\beta^2c^2n_2)\Delta(\rho v_2)\\
&\quad +(\gamma-1)\xi_2\Delta(\rho E)\Big]\\
&\quad +|\lambda_4|(H+\xi_2v_n)\Big[-(\xi_1(\gamma-1)\frac{|\mathbf{v}|^2}{2}+\beta^2c^2v_n)\Delta\rho\\
&\quad +(\xi_1(\gamma-1)v_1+\beta^2c^2n_1)\Delta(\rho v_1)+(\xi_1(\gamma-1)v_2+\beta^2c^2n_2)\Delta(\rho v_2)\\
&\quad -(\gamma-1)\xi_1\Delta(\rho E)\Big]\Big\}.
\end{aligned}$$

In this testcase, we have $v_n = v_2 = 0$ and thus, $\lambda_1 = \lambda_2 = 0$, as well as $\Delta(\rho v_2) = 0$. Thus, the above formula simplifies to

$$\begin{aligned}
\mathbf{D}_4\Delta\mathbf{u} &= \frac{H}{2\beta^2c^2\xi_3}\\
&\quad \Big(|\lambda_3|\Big[(\xi_2(\gamma-1)\frac{|\mathbf{v}|^2}{2}\Delta\rho-(\xi_2(\gamma-1)v_1+\beta^2c^2)\Delta(\rho v_1)+(\gamma-1)\xi_2\Delta(\rho E)\Big]\\
&\quad -|\lambda_4|\Big[(\xi_1(\gamma-1)\frac{|\mathbf{v}|^2}{2})\Delta\rho-(\xi_1(\gamma-1)v_1+\beta^2c^2)\Delta(\rho v_1)+(\gamma-1)\xi_1\Delta(\rho E))\Big]\Big)\\
&= \frac{H(\gamma-1)}{2\beta c\xi_3}(\xi_2-\xi_1)(\frac{|\mathbf{v}|^2}{2}\Delta\rho+v_1\Delta(\rho v_1)+\Delta(\rho E)),
\end{aligned}$$

as $|\lambda_4| = |\lambda_3| = \beta c$. Now, as in this case $\xi_2 - \xi_1$ equals $2\xi_3$, we obtain

$$f_4^{LFP} = \mathbf{D}_4 \Delta \mathbf{u} = \frac{H(\gamma-1)}{\beta c}\left(\frac{|\mathbf{v}|^2}{2}\Delta\rho + v_1\Delta(\rho v_1) + \Delta(\rho E)\right). \tag{5.1}$$

In the unpreconditioned case $\beta = 1$ the formula for the flux simplifies to:

$$f_4^{LF} = \breve{\mathbf{D}}_4 \Delta \mathbf{u} = \frac{H(\gamma-1)}{c}\left(\frac{|\mathbf{v}|^2}{2}\Delta\rho + v_1\Delta(\rho v_1) + \Delta(\rho E)\right). \tag{5.2}$$

Thus, the vertical fluxes differ by a factor of $1/\beta$. The update of a nonboundary cell is formed by the difference between the flux from the top of the cell and the flux from the bottom of the cell, as the numerical solution does not vary in $x_1$-direction. The update is though even in this simple testcase a complicated nonlinear function of the initial data. Nevertheless, we can deduct an asymptotic behavior. The total energy per unit volume $E$ and the total enthalpy per unit volume $H$ are $\mathcal{O}(M^{-2})$ if the nondimensionalization $\hat{p}_{ref} = \hat{\rho}_{ref}\hat{v}_{ref}^2$ is chosen. Thus, for a given initial pressure and density distribution in $x_2$-direction, we expect the update in the preconditioned case to increase of fourth order with the Mach number going to zero and in the unpreconditioned of third order. This can indeed be confirmed by numerical results. The tables show the energy flux update in an interior cell for the test problem at different Mach numbers.

| Mach number | 0.1 | 0.01 | 0.001 | 0.0001 | 0.00001 |
|---|---|---|---|---|---|
| Prec. flux | 0.001270 | 122.9158 | 1229132 | 12291317684 | $1.2291317658 \cdot 10E14$ |
| Unprec. flux | 0.001270 | 1.267485 | 1267.459 | 1267458.88783 | 1267458885.15 |

Vertical energy flux using a first order discretization at different Mach numbers

The flux behaves as predicted for Mach numbers smaller than 0.1, for higher Mach numbers the $\mathcal{O}(1)$ terms influence the flux. This effect of increasing flux can lead to steady states where the balance between the preconditioned flux and the gravitational source term is achieved at a very small and unphysical pressure difference. There are two ways to remedy this, as can be seen from (5.1). We can decrease the last factor and thereby the flux by decreasing the differences in the data either by refining the mesh or by using a method of higher order in space. In the same test case as above but using MUSCLE interpolation, the energy flux can be significantly decreased. This is demonstrated in the following tabular.

| Mach number | 0.1 | 0.01 | 0.001 | 0.0001 | 0.00001 |
|---|---|---|---|---|---|
| Prec. flux | $7.88449 \cdot 10E-9$ | 0.000854110 | 8.54112 | 85411.2 | 854111161 |
| Unprec. flux | $7.88449 \cdot 10E-9$ | $8.80744 \cdot 10E-6$ | 0.00880745 | 8.80745 | 8807.44 |

Vertical energy flux using a higher order discretization at different Mach numbers

The dependence on the Mach number is the same as in the first test case, as was expected after the analysis, but the size of the flux is decreased by a factor of $10^6$, which allows to

compute the correct pressure distribution up to an error of a few Pascal for moderately small Mach numbers. For $M = 10^{-5}$ a refinement of the grid is necessary, despite the higher order. Note that, as we have to use an implicit method due to the results from the stability analysis, decreasing the mesh width is not desirable, as this not only increases the number of unknowns, but also the condition number of the linear equation system to solve. Therefore, using the preconditioned approach with a first order discretization and an operator splitting is not a feasible method, a higher order discretization in space has to be used. Nevertheless, the results show that a pressure splitting as suggested in the introduction of this chapter is not necessary to compute a correct pressure distribution.

The reason for this is probably, that a linear pressure distribution is globally a very good approximation for the pressure field in a tunnel of five or ten meter height where one cell corresponds to about 25 cm. Thus the higher order method, which uses a linear representation in every cell has a very small discretization error in comparison to the first order method. For the meteorological problems considered by Botta, Klein, Langenberg and Lützenkirchen, where the height is on a scale of several kilometers and one cell is of the scale of dozens of meters, the pressure is truly nonlinear and this statement is no longer true.

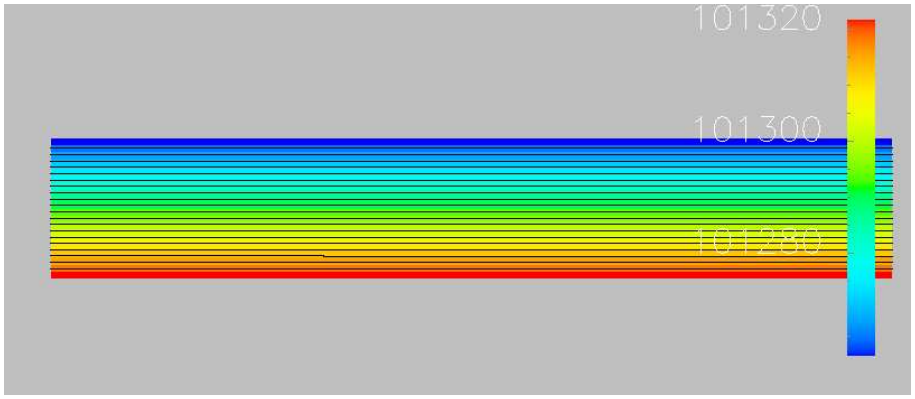


Figure 5.1: Pressure field in a small tunnel

Recently, Lee [32] demonstrated that for the here employed low Mach preconditioning techniques, the convergence rate towards the steady state is slowest in the energy equation and gets worse the smaller the Mach number. More, the convergence rate in the mass and momentum equations was not affected by the preconditioning. We believe that the above results are a pointer to why this is so.

## 5.4 Further Results for Buoyant Flows

To corroborate our impression that the higher order method is sufficient to compute the hydrostatic balance correctly, we proceed to more complicated test cases. The first is a

tunnel, where we prescribe a lower pressure at the outlet than at the inlet. There we expect a steady state, where the pressure isolines are still straight lines, but not parallel to the ceiling. This is indeed computed by the method using a higher order discretization in space, as shown by the next picture.

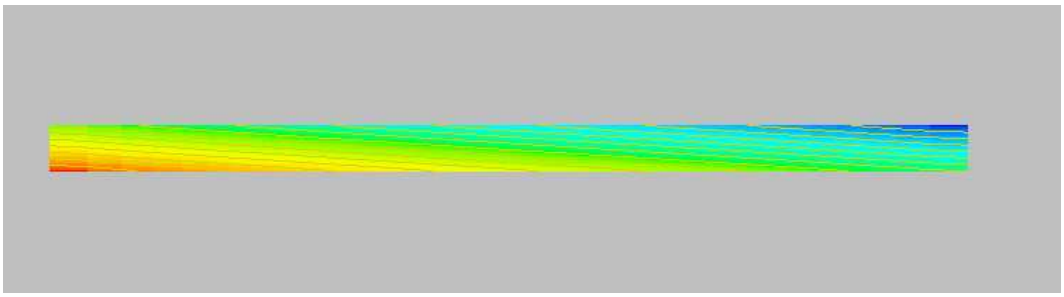

Figure 5.2: Pressure field with different inlet and outlet pressure

Furthermore, we computed the steady state in a short tunnel with two sharp bends. It starts level for six meters, then proceeds for 14 meters with a three % slope and continues again flat for another six meters. For the initial data, we use hydrostatic pressure and and a Mach number of 0.01. In the initial velocity field, the vertical component is set to zero. The expected pressure difference from formula (2.15) alone, which does not take the geometry into account, is 71 Pa. The computed pressure difference over all of the tunnel is 73.9 Pa. This is due to disturbances near the corners in the tunnel, which are the cause of the heightened pressure at the bottom of the first bend, which is higher than the pressure at the bottom of the entrance, as can be seen in figure 5.3. In the steady state, for a CFL number of 0.1 using the implicit midpoint rule, three Newton steps are needed and 16 or 17 GMRES iteration to reach the tolerance of $10^{-5}$ in the linear equation system.

## 5.5 Gravitation and a Heat Source

Having demonstrated that the preconditioned method is able to solve problems with gravitation, we now look at both gravitation and a heat source together. We skip the case where only the heat source is active, as this does not lead to interesting test cases.

For the first problem we consider, we use the sloped tunnel from above with the pressure and velocity field computed as a steady state as initial data. Then, a circular package of heat is placed near the entrance of the tunnel. The initial temperature in the hot zone is up to 450 Kelvin, as can be seen in picture 5.5. After 1.9 seconds, the package has moved with the flow about seven meters to the beginning of the slope and a bit upwards. The heat is distributed over a larger area with a temperature of 290 Kelvin in the hottest cell. Picture 5.6 shows that the package is no longer circular, but drawn out to the ceiling. After 3.7 seconds, the package has reached the second bend, which can be seen in picture 5.7. It is now more boomerang shaped, because the hottest air with a peak temperature of

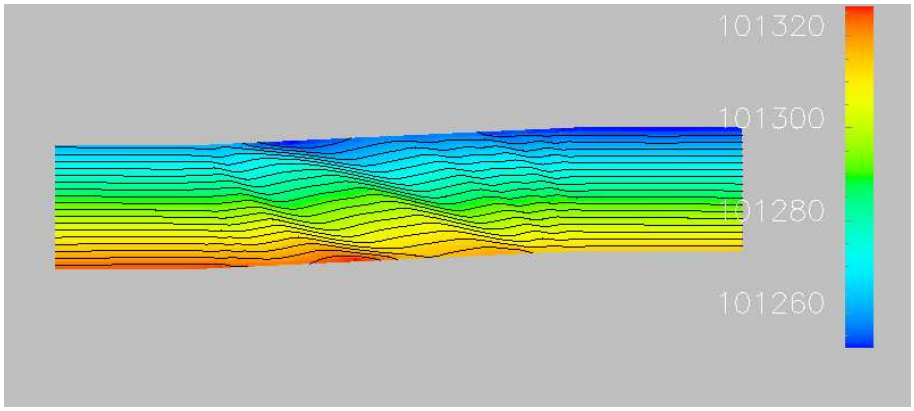


Figure 5.3: Pressure field in the bended tunnel

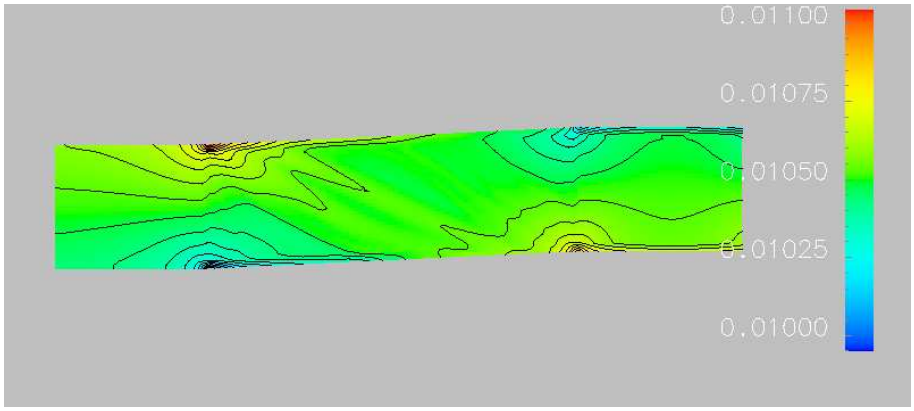


Figure 5.4: Mach number in the bended tunnel

285 Kelvin is in the center and flows toward the ceiling faster than the cooler parts of the packacke. This is what was expected to happen and thus we move on to fire events.

### 5.5.1 Simulation of a Fire Event

The final test case is similar to a fire event with a burning vehicle in the middle of a tunnel. We use a rectangular heat source of the size $3m \times 5m$, thus ranging from bottom to top of the tunnel. It is placed in the middle of a tunnel which is one kilometer long and has no slope. We expect the heat to get transported downstream with the flow and to stay primarily at the ceiling of the tunnel due to the buoancy forces. At the boundary, we prescribe the exact hydrostatic pressure as described in section 2.9. The initial conditions are obtained by first computing the steady state if the heat source is not active. As the prescribed data does not correspond exactly to the discrete solution, this steady state shows small disturbances near the tunnel entrance and exit, as can be seen in figure 5.6. However, these are only locally and do not lead to instabilities. This could in principal be diminished

by using Neumann boundary conditions to compute the steady state, where the pressure is not prescribed. However, it is not clear why using nonexact data at the boundary can increase the numerical solution.

We will perform three runs with different fires with a total power of ten MW, one MW and 0.1 MW. If we assume that the tunnel is ten meters wide, the heat source is distributed over a volume of $150m^3$ and we have to divide the total power by this to obtain the proper $\hat{q}_{ref}$. With an inflow Mach number of $Ma = 0.01$ this leads to a nondimensional parameter $Q$ of 32350, 3235 and 324, respectively, and the Froud number for a reference length of $\hat{x}_{ref} = 5m$ is $Fr = 0.488$. The grid we use is cartesian with $32 \times 464$ cells. These are smallest and quadratic in the middle of the tunnel and become thinner towards the exit, up to an aspect ratio of 1:16. The grid is demonstrated in the picture 5.9. This setting is similar to that described in [13], however there the fire is distributed over a volume of $400m^3$ and thus the power per unit volume is smaller. The position of the heat source is shown in picture 5.10. There, the light area marks the heat source, while the dark area is outside.

The simulations run until five seconds of realtime are reached. A first order operator splitting is used, for the time integration of the Euler equations we use the implicit midpoint rule. Up to three Newton steps are performed in every time step. Fewer steps are performed, if the euclidian norm of the relative nonlinear residual has dropped by a factor of 100 before. If this nonlinear tolerance was set to a factor of 10, divergence could happen. We start with a CFL number of 0.01, which is increased if fewer than three Newton steps were needed, up to a CFL number of 1.5. As for the linear equation systems, they are solved until the euclidian norm of the relative linear residual has dropped by a factor of $10^5$.

### 5.5.2 Description of the Results for the Fire Events

The pictures 5.11 up to 5.25 show the middle part of the tunnel at different times during the fire event. It can be clearly seen that the heat concentrates on the ceiling, due to the buoancy. Furthermore, it slowly drifts downstream, at about the rate of 3.6 m/s. A circulation of the flow, generated by hot air moving upwards can be seen in all cases in the velocity profiles or the Mach number distribution. Looking at the flow to the left and right of the fire, we see that the fire acts as a sort of wall for the flow. Downstream, the flow velocity decreases, but increases upstream. Another observation is that the speed of sound increases locally. This can be explained by the heat source: Additional heat leads to a boost in the internal energy, which is connected to the pressure, but not the total mass, and thus the speed of sound $c = \sqrt{\gamma \frac{p}{\rho}}$ is increased. This is bad for the time integration, because for a constant CFL number, an increase in the speed of sound leads to smaller time steps. In the case of the ten megawatt fire, this leads to a time step at five seconds, which is nearly ten times smaller than the time step at the beginning.

For the smallest fire with a total power of 0.1 megawatt, there is an increase of the temperature of only about two Kelvin. A propagation of hot air downstreams can be seen

for about 25 m. To the left of the fire, the temperature isolines are almost vertical, to the right the heat propagation concentrates near the cealing. The linear equation systems are so that for a CFL number of 0.7 we need 40 GMRES iterations per Newton step and three nonlinear iterations are needed in every time step.

After five seconds of the one megawatt fire event, the temperature has increased by about 30 Kelvin. To the left of the fire, the temperature isolines are almost vertical, to the right the heat propagation concentrates near the cealing. An effect of the fire can be observed up to twenty meters downstream, which coincides with the flow velocity. Three Newton iterations are needed in every time step, the linear equation systems are such that for a CFL number of one, 40-70 GMRES iterations are needed to fulfill the tolerance.

For the ten mega watt fire, the increase in temperature is immense, actually several thousand degrees Kelvin, in one single cell it is up to 14.000 Kelvin. However, this extreme heat is only in the top layer of cells. In the cells in the line next to the top, the temperature is between seven and eight tousand degrees Kelvin. and two meters away from the ceiling, directly in the area of the heat source, the temperature is less than one tousand Kelvin. Near the ceiling, there is a propagation of heat in upstream direction which leads to a strong shock. This is probably due to the extreme temperature gradients which leads to large pressure gradients which cause the air to move upstreams. Thus it can be observed, that the flow is absolutely not incompressible. To the right, the hot air has propagated up to 40 m.

As already pointed out in section 4.2.1, the linear equation systems are hard to solve. Already for CFL numbers around 0.5, a 100 GMRES iterations and more are needed. The computation takes about three days on a one GHz Pentium to compute one second of realtime. This is due to the large number of GMRES iterations: if three Newton steps are needed, as was usually the case, about 300 GMRES iterations are performed. The problem is thus significantly more difficult to solve than for the scenarios with less powerful fires, both for the nonlinear and the linear equations systems. It is also quite clear that the method is much too slow to be applied in practice, where the goal is to perform parameter studies on a PC.

A computation on a longer time scale is shown in figures 5.20 to 5.25. The one megawatt tunnel fire was computed beyond the five seconds, up to ten and twenty seconds real time. The heat does not increase significantly anymore, and the propagation of heat downstream is according to the basic flow velocity. The air circulates between bottom and ceiling, but in a steady way. This can also be seen in the nonlinear equation systems, where now one or at most two Newton steps are sufficient.

An important aspect of the analysis was the correct computation of the pressure field. Therefore, we take a close look at the numerical results for the pressure. There we see that for all flows, the pressure isolines become bended from vertical lines to flat parabolas. This was expected, as the heat increases inner and kinetic energy. The gradient of the inner energy is connected to the pressure by the equation of state and thus leads to a force. In horizontal direction this is balanced out by the gravitational force, which is why the isolines remain essentially vertical. In vertical direction, the gradient is there because we have a

continuous input of heat and thus the isolines become bended. However, even the shock for ten mega watt can only be seen as a very small disturbance in the pressure field, which is because we have a low Mach number and pressure differences even out very quickly if not balanced by some force. Thus, the method computes a physically reasonable pressure distribution. This can be seen in figure 5.26.

All in all, the numerical results are in agreement with physics as far as we can tell. In all cases the heat gets transported to the ceiling and propagates fastest downstream, where the additional kinetic energy through the fire leads to a significantly faster propagation for the stronger heat source. The pressure field is in line with the expectations.

### 5.5.3 Influence of the CFL Number

To illustrate the impact of the CFL number on the equation systems, we use the difficult problem with a ten megawatt fire after five seconds of real time and perform a single time step, using different CFL numbers.

| | Preconditioned | | Unpreconditioned | |
|---|---|---|---|---|
| CFL number | Newton steps | GMRES iterations | Newton steps | GMRES iterations |
| 0.1 | 3 | 50, 54, 51 | 1 | 3 |
| 0.5 | 3 | 84, 90, 91 | 2 | 5, 5 |
| 2.0 | 2 | 135, 146 | 3 | 9, 9, 9 |

Impact of the time step size on inner and outer iterations

As can be seen in the tabular, already for a CFL number of two, more than 100 GMRES iterations are needed in the preconditioned case. If we do not use low Mach number preconditioning, the linear equation systems are solved nearly immediately. However, already after one step, irregularities in the pressure field in the area of the heat source, can be observed. Furthermore, we would like to point out, that a restarted GMRES with a restart length of 40 needs seven restarts in the preconditioned case for a CFL number of two.

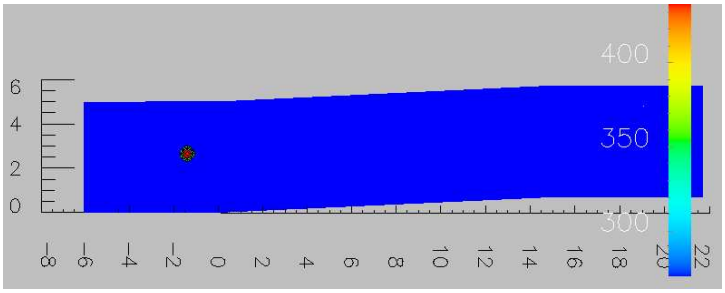


Figure 5.5: Initial position of the package of heat in the bended tunnel

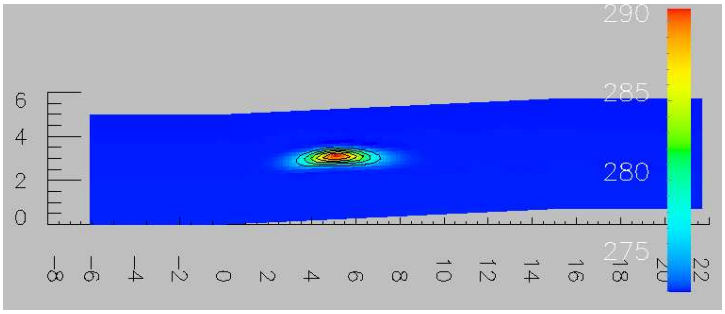


Figure 5.6: Temperature distribution after 1.9 seconds

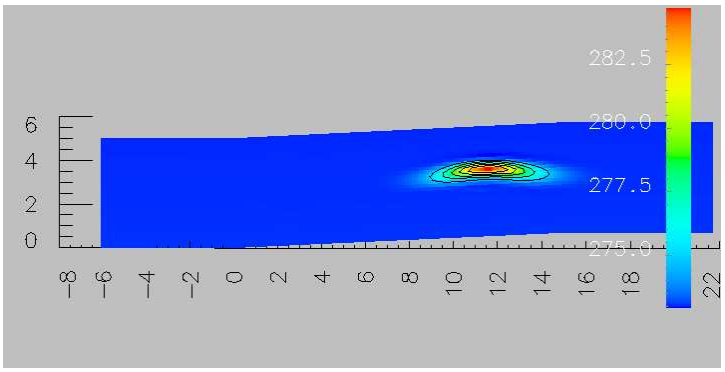


Figure 5.7: Temperature distribution after 3.7 seconds

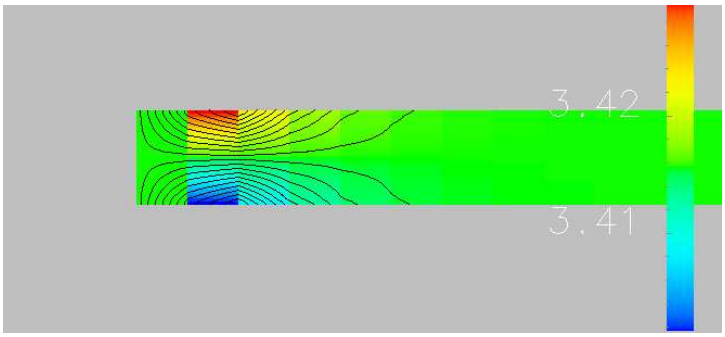


Figure 5.8: Influence of boundary conditions on intial solution $v_1$

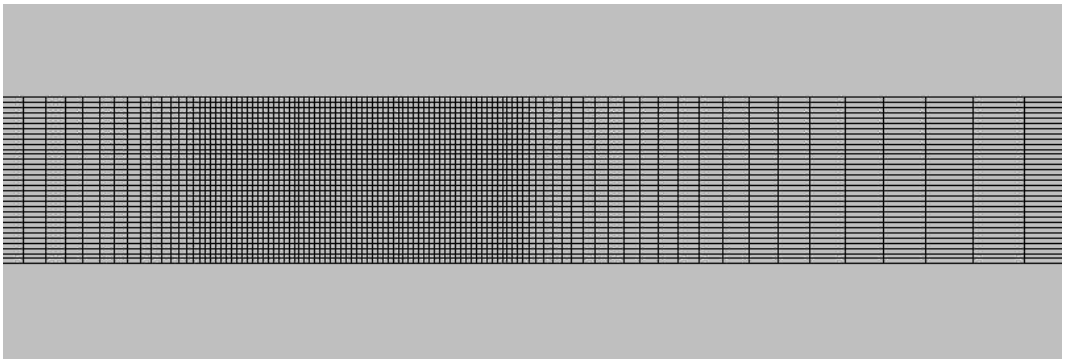

Figure 5.9: Segment of the grid

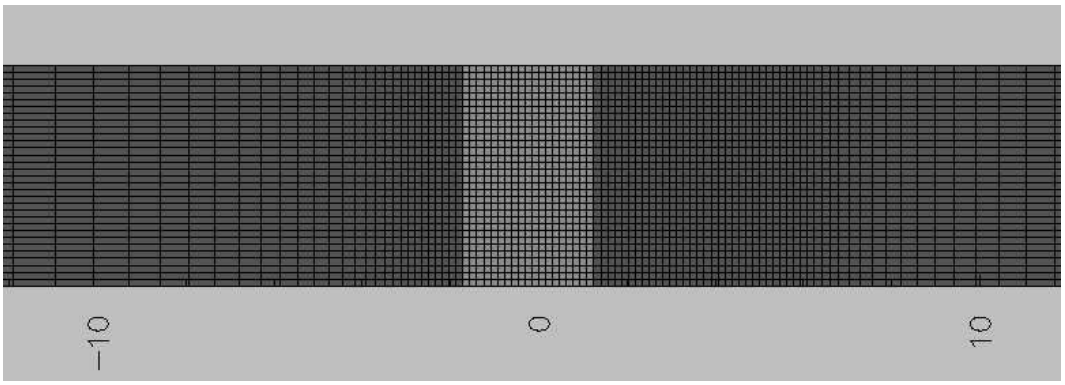


Figure 5.10: Position of the heat source in the tunnel

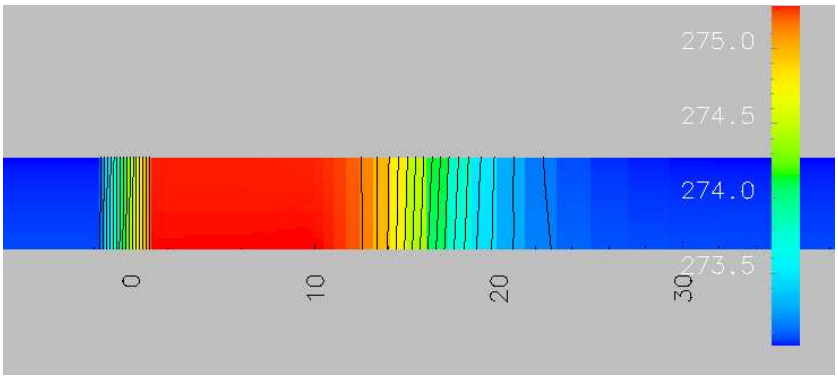


Figure 5.11: Temperature for 0.1 MW after 5 seconds

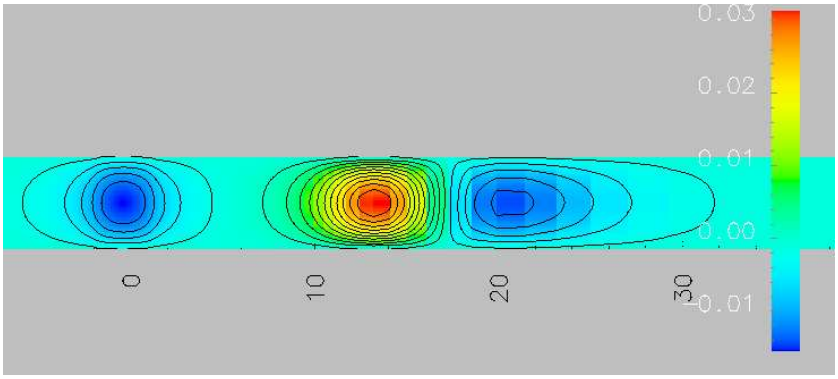


Figure 5.12: Horizontal velocity for 0.1 MW after 5 seconds

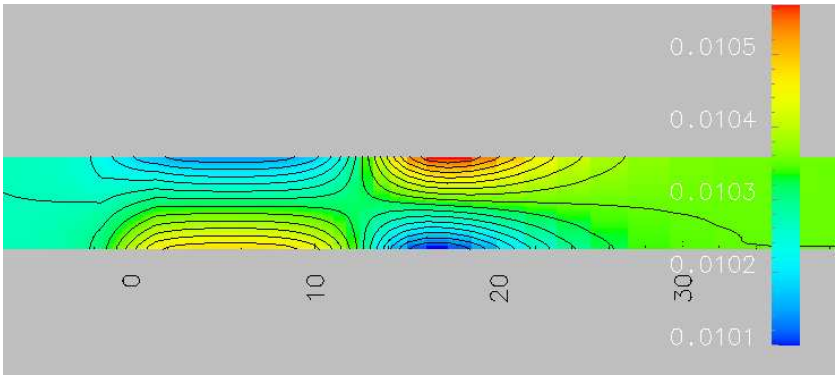


Figure 5.13: Mach number for 0.1 MW after 5 seconds

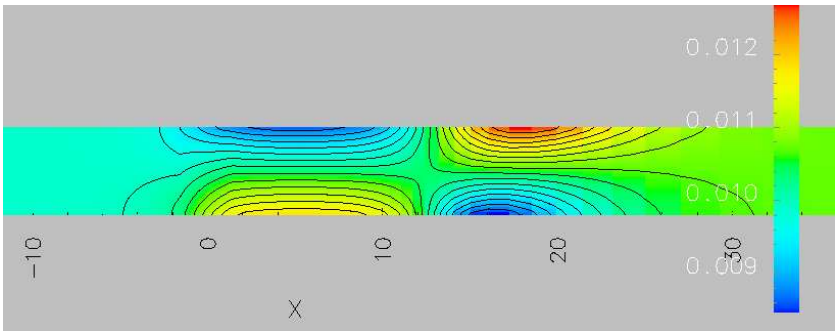


Figure 5.14: Mach number for 1 MW after 5 seconds

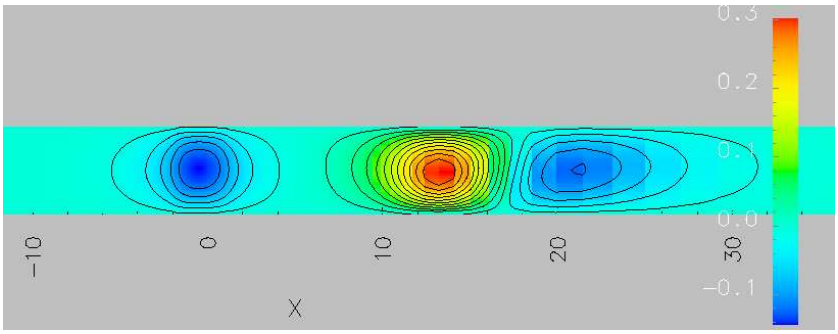


Figure 5.15: Horizontal velocity for 1 MW after 5 seconds

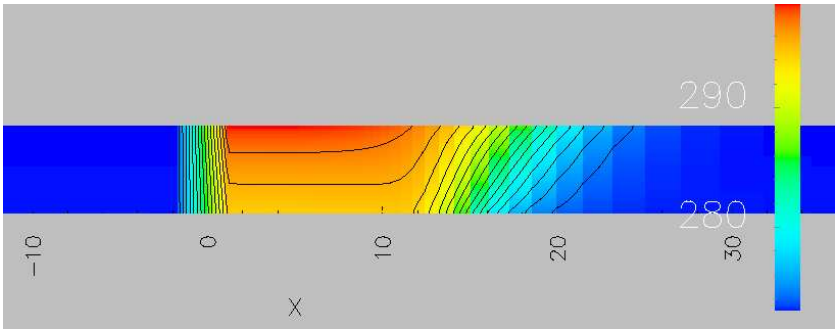


Figure 5.16: Temperature for 1 MW after 5 seconds

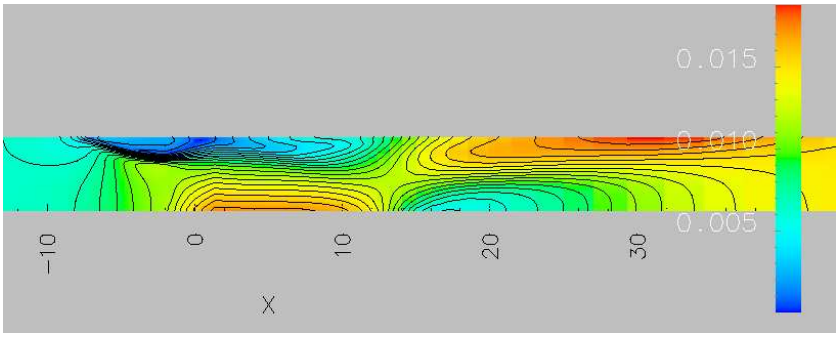


Figure 5.17: Mach number for 10 MW after 5 seconds

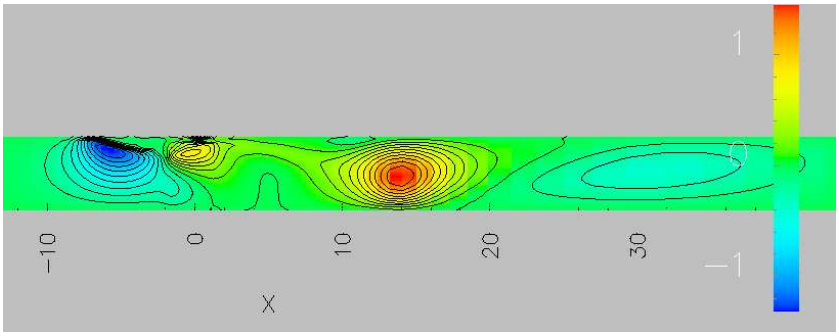


Figure 5.18: Horizontal velocity for 10 MW after 5 seconds

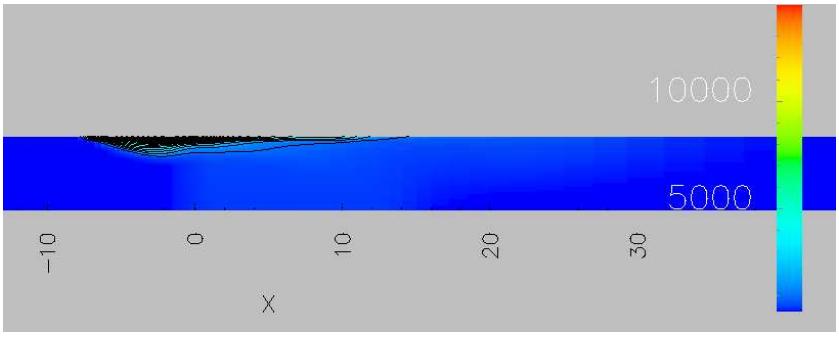


Figure 5.19: Temperature for 10 MW after 5 seconds

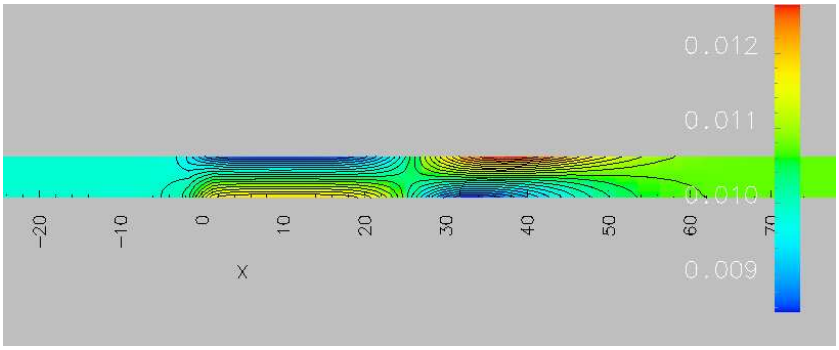


Figure 5.20: Mach number for 1 MW after 10 seconds

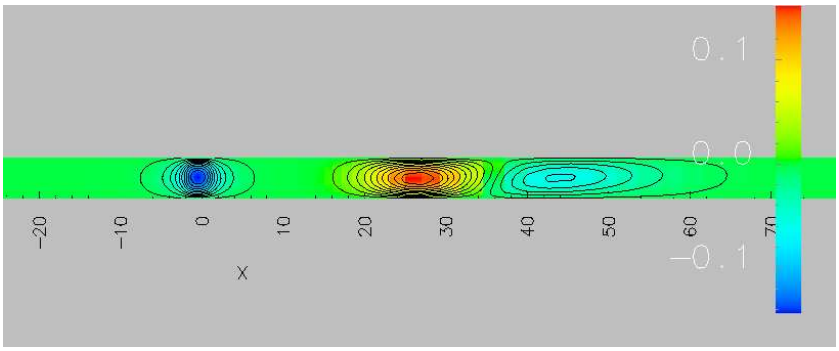


Figure 5.21: Horizontal velocity for 1 MW after 10 seconds

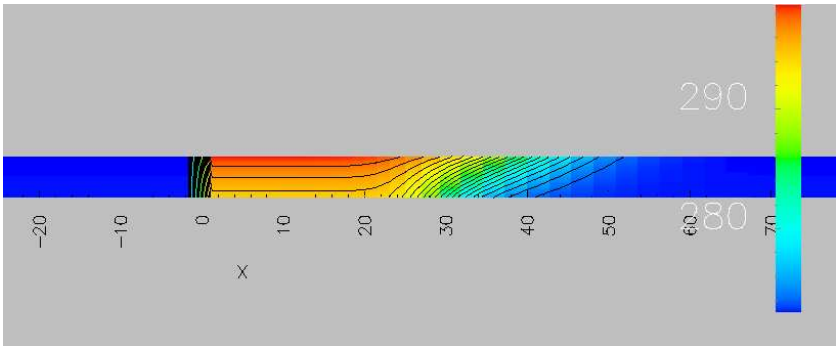


Figure 5.22: Temperature for 1 MW after 10 seconds

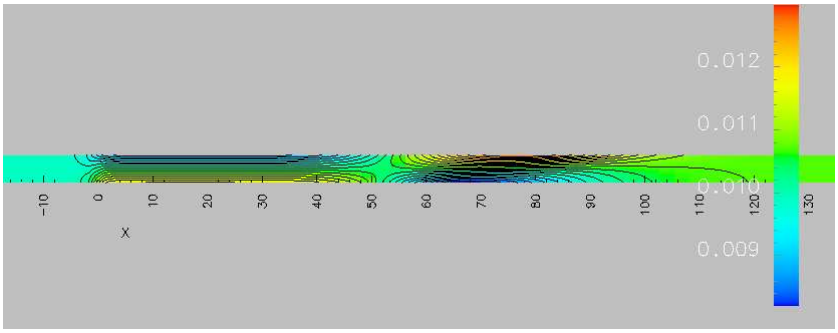


Figure 5.23: Mach number for 1 MW after 20 seconds

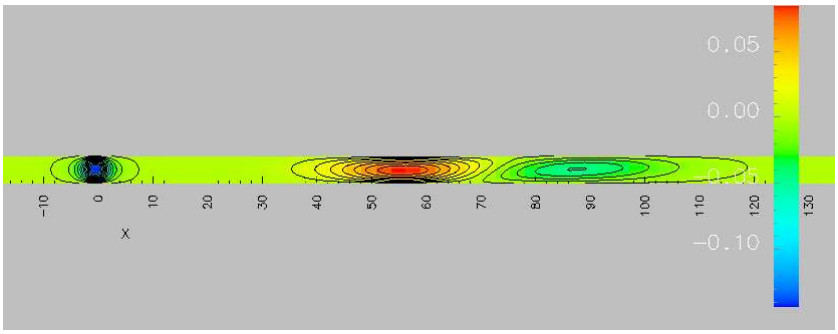


Figure 5.24: Horizontal velocity for 1 MW after 20 seconds

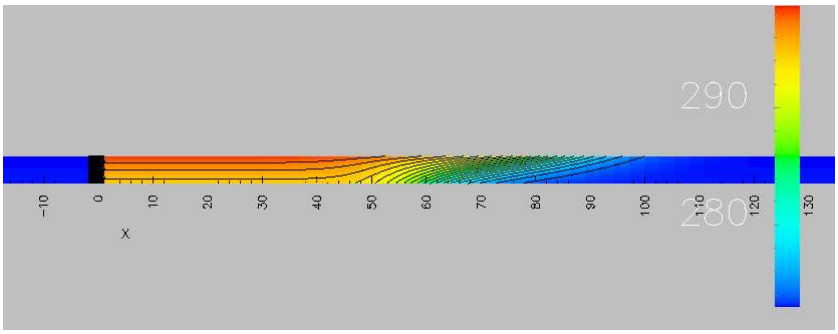


Figure 5.25: Temperature for 1 MW after 20 seconds

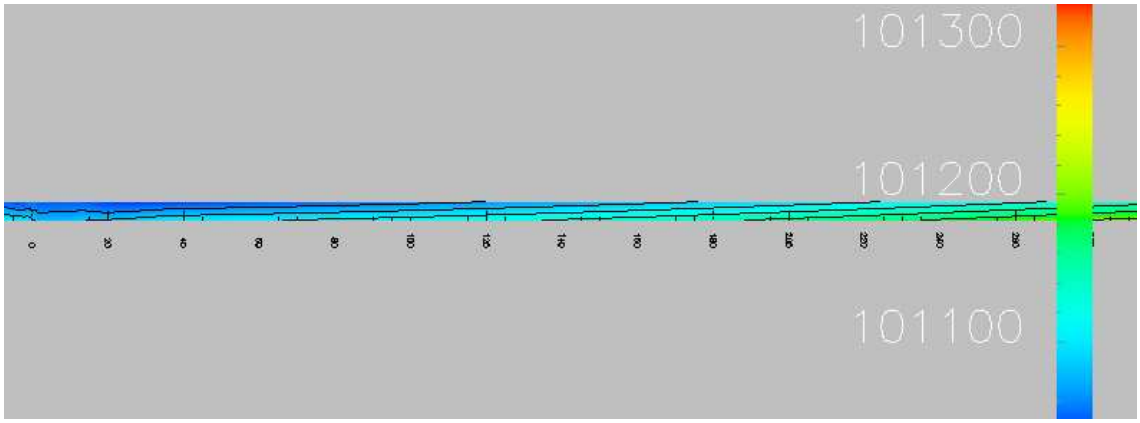


Figure 5.26: Pressure field during the fire event

# Chapter 6

# Summary and Outlook

In the thesis, a class of preconditioning techniques was used to extend the validity of a density based flow solver into the low Mach number regime. The behavior of the preconditioned schemes with respect to the class parameters was analyzed and thus the regime of suitable parameters could be narrowed down. For the remaining schemes, a stability analysis was performed. A von Neumann stability analysis showed that the stability region of the corresponding explicit scheme gets smaller with $M^2$, as $M$ tends to zero, thus rendering the explicit scheme unapplicable. Thus, implicit time integration methods have to be used in this context.

The method was then applied to problems with gravitation. There, the incorporation of the gravitational source term posed special difficulties. It was shown that a first order discretization needs an unacceptable fine grid in this context and that higher order discretizations have to be used.

Finally, in addition to gravitation, a heat source term was included in the model to simulate tunnel fires. Several test cases demonstrate the feasibility of the method.

The thesis focused on properties of the discretization. It turned out in the test problems that the solution algorithm for the appearing linear equation systems is unsatisfactory slow. Further work is thus required for the development of a fast solution algorithm. A better linear preconditioner for these problems might improve the speed dramatically. Once this is achieved, further test cases on longer time scales can be computed to compare with results obtained in experiments or by other authors.

# Appendix A

# One Dimensional Terms

In one spatial dimension, the transformation matrices between conserved and entropic variables are given by:

$$\mathbf{U} = \frac{\partial \mathbf{u}}{\partial \mathbf{w}} = \begin{pmatrix} \frac{1}{c^2} & 0 & -\frac{\rho}{\gamma} \\ \frac{v}{c^2} & \rho & -\frac{\rho v}{\gamma} \\ \frac{H}{c^2} & \rho v & -\frac{\rho |v|^2}{2\gamma} \end{pmatrix} \quad \text{and} \tag{A.1}$$

$$\mathbf{W} = \frac{\partial \mathbf{w}}{\partial \mathbf{u}} = \begin{pmatrix} \frac{1}{2}(\gamma-1)|v|^2 & -(\gamma-1)v & \gamma-1 \\ -\frac{v}{\rho} & \frac{1}{\rho} & 0 \\ \frac{(\gamma-1)|v|^2}{2p} - \frac{\gamma}{\rho} & -\frac{(\gamma-1)v}{p} & \frac{\gamma-1}{p} \end{pmatrix}. \tag{A.2}$$

The preconditioner is given by

$$\mathbf{Q} = \begin{pmatrix} \beta^2 & 0 & 0 \\ -\frac{\alpha v}{\rho c^2} & 1 & 0 \\ 0 & 0 & 1 \end{pmatrix}.$$

The matrices of eigenvectors that diagonalize the preconditioned Jacobian in entropy formulation are:

$$\mathbf{S} = \begin{pmatrix} 0 & 1 & 1 \\ 0 & \frac{\xi_1}{\rho\beta^2 c^2} & \frac{\xi_2}{\rho\beta^2 c^2} \\ 1 & 0 & 0 \end{pmatrix} \text{ and } \mathbf{S}^{-1} = \begin{pmatrix} 0 & 0 & 1 \\ \frac{\xi_2}{2\xi_3} & -\frac{\rho\beta^2 c^2}{2\xi_3} & 0 \\ -\frac{\xi_1}{2\xi_3} & \frac{\rho\beta^2 c^2}{2\xi_3} & 0 \end{pmatrix}. \tag{A.3}$$

Thus, we can compute the preconditioned dissipation matrix (4.20)

$$\bar{\mathbf{D}} = \mathbf{Q}^{-1}\mathbf{S}|\mathbf{\Lambda}|\mathbf{S}^{-1} = (\bar{d}_{ij})_{i,j=1,2,3} \tag{A.4}$$

with $\bar{d}_{3,1} = \bar{d}_{3,2} = \bar{d}_{2,3} = \bar{d}_{1,3} = 0$, $\bar{d}_{3,3} = |\lambda_1|$,
$\bar{d}_{1,1} = \frac{|\lambda_2|\xi_2 - |\lambda_3|\xi_1}{2\beta^2\xi_3}$, $\bar{d}_{1,2} = \frac{c^2\rho}{2\xi_3}(|\lambda_3| - |\lambda_2|)$,
$\bar{d}_{2,1} = \frac{\alpha v}{\rho c^2 2\xi_3}(|\lambda_2|\xi_2 - |\lambda_3|\xi_1) + \frac{\xi_1\xi_2}{2\beta^2 c^2\rho\xi_3}(|\lambda_2| - |\lambda_3|)$ and
$\bar{d}_{2,2} = \frac{\beta^2\alpha v}{2\xi_3}(|\lambda_3| - |\lambda_2|) + \frac{|\lambda_3|\xi_2 - |\lambda_2|\xi_1}{2\xi_3}$.
This matrix has the eigenvalues $\mu_1 = v_n$ and $\mu_{2,3} = \frac{a \pm \sqrt{b}}{2\xi_3}$ with

$$a = -\beta^2 c^2 - c^2 + \frac{\alpha}{2}(3v^2 - \beta^4 v + \beta^2 v^2 - \beta^2 v) + \frac{\alpha^2}{2}(\beta^2 v - v^2) \text{ and}$$

$$\begin{aligned} b \;=\; & \beta^4 v^2\alpha^4 + 4\beta^4 c^4 - 4\beta^4\alpha^2 v c^2 + \beta^4\alpha^2 v^2 + 2\beta^6 v^2\alpha^2 - 2\beta^6\alpha^2 v^3 - 2\beta^4\alpha^3 v^2 + 4\beta^4\alpha^3 v^3 \\ & -2\beta^2\alpha^4 v^3 - 2\beta^6\alpha^3 v^2 - 6\beta^2 v^3\alpha^2 - 7\beta^4 v^4\alpha^2 + 4\beta^2 v^3\alpha + \beta^8 v^2\alpha^2 + \alpha^4 v^4 - 6v^4\alpha^3 \\ & +4\beta^6 c^2\alpha v - 4v^2\alpha^2\beta^2 c^2 - 4v^2 c^2\beta^4 - 8\beta^2 c^4 - 4\beta^2 c^2 v\alpha + 4\beta^4 v^2 c^2\alpha + 4c^4 + 4v^4 \\ & +4\alpha^3 v^3\beta^2 - 4\beta^6 v^3\alpha + 6\beta^2 v^4\alpha^2 + 2\beta^2 v^4\alpha^3 + 4v^4\beta^6\alpha + 24v^2\beta^2 c^2 - 4c^2\alpha v^2 - 4v^2 c^2 \\ & +4\beta^2\alpha^2 v c^2 - 8\beta^2 v^4 - 8v^4\alpha + 13v^4\alpha^2 + 4v^4\beta^4 - 12v^4\beta^2\alpha. \end{aligned}$$

# Appendix B

# Rotational Invariance of the Lax-Friedrichs Flux

The Lax-Friedrichs Flux is given by (3.6):

$$\mathbf{f}^{LF}(\mathbf{u}_L, \mathbf{u}_R; \mathbf{n}) = \frac{1}{2}(\mathbf{f}(\mathbf{u}_L) + \mathbf{f}(\mathbf{u}_R))\mathbf{n} - \breve{\mathbf{D}}(\mathbf{u}_L, \mathbf{u}_R; \mathbf{n}) \cdot (\mathbf{u}_R - \mathbf{u}_L)),$$

where we have a matrix valued dissipation term

$$\breve{\mathbf{D}}(\mathbf{u}_L, \mathbf{u}_R; \mathbf{n}) = \breve{\mathbf{R}}(\frac{\mathbf{u}_L + \mathbf{u}_R}{2}; \mathbf{n})|\breve{\mathbf{\Lambda}}|(\frac{\mathbf{u}_L + \mathbf{u}_R}{2}; \mathbf{n})\breve{\mathbf{R}}^{-1}(\frac{\mathbf{u}_L + \mathbf{u}_R}{2}; \mathbf{n}).$$

Here, $\breve{\mathbf{R}}$ is the matrix of the conservative right eigenvalues and $|\breve{\mathbf{\Lambda}}|$ is a diagonalmatrix consisting of absolute values of the eigenvalues. Thus $\breve{\mathbf{R}}$ is given by

$$\breve{\mathbf{R}}(\mathbf{u}; \mathbf{n}) = \begin{pmatrix} 1 & 0 & \frac{\rho}{2c} & \frac{\rho}{2c} \\ v_1 & \rho n_2 & \frac{\rho}{2c}(v_1 + cn_1) & \frac{\rho}{2c}(v_1 - an_1) \\ v_2 & -\rho n_1 & \frac{\rho}{2c}(v_2 + cn_2) & \frac{\rho}{2c}(v_2 - an_2) \\ \frac{|v|^2}{2} & \rho(v_1 n_2 - v_2 n_1) & \frac{\rho}{2c}(E + \frac{p}{\rho} + cv \cdot n) & \frac{\rho}{2c}(E + \frac{p}{\rho} - cv \cdot n) \end{pmatrix}.$$

We want to prove the rotational invariance of this numerical flux function. Therefore, given

$$\mathbf{T}(\mathbf{n}) = \begin{pmatrix} 1 & 0 & 0 & 0 \\ 0 & n_1 & n_2 & 0 \\ 0 & -n_2 & n_1 & 0 \\ 0 & 0 & 0 & 1 \end{pmatrix},$$

we want to show that

$$\mathbf{T}^{-1}(\mathbf{n})\mathbf{f}^{LF}(\mathbf{T}(\mathbf{n})\mathbf{u}_L, \mathbf{T}(\mathbf{n})\mathbf{u}_R; (1,0)^T) = \mathbf{f}^{LF}(\mathbf{u}_L, \mathbf{u}_R; \mathbf{n}).$$

With $\mathbf{x} = \mathbf{T}(\mathbf{n})\mathbf{u}_L$ and $\mathbf{y} = \mathbf{T}(\mathbf{n})\mathbf{u}_R$, we have

$$\begin{aligned}
\mathbf{T}^{-1}(\mathbf{n})\mathbf{f}^{LF}(\mathbf{x}, \mathbf{y}; (1,0)^T) &= \mathbf{T}^{-1}(\mathbf{n})\frac{1}{2}(\mathbf{f}(\mathbf{x}) + \mathbf{f}(\mathbf{y}))(1,0)^T \\
&\quad -\breve{\mathbf{R}}(\frac{\mathbf{x}+\mathbf{y}}{2}; (1,0)^T)|\breve{\mathbf{\Lambda}}|\breve{\mathbf{R}}^{-1}(\frac{\mathbf{x}+\mathbf{y}}{2}; (1,0)^T))(\mathbf{y}-\mathbf{x}) \\
&= \mathbf{T}^{-1}(\mathbf{n})\frac{1}{2}(f_1(\mathbf{x}) + \mathbf{f}_1(\mathbf{y}) - \breve{\mathbf{D}}(\mathbf{x}, \mathbf{y}; (1,0)^T)(\mathbf{y}-\mathbf{x})) \\
&= \frac{1}{2}(\mathbf{f}(\mathbf{u}_L) + \mathbf{f}(\mathbf{u}_R) - \mathbf{T}^{-1}(\mathbf{n})\breve{\mathbf{D}}(\mathbf{x}, \mathbf{y}; (1,0)^T)(\mathbf{y}-\mathbf{x})).
\end{aligned}$$

We will now look at the last part:

$$\begin{aligned}
\mathbf{T}^{-1}(\mathbf{n})\breve{\mathbf{D}}(\mathbf{x}, \mathbf{y}; (1,0)^T)(\mathbf{y}-\mathbf{x}) &= \mathbf{T}^{-1}(\mathbf{n})\breve{\mathbf{R}}(\frac{\mathbf{x}+\mathbf{y}}{2}; (1,0)^T)|\breve{\mathbf{\Lambda}}|\breve{\mathbf{R}}^{-1}\mathbf{T}(\mathbf{n})(\mathbf{u}_R - \mathbf{u}_L) \\
&= \mathbf{T}^{-1}\breve{\mathbf{R}}|\breve{\mathbf{\Lambda}}|\breve{\mathbf{R}}^{-1}\mathbf{T}\mathbf{T}^{-1}\mathbf{T}(\mathbf{u}_R - \mathbf{u}_L),
\end{aligned}$$

with

$$\breve{\mathbf{R}}(\mathbf{T}(\mathbf{u}); (1,0)^T) = \begin{pmatrix} 1 & 0 & \frac{\rho}{2c} & \frac{\rho}{2c} \\ v_n & 0 & \frac{\rho}{2c}(v_n + c) & \frac{\rho}{2c}(v_n - c) \\ v_t & -\rho & \frac{\rho}{2c}v_t & \frac{\rho}{2c}v_t \\ \frac{|\mathbf{v}|^2}{2} & -\rho v_t & \frac{\rho}{2c}(E + \frac{p}{\rho} + cv_n) & \frac{\rho}{2c}(E + \frac{p}{\rho} - cv_n) \end{pmatrix}.$$

Because $\tilde{\mathbf{T}}(\mathbf{n})$ is a rotation matrix, it does not change scalar products of $\mathbf{v}$ and $\mathbf{n}$. Therefore, the eigenvalues remain the same and so does the diagonal matrix $|\breve{\mathbf{\Lambda}}|$. It is therefore sufficient to show that $\breve{\mathbf{R}}(\frac{\mathbf{x}+\mathbf{y}}{2}, (1,0)^T) = \mathbf{T}(\mathbf{n})\breve{\mathbf{R}}(\frac{\mathbf{u}_L+\mathbf{u}_R}{2}; \mathbf{n})$. For this, we first note that only the directions of $\mathbf{v}$ and $\mathbf{n}$ are affected by the rotation. It is therefore immediately clear that the first line of the two matrices is equal.

A simple calculation using $\mathbf{v} \cdot \mathbf{n} = v_n$ and $\mathbf{v} \cdot (n_2, -n_1)^T = v_t$ shows that this is also true for the second and third line. For the fourth line, we have to show that the change of variables through $\mathbf{T}$ does not affect the values of the matrix, which can easily be seen, as $\tilde{\mathbf{T}}(\mathbf{n})$ does not change scalar products.

# Appendix C

# The Preconditioned Flux

For the computation of the components of the dissipation vector (see (3.7))

$$\mathbf{D}\Delta\mathbf{u} = \mathbf{P}^{-1}\mathbf{R}|\mathbf{\Lambda}|\mathbf{R}^{-1}\Delta\mathbf{u}$$

for the relevant case $\alpha = 0$, we use the decomposition $\mathbf{D} = \mathbf{T}^g|\mathbf{\Lambda}|\mathbf{T}^d$, with

$$\mathbf{T}^g = \mathbf{P}^{-1}\mathbf{R}diag\{-\frac{\rho}{\gamma}, -\rho, 2, 2\}^{-1} \text{ and } \mathbf{T}^d = diag\{-\frac{\rho}{\gamma}, -\rho, 2, 2\}\mathbf{R}^{-1}.$$

Thus the auxiliary matrices $\mathbf{T}^g$ and $\mathbf{T}^d$ are given by

$$\mathbf{T}^g = \begin{pmatrix} 1 & 0 & \frac{1}{2\beta^\nu c^2} & \frac{1}{2\beta^\nu c^2} \\ v_1 & n_2 & \frac{1}{2\beta^\nu c^2}(v_1 + \xi_1 n_1) & \frac{1}{2\beta^\nu c^2}(v_1 + \xi_2 n_1) \\ v_2 & -n_1 & \frac{1}{2\beta^\nu c^2}(v_2 + \xi_1 n_2) & \frac{1}{2\beta^\nu c^2}(v_2 + \xi_2 n_2) \\ \frac{|\mathbf{v}|^2}{2} & -v_t & \frac{1}{2\beta^\nu c^2}(H + \xi_1 v_n) & \frac{1}{2\beta^\nu c^2}(H + \xi_2 v_n) \end{pmatrix}$$

and

$$\mathbf{T}^d = \begin{pmatrix} 1 - \frac{(\gamma-1)|\mathbf{v}|^2}{2c^2} & \frac{(\gamma-1)v_1}{c^2} & \frac{(\gamma-1)v_2}{c^2} & \frac{\gamma-1}{c^2} \\ v_t & n_2 & -n_1 & 0 \\ \frac{\xi_2(\gamma-1)\frac{|\mathbf{v}|^2}{2} + \beta^\nu c^2 v_n}{\xi_3} & -\frac{\xi_2(\gamma-1)v_1 + \beta^\nu c^2 n_1}{\xi_3} & -\frac{\xi_2(\gamma-1)v_2 + \beta^\nu c^2 n_2}{\xi_3} & \frac{\xi_2(\gamma-1)}{\xi_3} \\ \frac{\xi_1(\gamma-1)\frac{|\mathbf{v}|^2}{2} + \beta^\nu c^2 v_n}{\xi_3} & -\frac{\xi_1(\gamma-1)v_1 + \beta^\nu c^2 n_1}{\xi_3} & -\frac{\xi_1(\gamma-1)v_2 + \beta^\nu c^2 n_2}{\xi_3} & -\frac{\xi_1(\gamma-1)}{\xi_3} \end{pmatrix}.$$

We obtain:

$$\mathbf{D}_1(\mathbf{u}_R - \mathbf{u}_L) \;=\; |\lambda_1|(\Delta_{ji}\rho + \frac{\gamma-1}{c^2}\left(-\frac{|\mathbf{v}|^2}{2}\Delta_{ji}\rho + v_1\Delta_{ji}m_1 + v_2\Delta_{ji}m_2 - \Delta_{ji}(\rho E)\right))$$

$$
\begin{aligned}
&+\frac{1}{2\beta^\nu c^2\xi_3}\Big[|\lambda_3|((\xi_2\frac{(\gamma-1)|\mathbf{v}|^2}{2}+\beta^\nu c^2 v_n)\Delta_{ji}\rho\\
&-(\xi_2(\gamma-1)v_1+\beta^\nu c^2 n_1)\Delta_{ji}m_1-(\xi_2(\gamma-1)v_2+\beta^\nu c^2 n_2)\Delta_{ji}m_2)\\
&+|\lambda_4|(-(\xi_1\frac{(\gamma-1)|v|^2}{2}+\beta^\nu c^2 v_n)\Delta_{ji}\rho+(\xi_1(\gamma-1)v_1+\beta^\nu c^2 n_1)\Delta_{ji}m_1\\
&+(\xi_1(\gamma-1)v_2+\beta^\nu c^2 n_2)\Delta_{ji}m_2)+(\gamma-1)(|\lambda_3|\xi_2-|\lambda_4|\xi_1)\Delta_{ji}(\rho E)\Big]\,,
\end{aligned}
$$

$$
\begin{aligned}
\mathbf{D}_2(\mathbf{u}_j-\mathbf{u}_i) &= |v_n|[v_1\Delta_{ji}\rho+v_1\tfrac{\gamma-1}{c^2}(-\tfrac{|\mathbf{v}|^2}{2}\Delta_{ji}\rho+v_1\Delta_{ji}m_1+v_2\Delta_{ji}m_2-\Delta_{ji}(\rho E))\\
&\quad +n_2(v_t\Delta_{ji}\rho+n_2\Delta_{ji}m_1-n_1\Delta_{ji}m_2)]\\
&\quad +\tfrac{1}{2\beta^\nu c^2\xi_3}\,[|\lambda_3|(v_1+\xi_1 n_1)\\
&\quad \Big((\xi_2(\gamma-1)\tfrac{|\mathbf{v}|^2}{2}+\beta^\nu c^2 v_n)\Delta_{ji}\rho-(\xi_2(\gamma-1)v_1+\beta^\nu c^2 n_1)\Delta_{ji}m_1\\
&\quad -(\xi_2(\gamma-1)v_2+\beta^\nu c^2 n_2)\Delta_{ji}m_2+(\gamma-1)\xi_2\Delta_{ji}(\rho E))\\
&\quad +|\lambda_4|(v_1+\xi_2 n_1)\Big(-(\xi_1(\gamma-1)\tfrac{|v^2|}{2}+\beta^\nu c^2 v_n)\Delta_{ji}\rho+(\xi_1(\gamma-1)v_1+\beta^\nu c^2 n_1)\Delta_{ji}m_1\\
&\quad +(\xi_1(\gamma-1)v_2+\beta^\nu c^2 n_2)\Delta_{ji}m_2-(\gamma-1)\xi_1\Delta_{ji}(\rho E))]\,,
\end{aligned}
$$

$$
\begin{aligned}
\mathbf{D}_3(\mathbf{u}_R-\mathbf{u}_L) &= |v_n|[v_2\Delta_{ji}\rho+v_2\tfrac{\gamma-1}{c^2}(-\tfrac{|\mathbf{v}|^2}{2}\Delta_{ji}\rho+v_1\Delta_{ji}m_1+v_2\Delta_{ji}m_2-\Delta_{ji}(\rho E))\\
&\quad -n_1(v_t\Delta_{ji}\rho+n_2\Delta_{ji}m_1-n_1\Delta_{ji}m_2)]\\
&\quad +\tfrac{1}{2\beta^\nu c^2\xi_3}\,[|\lambda_3|(v_2+\xi_1 n_2)\\
&\quad \Big((\xi_2(\gamma-1)\tfrac{|\mathbf{v}|^2}{2}+\beta^\nu c^2 v_n)\Delta_{ji}\rho-(\xi_2(\gamma-1)v_1+\beta^\nu c^2 n_1)\Delta_{ji}m_1\\
&\quad -(\xi_2(\gamma-1)v_2+\beta^\nu c^2 n_2)\Delta_{ji}m_2+(\gamma-1)\xi_2\Delta_{ji}(\rho E))\\
&\quad +|\lambda_4|(v_2+\xi_2 n_2)\Big(-(\xi_1(\gamma-1)\tfrac{|\mathbf{v}|^2}{2}+\beta^\nu c^2 v_n)\Delta_{ji}\rho+(\xi_1(\gamma-1)v_1+\beta^\nu c^2 n_1)\Delta_{ji}m_1\\
&\quad +(\xi_1(\gamma-1)v_2+\beta^\nu c^2 n_2)\Delta_{ji}m_2-(\gamma-1)\xi_1\Delta_{ji}(\rho E))]\Big)\,,
\end{aligned}
$$

and

$$
\begin{aligned}
\mathbf{D}_4(\mathbf{u}_R-\mathbf{u}_L) &= |v_n|\tfrac{|\mathbf{v}|^2}{2}[(1-\tfrac{\gamma-1}{c^2}\tfrac{|v|^2}{2})\Delta_{ji}\rho+\tfrac{\gamma-1}{c^2}(v_1\Delta_{ji}m_1+v_2\Delta_{ji}m_2-\Delta_{ji}(\rho E))]\\
&\quad -|v_n|v_t(v_t\Delta_{ji}\rho+n_2\Delta_{ji}m_1-n_1\Delta_{ji}m_2)\\
&\quad +\tfrac{1}{2\beta^\nu c^2\xi_3}\,[|\lambda_3|(H+\xi_1 n_2)\\
&\quad ((\xi_2(\gamma-1)\tfrac{|\mathbf{v}|^2}{2}+\beta^\nu c^2 v_n)\Delta_{ji}\rho-(\xi_2(\gamma-1)v_1+\beta^\nu c^2 n_1)\Delta_{ji}m_1\\
&\quad -(\xi_2(\gamma-1)v_2+\beta^\nu c^2 n_2)\Delta_{ji}m_2+(\gamma-1)\xi_2\Delta_{ji}(\rho E))\\
&\quad +|\lambda_4|(H+\xi_2 n_2)\Big(-(\xi_1(\gamma-1)\tfrac{|\mathbf{v}|^2}{2}+\beta^\nu c^2 v_n)\Delta_{ji}\rho+(\xi_1(\gamma-1)v_1+\beta^\nu c^2 n_1)\Delta_{ji}m_1\\
&\quad +(\xi_1(\gamma-1)v_2+\beta^\nu c^2 n_2)\Delta_{ji}m_2-(\gamma-1)\xi_1\Delta_{ji}(\rho E))]\,.
\end{aligned}
$$

# Bibliography


[1] P. Birken. Preconditioning gmres for steady compressible inviscid flows. RWTH Aachen, Institut für Geometrie und Praktische Mathematik, Bericht Nr. 212, 2002.

[2] P. Birken and A. Meister. Stability of Preconditioned Finite Volume Schemes at Low Mach Numbers. *BIT*, 45(3), 2005. accepted.

[3] N. Botta, R. Klein, S. Langenberg, and S. Lützenkirchen. Well balanced finite volume methods for nearly hydrostatic flows. *J. Comput. Phys.*, 196:539–565, 2004.

[4] D. Choi and C. L. Merkle. The Application of Preconditioning in Viscous Flows. *J. Comput. Phys.*, 105:207–223, 1993.

[5] A. J. Chorin. A Numerical Method for Solving Incompressible Viscous Flow Problems. *J. Comput. Phys.*, 2:12–26, 1967.

[6] A. J. Chorin and J. Marsden. *A Mathematical Introduction to Fluid Mechanics.* Springer Verlag, New York, 1997.

[7] M. Crandall and A. Majda. The method of fractional steps for conservation laws. *Numer. Math.*, 34:285–314, 1980.

[8] I. Demirdžić, Ž. Lilek, and M. Perić. A Collocated Finite Volume Method for Predicting Flows at All Speeds. *Int. J. Num. Meth. Fluids*, 16:1029–1050, 1993.

[9] D.R. Durran. *Numerical Methods for Wave Equations in Geophysical Fluid Dynamics.* Springer, New York, 1999.

[10] O. Friedrich. Weighted Essential Non-Oscillatory Schemes for the Interpolation of Mean Values on Unstructured Grids. *J. Comput. Phys.*, 144:194–212, 1998.

[11] O. Friedrich. *Gewichtete wesentlich nicht-oszillierende Verfahren auf unstrukturierten Gittern.* Dissertation, Fachbereich Mathematik, Schwerpunkt Differentialgleichungen und Dynamische Systeme, Universität Hamburg, 1999.

[12] I. Gasser and J. Struckmeier. An asymptotic-induced one-dimensional model to describe fires in tunnels. *Math. Meth. Appl. Sci.*, Vol. 25:1231–1249, 2002.

[13] I. Gasser, J. Struckmeier, and I. Teleaga. Modelling and Simulation of Fires in Vehicle Tunnels. *Int. J. for Numerical Methods in Fluids*, 44 (3):277–296, 2004.

[14] E. Godlewski and P.-A. Raviart. *Numerical Approximation of Hyperbolic Systems of Conservation Laws*, volume 118 of *Applied Mathematical Sciences*. Springer, New York, Berlin, Heidelberg, 1996.

[15] S. K. Godunov. A Finite Difference Method for the Numerical Computation of Discontinuous Solutions of the Equations of Fluid Dynamics. *Mat. Sb.*, 47:357–393, 1959.

[16] A. Greenbaum, V. Pták, and Strakoš. Any nonincreasing convergence curve is possible for gmres. *SIAM J. Matrix Anal. Appl.*, 17 (3):465–469, 1996.

[17] J.J. Greenberg and A.Y. Leroux. A well-balanced scheme for the numerical processing of source terms in hyperbolic equations. *SIAM J. Numer. Anal.*, 33(1):1–16, 1996.

[18] H. Guillard and C. Viozat. On the Behaviour of Upwind Schemes in the Low Mach Number Limit. *Computers and Fluids*, Vol. 28:63–86, 1999.

[19] E. Hairer, S.P. Nørsett, and G. Wanner. *Solving Ordinary Differential Equations I.* Springer, Berlin, Heidelberg, New York, Series in Computational Mathematics 8, 2. edition, 2000.

[20] E. Hairer and G. Wanner. *Solving Ordinary Differential Equations II.* Springer, Berlin, Series in Computational Mathematics 14, 3. edition, 2004.

[21] F. H. Harlow and J. E. Welch. Numerical Calculation of Time-Dependent Viscous Incompressible Flow of Fluid with Free Surface. *Phys. of Fluids*, Vol. 8(12):2182–2189, 1965.

[22] C. Hirsch. *Numerical computation of internal and external flows*, volume 1. Wiley & Sons, Chicester, New York, 1988.

[23] C. Hirsch. *Numerical computation of internal and external flows*, volume 2. Wiley & Sons, Chicester, New York, 1988.

[24] L. Hoffmann and A. Meister. A Compressible Low Mach Number Scheme based on Image Processing and Asymptotic Analysis. *Computational Fluid Dynamics Journal*, Vol. 9:231–242, 2001.

[25] J. Kevorkian and J. D. Cole. *Multiple Scale and Singular Perturbation Methods*, volume 114 of *Applied Mathematical Sciences*. Springer, New York, Berlin, Heidelberg, 1996.

[26] S. Klainerman and A. Majda. Singular limits of quasilinear hyperbolic system with large parameters and the incompressible limit of compressible fluids. *Comm. Pure Appl. Math.*, 34:481–524, 1981.

[27] R. Klein. Semi-Implicit Extension of a Godunov-Type Scheme Based on Low Mach Number Asymptotics I: One-Dimensional Flow. *J. Comput. Phys.*, 121:213–237, 1995.

[28] R. Klein, N. Botta, T. Schneider, C.D. Munz, S. Roller, A. Meister, L. Hoffmann, and T. Sonar. Asymptotic adaptive methods for multi-scale problems in fluid mechanics. *Journal of Engineering Mathematics*, Vol. 9 (1/4)(2):261–343, 2001.

[29] D.A. Knoll and D.E. Keyes. Jacobian-free Newton-Krylov methods: a survey of approaches and applications. *J. Comp. Phys.*, 193:357–397, 2004.

[30] T. Kolb. Tunnelanlagen in Stuttgart. Untersuchung von Stuttgarter Tunnelanlagen mit Hilfe eines Brandsimulations-Programms. 2000.

[31] J. O. Langseth, A. Tveito, and R. Winther. On the convergence of operator splitting applied to conversation laws with source terms. *SIAM J. Num. Anal.*, 33(3):843–863, 1996.

[32] S.-H. Lee. Convergence characteristics of preconditioned euler equations. *J. Comp. Phys.*, 208:266–288, 2005.

[33] R. J. LeVeque. Hyperbolic Conservation Laws and Numerical Methods. High Resolution (Upwind and TVD) Methods for the Compressible Flow Equations, Selected Special Topics, Von Karman Institute for Fluid Dynamics, Rhode-Saint-Genèse, 1994.

[34] R. J. LeVeque. *Finite Volume methods for Hyperbolic Problems.* Cambridge University Press, Cambridge, 2002.

[35] R. Massjung. *Numerical Schemes and Well-Posedness in Nonlinear Aeroelasticity.* PhD thesis, RWTH Aachen, 2002.

[36] R. Massjung. Personal communication.

[37] U. Max. *Zur Berechnung der Ausbreitung von Feuer und Rauch in komplexen Gebäuden.* PhD thesis, University of Kassel, 1990.

[38] P. R. McHugh and D. A. Knoll. Comparison of standard and matrix-free implementations of several Newton-Krylov solvers. *AIAA J.*, 32(12):2394–2400, 1994.

[39] A. Meister. *Zur zeitgenauen numerischen Simulation reibungsbehafteter, kompressibler, turbulenter Strömungsfelder mit einer impliziten Finite-Volumen-Methode vom Box-Typ.* Dissertation, Technische Hochschule Darmstadt, 1996.

[40] A. Meister. Asymptotic Single and Multiple Scale Expansions in the Low Mach Number Limit. *SIAM J. Appl. Math.*, Vol. 60(1):256–271, 1999.

[41] A. Meister. *Numerik linearer Gleichungssysteme, Eine Einführung in moderne Verfahren.* Vieweg, Wiesbaden, 1999.

[42] A. Meister. *Analyse und Anwendung Asymptotik-basierter numerischer Verfahren zur Simulation reibungsbehafteter Strömungen in allen Mach-Zahlbereichen.* Habilitation, Universität Hamburg, 2001.

[43] A. Meister. Asymptotic based preconditioning technique for low Mach number flows. *Z. Angew. Math. Mech.*, 83(1):3–25, 2003.

[44] A. Meister. Viscous Flow Fields at all Speeds: Analysis and Numerical Simulation. *Journal of Applied Mathematics and Physics (ZAMP)*, 54:1010–1049, 2003.

[45] A. Meister and C. Vömel. Efficient Preconditioning of Linear Systems arising from the Discretization of Hyperbolic Conservation Laws. *Advances in Computational Mathematics*, Vol.14(1):49–73, 2001.

[46] B. Müller. Low Mach number asymptotics of the Navier-Stokes equations. *J. of Engineering Mathematics*, 34:97–109, 1998.

[47] N.T.-H. Nguyen-Bui, B. Dubroca, and P.-H. Maire. Application of turkel preconditioned method in external free convection and incompressible flows. In *Conference on Mathematical and Numerical Aspects of Low Mach Number Flows*, 2004.

[48] S. M. Olenick and D. J. Carpenter. An Updated International Survey of Computer Models for Fire and Smoke. *J. of Fire Protection Engineering*, 13:87–110, 2003.

[49] S. V. Patankar and D. B. Spalding. A Calculation Procedure for Heat, Mass and Momentum Transfer in Three-dimensional Parabolic Flows. *Int. J. Heat Mass Transfer*, 15:1787–1805, 1972.

[50] N. Qin, D. K. Ludlow, and S. T. Shaw. A matrix–free preconditioned Newton/GMRES method for unsteady Navier-Stokes solutions. *Int. J. Num. Meth. Fluids*, 33:223–248, 2000.

[51] A. Reusken. Convergence Analysis of the Gauss-Seidel Preconditioner for Discretized One Dimensional Euler Equations. *SIAM J. on Num. Analysis*, 41 (4):1388–1405, 2003.

[52] P. L. Roe. Approximate Riemann Solvers, Parameter Vectors, and Difference Schemes. *J. Comput. Phys.*, 43:357–372, 1981.

[53] Y. Saad. *Iterative Methods for Sparse Linear Systems.* PWS Publishing Company, Boston, 1996.

[54] Y. Saad and M. H. Schultz. GMRES: A generalized minimal residual algorithm for solving nonsymmetric linear systems. *SIAM J. Sci. Stat. Comput.*, 7:856–869, 1986.

[55] F. Schimmel. *Development and Test of an Atmosperic Model Employing Adaptive Numerical Methods.* Dissertation, Universität Hamburg, 2002.

[56] T. Schneider, N. Botta, K. J. Geratz, and R. Klein. Semi-Implicit Extension of a Godunov-Type Compressible Solver Based on Low Mach Number Asymptotics II: Multi-Dimesional, Variable Density Zero Mach Number Flow. *J. Comput. Phys.*, 155:248–286, 1999.

[57] J. Sesterhenn, B. Müller, and H. Thomann. On the cancellation problem in calculating compressible low mach number flows. In J.-A. Désidéri, C. Hirsch, P. LeTallec, M. Pandolfi, and J. Périaux, editors, *3rd ECOMAS CFD Conference, Paris, 9-13 September 1996*, pages 408–413, Chichester, 1996. Wiley.

[58] J.-S. Shuen, K.-H. Chen, and Y. Choi. A Coupled Implicit Method for Chemical Non-equilibrium Flows at All Speeds. *J. Comput. Phys.*, 106:306–318, 1993.

[59] G. Strang. On the construction and comparison of difference schemes. *SIAM J. Num. Anal.*, 5, 1968.

[60] T. Tang and Z.-H. Teng. Error bounds for fractional step methods for conservation laws with source terms. *SIAM J. Num. Anal.*, 32(1):110–127, 1995.

[61] E. F. Toro. *Riemann Solvers and Numerical Methods for Fluid Dynamics*. Springer, Berlin, Heidelberg, New York, 2. edition, 1999.

[62] L. N. Trefethen. Pseudospectra of linear operators. *SIAM Review*, 39 (3):383–406, 1997.

[63] E. Turkel. Preconditioned Methods for Solving the Incompressible and Low Speed Compressible Equations. *J. Comput. Phys.*, 72:277–298, 1987.

[64] E. Turkel and V. Vatsa. Choice of Variables and Preconditioning for Time Dependent problems. *AIAA Paper*, 2003-3692 CP, 2003. AIAA 16th Computational Fluid Dynamics Conference, Orlando.

[65] H. A. van der Vorst. *Iterative Krylov Methods for Large Linear Systems*, volume 13 of *Cambridge Monographs on Applied and Computational Mathematics*. Cambridge University Press, Cambridge, 2003.

[66] B. van Leer. Flux-vector splitting for the Euler equations. In E. Krause, editor, *Eighth International Conference on Numerical Methods in Fluid Dynamics*, number 170 in Lecture Notes in Physics, pages 507–512, Berlin, 1982. Springer Verlag.

[67] B. van Leer, W.-T. Lee, and P. Roe. Characteristic Time-Stepping or Local Preconditioning of the Euler Equations. *AIAA Paper*, AIAA-91-1552, 1991.

[68] V. Venkatakrishnan. Convergence to Steady State Solutions of the Euler Equations on unstructured Grids with Limiters. *J. Comp. Phys.*, 118, 1995.

[69] G. Volpe. Performance of Compressible Flow Codes at Low Mach Numbers. *AIAA J.*, 31(1):49–56, 1993.

[70] Y. Wada and M.-S. Liou. A Flux Splitting Scheme with High-Resolution and Robustness for Discontinuities. *AIAA Paper*, 94–0083, 1994.

[71] J. M. Weiss and W. A. Smith. Preconditioning Applied to Variable and Constant Density Flows. *AIAA J.*, 33(11):2050–2057, 1995.

[72] I. Wenneker, A. Segal, and P. Wesseling. A Mach-uniform unstructured staggered grid method. *I. J. Numerical Methods in Fluids*, 40:1209–1235, 2002.

Hiermit versichere ich, dass ich die vorliegende Dissertation selbstständig und ohne erlaubte Hilfe angefertigt und andere als die in der Dissertation angegebenen Hilfsmittel nicht benutzt habe. Alle Stellen, die wörtlich oder sinngemäß aus veröffentlichten oder unveröffentlichen Schriften entnommen sind, habe ich als solche kenntlich gemacht. Kein Teil dieser Arbeit ist in einem anderen Promotions- oder Habilitationsverfahren verwendet worden.